



Sapienza University of Rome

Faculty of Mathematical, Physical and Natural Sciences

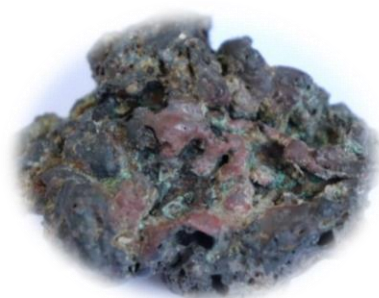
ARCHMAT

(ERASMUS MUNDUS MASTER IN ARCHAeological MATerials Science)

Scienze e Tecnologie per la Conservazione dei Beni Culturali

An Archaeometric Study of Copper Slags from Early Bronze Age I at
Arslantape, Eastern Anatolia, Turkey

Sabikun Naher (1874335)



Supervisor: ANNA CANDIDA FELICI
Department of Basic and Applied Sciences for Engineering
Sapienza University of Rome

Co-Supervisor: FRANCESCA BALOSSI RESTELLI
Department of Antiquity Sciences
Sapienza University of Rome

Co-Supervisor: GABRIELE FAVERO
Department of Chemistry and Drug Technologies
Sapienza University of Rome

Rome, October 2019



ARISTOTLE
UNIVERSITY OF
THESSALONIKI



UNIVERSIDADE
DE ÉVORA



SAPIENZA
UNIVERSITÀ DI ROMA

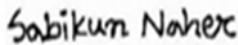


DECLARATION

I hereby declare that this thesis and abstract is my original work and that to the best of my knowledge, it neither contains any material previously published by another person, nor material that has been accepted for the award of a degree or any other qualification at this University or elsewhere, except where due acknowledgement has been made in the text. Where I have consulted the published or unpublished works of others, I have stated explicitly both in the text and references.

This research was done under the supervision and guidance of Professor Anna Candida Felici of the Department of Basic and Applied Sciences for Engineering and co-supervisions of Dr. Francesca Balossi Restelli of the Department of Antiquity Sciences and Professor Gabriele Favero of the Department of Chemistry and Drug Technologies, Sapienza University of Rome, Italy.

Sabikun Naher
(Student's Name)
Student ID: 1874335


(Signature)
Date: 18th October, 2019

Anna Candida Felici
(Supervisor's Name)
Department of Basic and Applied
Sciences for Engineering
Sapienza University of Rome



(Signature)
Date: 18th October, 2019

TABLE OF CONTENTS

List of Figures.....	4
List of Tables.....	6
List of Appendix.....	6
ACKNOWLEDGMENTS.....	7
ABSTRACT.....	8
CHAPTER 1: INTRODUCTION.....	9
1.1 Research background.....	9
1.2 Aims and objectives.....	10
1.3 Structure of the study.....	10
CHAPTER 2: SLAGS AND CRUCIBLES: A GENERAL OVERVIEW.....	11
2.1 The term ‘slag’.....	11
2.2 The formation of slags.....	12
2.3 Types of copper slags.....	13
2.4 The term ‘crucible’.....	14
2.5 Early Bronze Age crucibles.....	15
2.6 General attributes related to the Early Bronze Age crucibles.....	15
CHAPTER 3: ARCHAEOLOGICAL AND GEOLOGICAL SETTINGS.....	18
3.1 The Site of Arslantepe.....	18
3.2 A brief history of excavation at Arslantepe.....	18
3.3 Stratigraphic sequence of Arslantepe.....	19
3.4 Arslantepe in the Early Bronze Age I.....	21
3.5 Geological Setting of Arslantepe and Eastern Anatolia.....	23
3.5.1 Geological overview of Arslantepe and Eastern Anatolia.....	23
3.5.2 Ancient ore deposits in Eastern Anatolia.....	24
CHAPTER 4: MATERIALS AND METHODS.....	25
4.1 Materials.....	25
4.1.1 Stratigraphic context.....	25
4.2 X-ray fluorescence (XRF) spectroscopy for chemical characterization.....	29
4.2.1 Working principle.....	29
4.2.2 Analytical parameters.....	30
4.3 X-Ray Diffraction (XRD) for mineralogical identification.....	30
4.3.1 Working principle.....	30
4.3.2 Analytical parameters.....	32
4.4 Scanning Electron Microscope with EDS for microstructure study.....	32
4.4.1 Working principle.....	32
4.4.2 Analytical parameters.....	34
CHAPTER 5: RESULTS.....	34
5.1 EDXRF analysis: Chemical composition.....	35
5.2 Powder XRD analysis: Mineralogical phases.....	39
5.3 SEM-EDS analysis: Microstructure.....	49
CHAPTER 6: DISCUSSION.....	59
6.1 Type of slags and relevant metallurgical processes.....	59
6.2 Nature of thermodynamics.....	60
6.3 Nature of the ore.....	63
6.4 Crucible properties.....	63
6.5 Weathering phenomenon.....	65
CHAPTER 7: FINAL REMARKS.....	67
7.1 Research contributions.....	67
7.2 Prospects for future research.....	68
7.3 Limitations.....	68
RERERENCES.....	70
APPENDIX.....	75

List of Figures

Fig. 1: The metallurgical chain from ore to metal. Slags can be formed by a wide range of activities, e.g. by smelting ores or by melting metal (e.g., by casting, alloying, or refining processes) within this <i>chaîne opératoire</i> system (after Hauptmann,2014:92).	11
Fig. 2: Key factors related to the ancient slag formation.....	12
Fig. 3: Location of Arslantepe in Eastern Anatolia (area location at top right) (from Vignola Masi et al, 2018).....	18
Fig. 4: The Arslantepe mound in the Malatya plain, eastern Turkey (from Frangipani, 2016)19	
Fig. 5: Early Bronze Age I metals from Arslantepe, periods VIB1 and VIB2 (Left), and the upper town fortification wall (mud-brick elevation and stone foundations) from period VIB2 (right) (from Frangipane, 2017:177, 179).....	22
Fig. 6: A general geological map of Eastern Anatolia (from Garzanti, <i>et al</i> , 2016:109).....	23
Fig. 7: Known major ore sources in Eastern Anatolian region (modified after Frangipane & Palmieri, 1994-1995:67)	24
Fig. 8: Topographic plan of the settlement of Arslantepe-VI B2 (Early Bronze Age I) showing the distribution of metal objects, crucibles, slag and ores. The finding location of present analyzed slag samples marked in a red circle. (taken from Di Nocera, 2013:126).....	26
Fig. 9a: Photographic images of analyzed slag samples Fig.7a: Photographic images of analyzed slag samples.....	27
Fig. 9b: Photographic images of analyzed slag samples.....	28
Fig. 10a: Photographic images of analyzed crucible fragments.....	28
Fig. 10b: 3D images of analyzed crucible fragments.....	28
Fig. 11: Production of characteristic radiation (after Brouwer, 2011:18).....	29
Fig. 12: Schematic diagram of XRD (left) and Bragg's law (right) (retrieved from http://reference.iucr.org/dictionary).....	31
Fig. 13: Schematic diagram of a scanning electron microscope (left) and electron-matter interaction (right) (retrieved from https://www.nanoimages.com/sem-technology/overview/).....	33
Fig. 14: The XRF results for iron, silicon and aluminum contents in analyzed slag samples, results are presented as normalized mass fractions (%).....	35
Fig. 15: The XRF results for copper content in analyzed slag samples, results are presented as normalized mass fractions (%).....	36
Fig. 16: The XRF results for sulphur content in analyzed slag samples, results are presented as normalized mass fractions (%).....	36
Fig. 17: X-ray diffraction (XRD) patterns of slag sample 133 A929 1(i).....	39
Fig. 18: X-ray diffraction (XRD) patterns of slag sample 133 A929 1(ii).....	40
Fig. 19: X-ray diffraction (XRD) patterns of slag sample 133 A929 1(iii).....	41
Fig. 20: X-ray diffraction (XRD) patterns of slag sample 133 A929 1(iv).....	42
Fig. 21: X-ray diffraction (XRD) patterns of slag sample 133 A929 1(v).....	43
Fig. 22: X-ray diffraction (XRD) patterns of slag sample 144 A929 1a(i).....	44
Fig. 23: X-ray diffraction (XRD) patterns of slag sample 144 A929 1a(ii).....	45
Fig. 24: X-ray diffraction (XRD) patterns of slag sample 146 A929 1c(i).....	46
Fig. 25: X-ray diffraction (XRD) patterns of slag sample 146 A929 1c(iv).....	47
Fig. 26: Mass fraction (wt%) of quartz and fayalite in analyzed 9 slag samples.....	48
Fig. 27: SEM-EDS backscattered image (a), combined map (b), and EDS spectrum (c) of sample 133 A929 1(i).	49
Fig. 28: SEM-EDS elemental maps of sample 133 A929 1(i).....	50
Fig. 29: SEM-EDS backscattered image (a), combined map (b), and EDS spectrum (c) of	

sample 133 A929 1(iv).....	51
Fig. 30: SEM-EDS elemental maps of sample 133 A929 1(iv).....	52
Fig. 31: SEM-EDS backscattered image (a), combined map (b) and EDS spectrum of spot 1(c), EDS spectrum of spot 2 (d) of sample 144 A929 1a(iii).....	53
Fig. 32: SEM-EDS elemental maps of sample 144 A929 1a(iii).....	54
Fig. 33: SEM-EDS backscattered image (a), combined map (b), and EDS spectrum (c) of sample 144 A929 1a(iv).....	55
Fig. 34: SEM-EDS elemental maps of sample 144 A929 1a(iv).....	56
Fig. 35: SEM-EDS backscattered image (a), combined map (b), and EDS spectrum (c) of sample 146 A929 1c(i).....	57
Fig. 36: SEM-EDS elemental maps of sample 146 A929 1c(i).....	58
Fig. 37: (a) Ternary diagram of Si-Fe-Mg. Here FeO-SiO ₂ binary are shown on one side of the triangle, and an analogous MgO-SiO ₂ binary on the other side of the triangle. The solid solution series between the olivine and pyroxene end members form horizontal lines parallel to the base of the triangle. (b) Phase diagram for the components forsterite and fayalite. Here are graphically represented the equilibrium relationships governed by the laws of thermodynamics between these two minerals. (retrieved from http://lib.znate.ru/docs/index20150.html).....	61
Fig. 38: The phase diagram for SiO ₂	62
(https://serc.carleton.edu/research_education/equilibria/simplephasediagrams.html).	
Fig. 39: (A1) Slag and vitrified area of crucible sample 133 A929 1A, (A2) magnified detail of the same area, (A3) stereomicroscope image of the same area, (A4) A core area of the crucible sample 133 A929 1A, (A5) stereomicroscope image of the unidentified white inclusion in the same core area, (B1) slag and vitrified area of crucible sample 133 A929 1B, (B2) magnified detail of the same area, (B3) stereomicroscope image of the same area.....	64
Fig. 40: Ternary compositional diagram of iron-titanium-oxide solid solution magnetic minerals. During low temperature oxidation, the bulk composition follows the horizontal dashed lines, where z is the oxidation parameter and x is the titanomagnetite composition parameter. (https://www.sciencedirect.com/topics/earth-and-planetary-sciences/maghemite).....	66

List of Tables

Table 1: Technical attributes of crucibles (after Bayley & Rehren, 2007).....	17
Table 2: Archaeological phases and their chronologies of Arslantepe (Vignola <i>et al.</i> , 2018).	20
Table 3: Summary of the analytical methods used for the samples' characterization.....	34
Table 4: EDXRF elemental analysis of 15 slags samples. Results are presented as averages values of normalized mass fractions (%) with dispersion values.....	37
Table 5: XRD results of analyzed slag samples.....	48

List of Appendix

1.1- 3 EDXRF elemental analysis of three different points of each slag samples, results are shown as normalized mass fractions (%).....	75-77
2. 1-10 Some examples of EDXRF spectrums of analyzed slag and crucible samples.....	78-87
3.1 SEM-EDS backscattered image and spectrums of analyzed spots of sample 133 A929 1(i).....	88
3.2 SEM-EDS backscattered image and spectrums of analyzed spot of sample 133 A929 1(iv).....	89
3.3 SEM-EDS spectrums of analyzed spots of sample 133 A929 1(iv).....	90
3.4 SEM-EDS backscattered image and spectrums of analyzed spots of sample 144 A929 1(iii).....	91
3.5 SEM-EDS backscattered image and spectrums of analyzed spots of sample 144 A929 1(iv).....	92
3.6 SEM-EDS backscattered image and spectrums of analyzed spots of sample 146 A929 1(i).....	93
3.7 SEM-EDS spectrums of analyzed spots of sample 146 A929 1(i).....	94
4.1 Images of different analytical instruments and tools used in the present study.	95

ACKNOWLEDGEMENTS

The work presented here is a result of the collaborative effort of many people and it is my pleasure to thank everyone who made this possible.

First and foremost, I am indebted to my supervisor Prof. Anna Candida Felici, for her invaluable scientific guidance, enthusiastic supervision and encouragement throughout my thesis research work. I am very grateful for her support, patience and her efforts in explaining and teaching me the concepts of archaeometry techniques; in particular, X-ray fluorescence spectroscopy.

I also like to thank to my co-supervisors Dr. Francesca Balossi Restelli and Prof. Gabriele Favero for their friendly attitude to accept my appeal for conducting this project on a first meet up at their office. Besides my supervisors I am also grateful to Prof. Nick Schiavon, Prof. Jose Mirao, Prof. Patricia Moita, Prof. Antonio Candeias, Dr. Carlo Bottaini, Anna Tsoupra, Sara Valadas and Ana Cardoso for their invaluable contributions during my lab works in Hercules laboratory, University of Evora, Portugal.

A very special thanks to Dr. Gabriel Maria Ingo (ISMN-CNR), who provided insightful comments and feedback on the findings of the present work. I am also thankful to Prof. Laura Sadori and Claudia Moricca for their support regarding the stereomicroscope observation of crucible samples.

I must express my profound gratitude to my parents Md. Habibur Rahman and Salina Rahman, to my siblings Mesbahul Alam Salim, to my sister in law Roushon Ara Parvin Sume, to my uncle Shafiqul Islam Khan, Mosharaf Hossain and to my beloved friends Tania Jahan, Suvasish Kumar Jib Barua, Rabeya Akter Rabu and Jasmine Jaim for their unconditional support, encouragement, inspiration and wise advices throughout my studies. Their constant support plays a vital role throughout my life in abroad.

I would like to express my sincere gratitude to my mentor Dr Pranab Kumar Chattopadhyay for introducing me to the world of archaeometallurgy. I am also grateful to my mentors of Bangladesh-Prof. Syed M. Kamrul Ahsan, Prof. Mozammel Hoque, Prof. Seema Hoque, Prof. Swadhin Sen, Prof. Masood Imran Mannu, Prof. Maliha Nargis Ahmed, and my seniors Rupali Akhter, M Kamal H Akanda, Nurul Kabir for encouraging me to pursue a higher study in this particular field. I am also express my appreciation to my juniors Jesmin Nahar Jhumur, Arif Hossain, Md. Arifujjaman, Habibullah Habib and Nazifa Raihana Rafa for their moral support and various helps during the last two years.

I am also indebted to my fellow ARCHMAT colleagues: Dulce Elizabeth Valdez Madrid, Erwin M.U. Saraka, Liao Yun-Wen, Samah Al-Khasoneh, Basira Mir Makhmad, Zahra Haghighi, Judith Margarita Lopez Aceves, Samantha Hruban, Yang Zhou, Phylida Bailey, Maria Elisavet Samoili, Yuliia Storozhylova, Phoebe Tang Sum Yu, Adam Gasper and Alvaro Felipe Ortega Gonzalez for their priceless friendships, enormous support and motivation during the last two years. It's been really wonderful studying with all of them.

And finally, I thank the ARCHMAT consortium for selecting me for this program and providing me the Erasmus Mundus scholarship, which made possible of this thesis work.

ABSTRACT

15 copper slags and 2 crucible fragments from the village of the Early Bronze Age I (V1B2 period, 3100-2900 BC), at Arslantepe, Eastern Anatolia, Turkey, have been analyzed with energy dispersive X-ray fluorescence spectroscopy (EDXRF), powder X-ray diffraction (XRD) and scanning electron microscopy with energy dispersive spectroscopy (SEM-EDS) to determine the chemical and mineralogical composition and microstructures as well. The compositional analysis confirms the presence of iron, silicon, and aluminum as the significant elements in the copper slags with the modest level of copper and calcium, and low concentrations of sulphur, potassium, titanium, vanadium, chromium, manganese, zinc, molybdenum and strontium. Powder X-ray diffraction analysis reveals that quartz and fayalite are the major crystalline phases along with the magnetite as minor phase present in the analyzed slag samples. However, the mineralogical composition and SEM-EDS images indicates that some of the analyzed slags were the product of primary copper smelting and other might be formed during the works of metal. The presence of well-formed fayalite crystals in one analyzed slag sample indicates the specific thermodynamics condition, that is heating condition was well controlled during the smelting activities. Through EDXRF, the presence of low concentration of sulphur in all slag samples and the association of copper with sulphur in SEM-EDS image of one sample suggests that ancient metal workers might be exploiting some minerals as a copper ore that were associated with sulphur.

Keywords: Slags, Crucibles, Early Bronze Age, Arslantepe, EDXRF, XRD, SEM-EDS, Fayalite

CHAPTER 1: INTRODUCTION

1.1 Research background

Archaeometry is an interdisciplinary research area where complementary approaches cooperate to investigate cultural heritage materials. It can be considered a bridge between humanities, such as archaeology and art history, and natural sciences, as chemistry, physics, biology and geology. Archaeometric research includes a wide range of studies and can be defined as the application of scientific techniques for the knowledge and characterization of artefacts and their involvement with humans and environment (Castellano, Martini, & Sibilla, 2007). The age, use, production technique, provenance and environmental data are some of the achievable information as result of this investigation. However, there are several examples that have demonstrate the potentiality of archaeometric research in the field of slag analysis (Bachmann, 1982).

In human history, intentional smelting of ores to produce metal is marked as one of the remarkable achievements and slags are one of the important evidences to understand this past pyrometallurgical activities. Slags and crucibles serve a variety of functions in the physicochemical processes of metallurgical production. Hence, the examination of macroscopic features and chemical, mineralogical and micro-structural compositions of ancient slags and crucibles can give the answers of many questions regarding archaeometallurgy and history of technology (Bachmann, 1982; Hauptmann, 2009). In Arslantepe, an ancient archaeological site in the Eastern Anatolian region of Turkey, abundant metal artifacts of silver, gold, copper and lead have been found. For example, 100 metal objects were found both in a palace and a royal tomb from Arslantepe V I A - B1 (3400-3100 BC) that were published by Frangipane *et al.* (2002) and Hauptmann *et al.* (2003a). The analytic investigations have shown that the jewelry was produced from a silver-copper alloy. Furthermore, a kind of arsenic enriched copper, partly nickel-bearing, was used in order to produce high-status objects, weapons (also swords and spearheads) and tools. But archaeological evidence shows that smelting in the site is attested apparently only for copper (Caneva and Palmiri: 1983). In particular, plentiful metallurgical activities have been identified in the Arslantepe at Early Bronze Ib village (3100-2900 BC), where fragments of crucibles and various kilograms of slags have been brought to light in a small courtyard and street. Most evidently in this area worked by the metallurgists. In this aspect, present archaeometric study

of copper slags and crucible fragments from Early Bronze Age Ib could shed new light on past smelting activities and metallurgical advancement of this particular area.

1.2 Aims and Objectives

For this research 15 slags samples and 2 crucible fragments were collected from Early Bronze Age Ib at Arslantepe, Eastern Anatolia, Turkey, for various archaeometric analyses. The main purposes of this study are:

- To examine the chemical composition of the samples.
- To determine the mineralogical composition of the samples.
- To study the microstructure of the samples
- To achieve a practical knowledge to conduct an archaeometric research in the field of archaeometallurgy.

1.3 Structure of the study

The whole thesis work is divided into seven chapters. Chapter 1 starts with the background of the research. This chapter also contains explanation of the research aim and objectives and explains the research structure.

Chapter 2 consists of a general overview of slags and crucibles focusing on the terminology of slag and crucible, type of the early bronze age slags and general attributes related to the early bronze age crucibles. Chapter 3 provides the archaeological and geological background of Arslantepe and Eastern Anatolia to contextualize the site, its excavation history, chronological phases and geological setting as well.

Chapter 4 is about the materials and methods. This chapter gives a general description of the samples and also describe the working principles and analytical parameters of the three archaeometric techniques used in the study.

Chapter 5 reports the result of the chemical characterization of slag and crucible samples by EDXRF, the mineral characterization by XRD, and the analysis of microstructure by SEM-EDS. Chapter 6 presents a comprehensive discussion and the technical interpretation of the results obtained with all three archaeometric techniques used in the study.

Chapter 7 which is the last chapter of this study, comprises summery and practical recommendations for future studies and limitation of the research as well.

CHAPTER 2: SLAGS AND CRUCIBLES: A GENERAL OVERVIEW

2.1 The term ‘slag’

In very general terms, a slag can be defined as a waste material of the pyrometallurgical process, which is mainly formed by the combination of gangue from the ore (mainly silicate complex) and with some of the iron oxide in the charge acting as a flux. Therefore, most of the ancient metallurgical slags are ferrous silicates, no matter whether they are the byproducts of iron or non-ferrous metal production (Bachmann, 1982; Hauptmann, 2014). Since slags are the product of complicated thermodynamics processes in relation to the type of temperature and the type of environment (more or less reducing/oxidizing) of the furnace and crucibles, the structure of the slags and their chemical composition become remarkably resistant to weathering (Hauptmann, 2007, 2014). Despite their good preservation over time, it is often difficult to classify at which point of the production process the slag originated, especially if there is no additional archaeological context available.

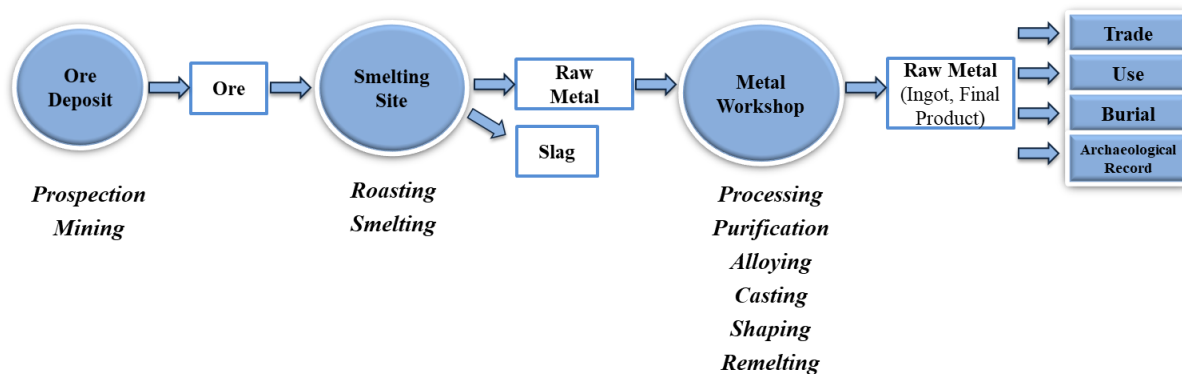


Fig. 1: The metallurgical chain from ore to metal. Slags can be formed by a wide range of activities, e.g. by smelting ores or by melting metal (e.g., by casting, alloying, or refining processes) within this *chaîne opératoire* system (after Hauptmann, 2014:92)

The metallurgical activities start at the ore deposit with ore extraction and enrichment followed by technological steps of the smelting processes, producing raw metal and other intermediate products like metallurgical slags. Slags are mainly residues of ore-smelting processes, but they can also be formed by a variety of other metallurgical activities within the ‘*chaîne opératoire*’ of metal production (Fig.1) (Hauptmann, 2014). Thus, ancient slags can be very crucial for the study of archaeometallurgical processes that produced them. By combination of the various archaeometric techniques, a wide range of technical information can be obtained from ancient slags. For example, elemental analyses can provide an idea of the bulk composition of the slags, e.g. is the acidic slag (e.g. the presence of SiO₂, Al₂O₃, TiO₂, etc.) or basic (e.g. the presence FeO, MnO, CaO, MgO, etc) (Delrue, 2008). It can also highlight the efficiency of the process

and give an idea on how much metal was lost. By examining the crystalline phases, slag's solidification temperatures and the reducing environment can also be determined. The microstructure and the non-metallic phases and metallic inclusions may provide supplementary information on the structure of the slag (segregation, which impurities are present, etc.) (Hauptmann, 2007, 2014).

2.2 Formation of slags

Slags are mainly a collection of impurities separated from metals during the ore-smelting processes. Hence, the type of the ore is one of the key factors related to the formation of slags, the purer the ore, the less slag will be formed (Bachmann, 1982, Bourgarit, 2007). Refining processes, like crucible melting can reduce the noticeable amount of slag and sometimes left none at all, perhaps only some dross or a slagging ('glazing', vitrification) of the ceramic material of the crucible used for the operation (Bachmann, 1982). However, sometimes the ores plus associated gangue can influence the bulk chemical composition for the slag formation. Such ores are called self-fluxing (Bachmann, 1982, Bourgarit, 2007). Without this property, it is not possible to achieve a sufficient separation of metal and impurities during the smelting process. Over the time and experience, ancient metallurgist gradually learned the proper use of flux to produce a good slag, i.e. a slag of low melting point and viscosity which could take up all impurities. Therefore, the composition and the properties of metallurgical slags can be influenced by several factors, e.g. nature of ores and gangue, type of fluxes added, quality of furnace constructing materials (including lining, bricks, ceramic pipes called tuyeres, temper added to clays used as furnace linings, etc.), charcoal and wood ashes, process conditions (heat distribution, air intake, furnace profile and height, retention time of slags within the furnace), cooling conditions, and weathering phenomenon (dependent on time, climate and mode of deposition) (Fig. 2) (Bachmann, 1982, Hauptmann, 2007, 2014).

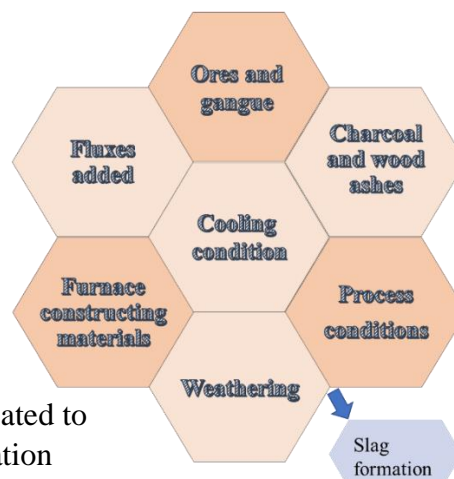


Fig. 2: Key factors related to the ancient slag formation

Each piece of slag may be a genuine chemical footprint of all or part of these influences. In particular, it may bring new insights on the process reconstruction. In spite of the many complex influences that have to be considered, certain assumptions and simplifications can be made when dealing with ancient slags as compared with modern products:

- Ancient slags were produced under limited firing control and the temperature of the smelting furnaces and hearths rarely exceeded 1300 to 1400 degrees centigrade; in most cases they were lower; (Bachmann, 1982, Hauptmann, 2007, 2014)
- Wood and charcoal were the main materials to produced heat and reduction, other materials remain unknown. In some cases, in China around 4th century AD and probably even earlier coal was used for smelting iron; (Bachmann, 1982, Bourgarit,2007).
- Preferably, local resources were used for the construction and lining of furnaces material. High quality refractories can be ruled out of antiquity (Bourgarit, 2007).

2.3 Types of copper slags

In general, slags can be divided in two categories; ferrous slags (e.g., iron) and non-ferrous slags (e.g., copper, tin) (Bachmann, 1982, Hauptmann, 2007, 2014). It is often very difficult to differentiate between these two categories by naked eye, especially copper slags and iron slags look almost the same. Sometimes green spots can be found on the slag's surface as weathering products of secondary copper minerals formed due to the metal inclusions in the slag. This could be a good indication of copper slags (Bachmann,1982). Without this color indication, only chemical analysis can help to identify whether the particular piece of slag is copper, iron, or tin etc.

However, copper slags are mainly byproduct of non-ferrous metallurgy and based on technological grounds, this type of slag can be divided into two main groups:

- smelting slags
- crucible slags (melting/refining/ casting slags).

Smelting slags are the waste product of primary smelting operations and therefore typically (though not exclusively) formed inside the furnaces (e.g., furnace slag, tap slag). On the other hand, crucible slags are generally formed inside the crucibles and usually associated with secondary metallurgy (Craddock, 1995; Redemakers, 2015). They are frequently attached to the wall of the crucibles and as a result of reactions between the metals and crucibles material,

charcoal ash and silica rich fluxes, the composition of this type of slag is commonly alkali-aluminum-silicates (Bachmann,1982). Based on macroscopic study of the external characteristics, it is often possible to distinct these two kinds of slags: smelting slags (from furnaces) are usually well crystallized and have few large pores, while crucible slags are heterogenous, glassy and porous, have small size and weight (Bachmann,1982). There are several archaeological findings which support that even in the early stage of metallurgy a highly developed technology was known, for example in Los Millares in southwest Spain or in the chalcolithic site of Shiqmim in Israel, where not only smelting slags are mainly composed of ferrous silicate (fayalite), iron-rich and poor of the extracted metal, but also, the crucible refining ones are characterized by a higher valent content of oxides and sometimes residue of wood ash in the matrix (Bourgarit, 2007).

2.4 The term ‘crucible’

The term ‘crucible’ refers to a wide range of ceramic vessels generally used for a variety of metallurgical processes, ranging from primary smelting to secondary processes like refining, alloying and casting (Bayley & Rehren, 2007; Rehren, 2003). In archaeological contexts, crucible fragments are more common, rather than a complete one. Through the metallurgical processes from ore to the finished object, ancient metallurgist used a wide range of tools and techniques. Crucibles are one of the prominent parts of this range and, apart from slags, they are also a crucial remains to reconstruct the past metallurgical process. There is a common misunderstanding in the assumption that furnace is the core place where most of the chemical reactions of smelting occurred and crucibles were only used to change temporarily the physical state of metal, and they were indeed used to melt and cast non-ferrous metals and alloys. But in recent past, through the work of various scholars, it is evident that they had numerous and often crucial roles in smelting, refining and alloying of almost all the metals of antiquity (Rehren, 2003). However, crucibles can be defined as free-standing movable containers or reaction vessels being used for high-temperature metallurgical processes.

The environments within a single crucible depends on a variety of factors, e.g. fluctuation of temperature, oxygen supply and material presence on it (Rademakers, & Rehren, 2014; Rehren & Thornton, 2009). Moreover, a crucible can be recurrently reused throughout its life span, typically involving (some) pre-firing (solid), heating, slagging (liquid) and cooling (solid). These stages might not occur in a linear line and can be overlapped on each other and hence, the recovered fragment may not be essentially characterized. Furthermore, post-burial

conditions like weathering and rupturing can further contaminate the representativeness of a fragment for understanding ancient metallurgical processes (Rademakers, & Rehren, 2014; Rehren & Thornton, 2009).

2.5 Early Bronze Age crucibles

At the beginning of extractive metallurgy, crucibles were preferred to extract metal from the ores. They continued to be used for various purposes even after the introduction of furnaces for metal smelting, such as to assess the purity of the ore, for refining gold and silver, or for the production of zinc and brass (Rehren, 2003). However, early copper smelting crucibles were very simple usually made of clay, which generally lacks the refractory properties and look like wide shallow vessels (Martinón-Torres & Rehren, 2014; Rehren, 2003). Later during the Chalcolithic and Early Bronze Age period, the form of crucibles had slightly changed. In these periods, the reduction of small amounts of copper rich ore was done in crucibles with almost no slag formation (Rehren, 2003). In these two periods, usually crucibles were heated from the top by using blow pipes and they had handles, knobs or pouring spouts allowing them to be more easily handled and poured. Early examples of this kind have been found in Feinan, Jordan (Hauptmann, 2007). However, due to the poor preservation of the crucibles there is no evidence of a pouring spout.

The functional role of the crucible during these periods was to keep the high temperatures and specific atmospheric conditions necessary to drive the smelting or melting processes (Bayley & Rehren, 2007; Rehren, 2003). For the successful metallurgical operation, achieving and containing high temperatures and simultaneously controlling the amount of gases such as oxygen or carbon monoxide were very much important. Therefore, in early bronze age, the specific shape of crucible allows to balance between the circulation of oxygen to keep the fuel to burn, and, at the same time, minimized the flow of air to ensure the reducing conditions required to transform ore into metal, or to prevent the metal from burning before it is being cast (Bayley & Rehren, 2007).

2.6 Some technical attributes related to Early Bronze Age crucibles

Crucibles and the processes carried out in them can be very diverse. To be workable and to be influential to the dynamic metallurgical processes, such as redox conditions, thermal fluctuation, presence of charge constituents, melting speed etc., the early bronze age crucible were often designed to achieve some physical and chemical properties (Adriaens, Yener &

Adams, 1999). However, these technical properties can be very much interconnected. The most important attributes related to crucible are:

Crucible fabrics: Crucible fabrics must be sufficiently refractories to resist the heat and to hold the weight of the metal both in their hot and cold state. In general, the refractories can be defined as substances that are not very much sensitive to chemical and thermal fluctuation, and much resistant than domestic ceramics (Craddock, 2013; Freestone, 1989; Martín-Torres, M. & Rehren, 2014). Usually iron, alkalis, and alkali earth elements can act as fluxes so, ceramic rich in silica and/or alumina and poor in iron could be ideal for crucible process. Moreover, crucibles need to be moderately inert, so that they can remain stable in contact with metal oxides (especially lead oxide) and alkalis produced from the fuel ash (Craddock, 2013; Rehren & Thornton, 2009).

From the very beginning of metallurgy until after the Late Bronze Age, crucibles were almost exclusively made of local clay used for domestic pottery and not truly refractories (Martín-Torres, & Rehren, 2014; Rehren & Thornton, 2009). Selection of specific clays for crucible fabrics is not evident in these periods, rather the required properties were achieved by adding different tempers. The main temper chosen for crucible fabrics throughout the Bronze Age was organic materials, such as straw or chaff. When these organic tempers burnt out, they left voids which allow to maximized heat transfer from the fuel to the metal by enabling direct contact between the two, while also providing a reducing environment to avoid excessive oxidation of the metal (Martín-Torres, & Rehren, 2014; Bayley & Thornton, 2007).

Crucible forms: Most Early Bronze Age crucibles were flat-bottomed vessels with shallow open forms (Bayley & Rehren, 2007). These particular forms of the crucibles were very much interrelated with the nature of refractoriness and the practice of heating of that period. As above mentioned, Early Bronze Age crucibles were made of less refractory clay, and hence, they were not truly thermal shock resistance. They were usually heated from above so that underside of the crucible could remain relatively cool. In these cases, the cooler outer zone provided the required strength even if the inside had been melted or fluxed (Bayley & Rehren, 2007; Rehren & Thornton, 2009)

From Roman times onwards, crucibles were refractory which allowed heating from bellow. Usually crucibles of these periods had rounded and pointed bases with a narrow opening near the top and usually tend to be relatively taller. These modified forms help to increase heat

transfer from below while reducing the loss of heat from the upper surface of the melt. Thus, crucible forms help to manipulate them in the fire (Bayley & Rehren, 2007; Martínón-Torres, M. & Rehren, 2014).

Thermal properties: All type of crucibles need to achieve some thermal properties, e.g., ability to remain integrated when temperature goes high, or withstand even temperature changes suddenly, and also ability to hold substantial charges, while manipulating them in a hot state (Bayley & Rehren, 2007). Early metalworkers very frequently tried to improve crucible form and fabric to achieve these certain types of thermal properties. They try to do so by optimizing wall thickness or vessel shape and by adding organic tempers with the clay (Bayley & Rehren, 2007). Early Bronze Age crucibles with wide opening and shallow deep help to raise temperature relatively easily while heated from above and their tempered fabric also acts as thermal insulation to increase retention time and hold its mechanical integrity while temperature goes high. Table 1 summarizes a crucible classification based on technical attributes or design features.

Table 1: Technical attributes of crucibles (after Bayley & Rehren, 2007)

small size shallow form ceramic not refractory thick walls heated from above Round/ pointed base	small size deep form ± lid refractory ceramic thin walls heated from below Round/ pointed base	larger size deep form refractory ceramic thin walls heated from below flat base
--	---	--

CHAPTER 3: ARCHAEOLOGICAL AND GEOLOGICAL SETTINGS

3.1 The site of Arslantepe

Arslantepe is an important archaeological site in Turkey. It is located in the Malatya plain of Eastern Anatolia, 6km north of the modern Malatya city and 15 km south of the west bank of the river Euphrates (Fig.3) (Piccione et al., 2015). The whole site is surrounded by mountains, which, in the past, were covered by forests (Sadori, Susanna, and Restelli, 2008). It is a 4 hectares and 30 m. high archaeological mound dominating the plain and shaped by the superimposed settlements, built for millennia in the same place (Frangipane, 2016) (Fig.4). Situated between the Caucasus on the one hand, and the great civilizations of Mesopotamia on the other, this site been engaged almost uninterrupted sequence of occupation spanning from the 5th millennium BC, until the Roman and Byzantine periods (Vignola et al, 2018, 2019).



Fig. 3: Location of Arslantepe in Eastern Anatolia (area location at top right) (from Vignola Masi et al, 2018)

3.2 A brief history of excavation at Arslantepe

French archaeologist Louis Delporte was the first scholar who discovered the site Arslantepe and conducted excavation from 1932 to 1983 (Frangipane, 2012). During this time period he successfully excavated the upper part of mound and exposed the extraordinary ruins of Iron age buildings, which include so called neo-Assyrian palace dated to 7th century BC and well-known Lions' Gate dated to 10-9th centuries BC (Frangipane, 2012). The gate was adorned by

two stone carved lions' statues which was very prominent and perhaps one of the reasons to named the site as Arslantepe, which means "Lion Hill" (Frangipane, 2012). Due to the second world war Delaporte stopped his mission and immediately after, from 1946 to 1951, another French scholar Claude F.A. Schaeffer continued the investigations (Frangipane, 2012).



Fig.4: The Arslantepe mound in the Malatya plain, eastern Turkey (from Frangipani, 2016)

After a short break, the French mission was substituted by an Italian one and in 1961, under the financial contribution of La Sapienza University of Rome, an Italian team headed by Professors P. Meriggi and S. Puglisi, started the excavation at Arslantepe. This mission is still ongoing and has advanced as one of the major archaeological projects of the university. The Hittitologist Meriggi only took part of the first few expeditions and later left the direction to Puglisi, a palaeoethnologist, who expanded and regularly conducted yearly investigations under regular permit from the Turkish government. During the 1970s, Alba Palmieri took over the supervision of the excavation and later it continues under the direction of Marcella Frangipane.

3.3 Stratigraphic sequence of Arslantepe

The many decades of extensive and stratigraphic excavations at the site Arslantepe have brought to light a continuous sequence of settlements from the 5th to the 1st millennium BCE (Vignola *et al*, 2017, 2018, 2019). The general sequence of the excavated levels is now divided into eight main periods (I–VIII, Table 2).

Table 2: Archaeological phases and their chronologies of Arslantepe (Vignola *et al.*, 2019)

Chronological sequence of Eastern Anatolia	Arslatepe Periods	Dates (C14 calibrated)	Contemporary Near Eastern civilizations
Late Roman and Byzantine	I		
Iron Age	II-III	1100-712 BCE	Neo-Hittite Kingdoms
Late Bronze Age II	IV	1600-1200 BCE	Hittite Empire
Late Bronze Age I	V B	1750-1600 BCE	Early Hittite
Middle Bronze Age	V A	2000-1750 BCE	Palaeo-Assyrian colonies
Early Bronze Age III	VI D	2500-2000 BCE	Early Dynastic III B, Akkad, Ur III
Early Bronze Age II	VI C	2750-2500 BCE	Early Dynastic II-III A
Early Bronze Age Ib	VI B2	3100-2900 BCE	Jemdet-Nasr, Early Dynastic I
Early Bronze Age Ia	VI B1	3200-3100 BCE	Jemdet-Nasr, Early Dynastic I
Late Chalcolithic 5	VI A	3400-3200 BCE	Late Uruk (Mesopotamia)
Late Chalcolithic 3-4	VII	3900-3400 BCE	Early and Middle Uruk
Late Chalcolithic 1-2	VIII	4700-3900 BCE	late Ubaid

The earliest documented period at this site is VIII (4700-3900 BCE), which match to the Late Chalcolithic 1-2. This period was characterized by small domestic units with kitchens, storages and living areas for each household and witnessed the emergence of a local *elite* and the organization of mass-produced pottery. Following two periods VII (3900-3400 BCE) and VIA (3400-3200 BCE) refers to the Late Chalcolithic 2-3 and 5 respectively and gradually shown the development towards the first state organization. In the Period VIA, a monumental Palatial complex is found which is a more than 4000 mq building with 3m walls in height. This was a place where a wide range of cultic, centralizing and redistributive activities took place (Frangipane, 2012, 2016). Archaeological evidence clearly shown that during this late 4th millennium BCE a very hierarchical and politically centralized society developed and Arslantepe became an important center of the upper Euphrates region and involved with an extensive network to the Near East (Frangipane, 2012, 2016).

The period VI B1 (3200-3100 BCE) was a short phase, which refers to the beginning of Early Bronze Age I. At the beginning of this period, Arslantepe witnessed a devastating fire, which destroyed the palace and ended the centralized system forever (Frangipane, 2016). This cultural period is characterized by a rather generalized change, which is particularly evident in its material culture (i.e., pottery production), testifying the collapse of the socioeconomic system and the increase in links with the pastoral communities from the Transcaucasia regions. Periods VI B2 (3100-2900 BCE), VI C (2750-2500 BCE) and VI D (2500-2000 BCE) corresponding to the Early Bronze Age Ib, II and III respectively, are characterized by sequences of villages

occupied by more or less sedentary people. As a proof of the alternating dominance of different communities in the plain, a farmers' village was built up on the mound in the VI B2 period. Besides, the presence of fortification walls in period VI D, deeply revealed the persistence of conflicts in the region (Frangipane, 2012). The Period VA (2000-1750 BCE) and VB (1750-1600 BCE) linked to the Middle Bronze Age and Late Bronze Age I and showed the gradual development (Vignola *et al.*, 2018).

Period IV (1600-1200 BCE) and period III-II (1100-712 BCE) corresponding to the Late Bronze Age II and Iron Age respectively. During these time span, Hittite state expansion very much influenced the settlement of Arslantepe and for the first time it becomes one of the provinces of the Hittite Empire and later (period III) capital of a Neo-Hittite kingdom until its destruction by Akkadian king Sargon II in 712 BCE. Later, this site was randomly occupied by small households in the Late Roman and Byzantine period. Last occupation of the mound is that of a Christian cemetery (Frangipane, 2012).

Thus, the archaeological sequence showed that during the long history of the settlement, Arslantepe went through a discursive transformation from village to monumental central place and back to small village, then large, fortified village and back to be a monumental central place in the Late Bronze Age in Neo-Hittite times. In the final phases the site once again becomes home to a small village of agriculturalists in the Roman and Byzantine periods (Frangipane, 2012).

3.4 Arslantepe in the Early Bronze Age I

The Early Bronze Age I began at Arslantepe with the sudden destruction of earlier VI A 'temple-palace complex' and the collapse of the centralized state system (Frangipane, 2012; Frangipane *et al.* 2016). At this site, periods VI B1 and VI B2 correspond to the Early Bronze Age I (respectively dated at 3200-3100 and 3100-2900 BCE). The VI B1 period was more seasonal and ephemeral, while VI B2 was fortified and more permanent. The first phase of the Early Bronze I (period VI B1) is characterized by small and simple private dwellings, constituted by wattle and daub huts and fences for herding. The simple village built upon the demolished ruins of the VIA crushed palace and most probably inhabitants by groups of Transcaucasia pastoralists who shared the customs and cultural features with the eastern Anatolian and Transcaucasia world (Frangipane, 2016). Red-Black, burnished pottery was dominant at this period and they were exclusively handmade. In terms of firing techniques and

aesthetic standards this type of pottery was very much resemble to the earlier Late Chalcolithic Red-Black Ware, but presence of new shapes indicates the inclusion of Transcaucasian culture. This short life (about one century) period ends with a widespread conflagration (Frangipane, 2012).

In the second phase of the Early Bronze I (period VI B2) there was a revival of mudbrick construction traditions and of wheel made light-colored pottery of local and Uruk inspiration. A series of living complexes along with narrow perpendicular streets marked the settlement of this period. Each house comprises single or double large rectangular rooms and each room contains a circular hearth and sometimes have rectangular or sub-rectangular fittings. From some of the fitting an abundant *in situ* carbonized botanic remains were found which suggest to interpreted them as *silos* or a type of ‘cupboard’ for keeping dry goods (Frangipane, 1993). Other features, such as small storage-rooms, sheds with preserved animal skeletons and courtyards with different plan, sometimes with semicircular ovens were also found in some of the best-preserved houses. The northern sector of the settlement also comprises some specialized activity areas, such as metalworking and animal butchery (Frangipane, Palmieri 1983; Bökönyi 1983). One of the important features of this period is a long and wide curvilinear mud brick wall which surrounded and protected the highest sector of the site (fig. 5) (Frangipane 2012, 2017). This fascinating feature indicating the conflict in socioeconomic system during the early phases of the Bronze Age and the presence of social élites as well. However, some archaeological records of this period clearly shown the reemergence of the Late Chalcolithic traditions; e.g. the reappearance of wheel-thrown, light-colored pottery in the Syrian-Mesopotamian fashion. (Piccione, 2010).

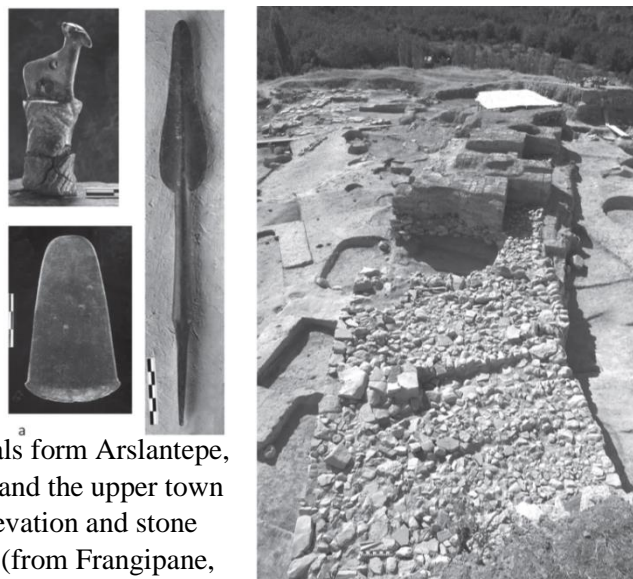


Fig. 5: Early Bronze Age I metals from Arslantepe, periods VIB1 and VIB2 (Left), and the upper town fortification wall (mud-brick elevation and stone foundations) from period VIB2 (from Frangipane, 2017:177,179)

3.5 Geological Setting of Arslantepe and Eastern Anatolia

3.5.1 Geological overview of Arslantepe and Eastern Anatolia

The site of Arslantepe is located in an eccentric position on the Malatya plain in the modern village of Orduzu on the western margin of the eastern Anatolian region, between the eastern part of the Taurus mountain chain and the Anti-Taurus (Manuelli, 2013:25). The Orduzu volcanics are located about 1 km east of the site and are part of the widespread Yamadağ volcanics in the Malatya region, which form the western part of the Neogene volcanism in eastern Anatolia. The Orduzu comprise rhyolite, rhyolitic dykes, trachyandesite basaltic trachyandesite dykes, and Quartz-micromonzonitic dykes. The Yamadağ volcanics constitutes a vast volcanic sequence which mainly comprises rhyolitic lava, andesitic lava and pyroclastic intercalations, and basaltic/andesitic to andesitic/dacitic lava flows (Yalçın *et al.* 1998; Kürüm *et al.* 2004).

However, the whole Anatolia landscape is very complicated. It is a varied mountainous and steppe landscape and rich in metal-bearing mineral concentrations. As part of a larger metallogenic belt within the Alpine-Himalayan orogenic system, Anatolia has extensive polymetallic deposits of copper, iron, lead, silver and zinc, in addition to rarer deposits of antimony, arsenic, nickel, gold and tin. The three largest massive sulfide ore bodies include the metallogenic zones of Ergani in the eastern Taurus and Küre and Murgul/Göktas along the central and eastern Pontide belt (Lehner, Joseph & Yener, 2013). The geological history of the Anatolian landmass resulted in mineralizations of different ages, which is a decisive factor in the success of extensive lead isotope research conducted in Anatolia (Lehner, Joseph & Yener, 2013).

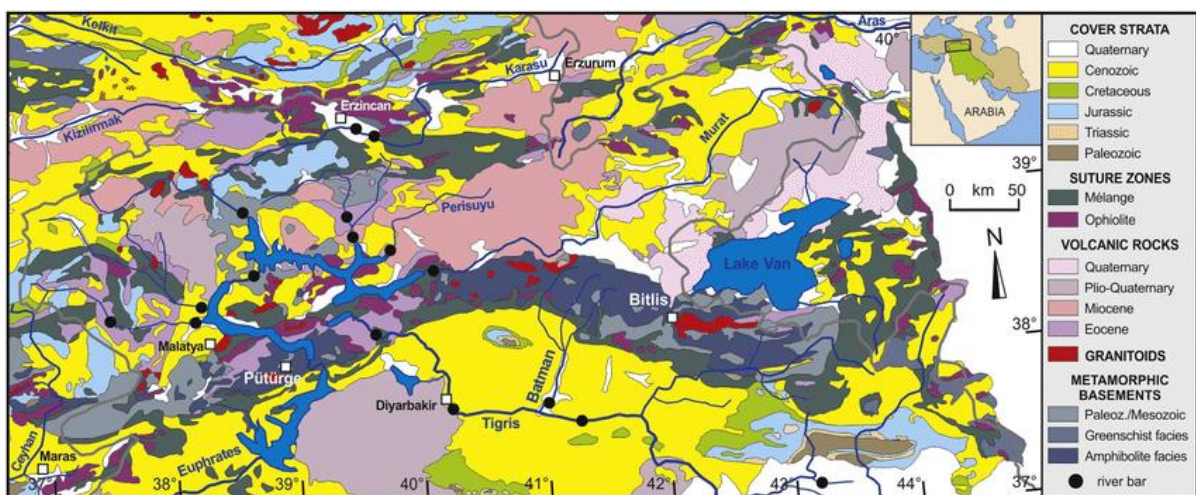


Fig. 6: A general geological map of Eastern Anatolia (from Garzanti, *et al.*, 2016:109)

3.5.2 Ancient ore deposits in Eastern Anatolia

The geographic distribution of ore bodies are follows of the Pontide and Tauride orogenic belts in northern and southern Turkey. Polymetallic copper and lead-zinc-silver ores are particularly abundant in the eastern sectors of these regions. Arsenic and antimony rich ores of the fahlerz-type are evident in both Pontide and Tauride sources and from fourth-millennium BC archaeological deposits at Norsuntepe and Arslantepe along the Upper Euphrates. A major copper-nickel sulfide deposit near modern Bitlis in eastern Turkey has also been reported (Lehner, Joseph & Yener, 2013).

Despite a relative abundance of ore sources, their spotty distribution created special stresses that influenced how they were extracted, refined, smelted, and transported (Craddock 1995). In other words, geographic and social parameters of mining regions had significant influence on technological organization and socioeconomic process (Knapp 1998). Distance from the raw materials to fuel and food supplies, as well as seasonal weather conditions, were key factors in how they were utilized. The dynamic and costly ventures of mining and smelting activities often had considerable impact on the environment, leading to deforestation, alterations of drainage routes, and other problems. Transportation is often limited to navigable rivers and wide intermontane valleys, and even then, it was largely a seasonal enterprise. movement of goods across central Anatolia was often abruptly postponed due to poor weather, and this likely had significant effects on trade relations and the exchange rates of metal types (Dercksen 1996).

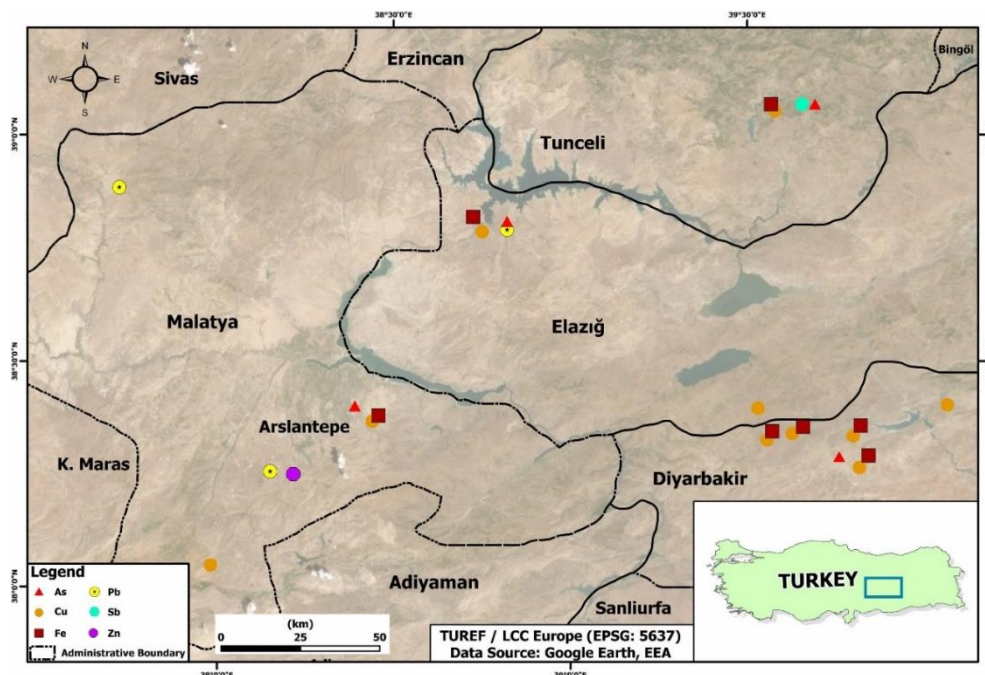


Fig. 7: Known major ore sources in Eastern Anatolian region (modified after Frangipane & Palmieri, 1994- 1995:67)

CHAPTER 4: MATERIALS AND METHODS

4.1 Materials

In total 15 slag samples and 2 crucible fragments were selected and subjected to different archaeometric analyses: EDXRF analysis, Powder XRD analysis and SEM-EDX analysis. The diameter of the slag samples varies between 2 and 6 cm and a depth of 1 to 3 cm. The outer side often has spots that are red oxidized. The interior side is often irregular with bulbs and backed clay attached sometimes with a 0.1 cm thickness. The bulbs often have green spots. In section the grain is fine, grey or black and has a low porosity. The slags are magnetic.

Both crucible fragments are small body fragments and hence, allow no reliable reconstruction of their original shape. Inner side they are heavily vitrified, while the core is less vitrified, and the exterior is only slightly baked. There is slag on their interiors and a green staining indicative of copper corrosion products. Thickness of both fragments varies from 1 to 2 cm. The outer surfaces are rich in traces of organic temper

4.1.1 Stratigraphic context

Stratigraphically all analyzed slag samples and crucible fragments belong to Arslantepe period VI B2, chronologically which is correspondent to Early Bronze Ib (3100-2900 BC). During the 1998 excavation session, these slag samples were recovered from the archaeological context A929, which is mainly a street (Fig. 8). In this period, fragments of crucibles and various kilograms of slags were also concentrated in and around buildings described as workshops, together with ore fragments and stone grinding tools, but apart from some burnt hollows there was no indication of furnaces, and no tuyeres were found (Palmieri, *et al*, 1999).

All samples were photographed for record purposes by using Canon EOS 2000D (Fig 9a, 9b, and 10a). Besides, some 3D images of crucible fragments were also created using Nikon D3100 and Agisoft profession software (fig.10b).

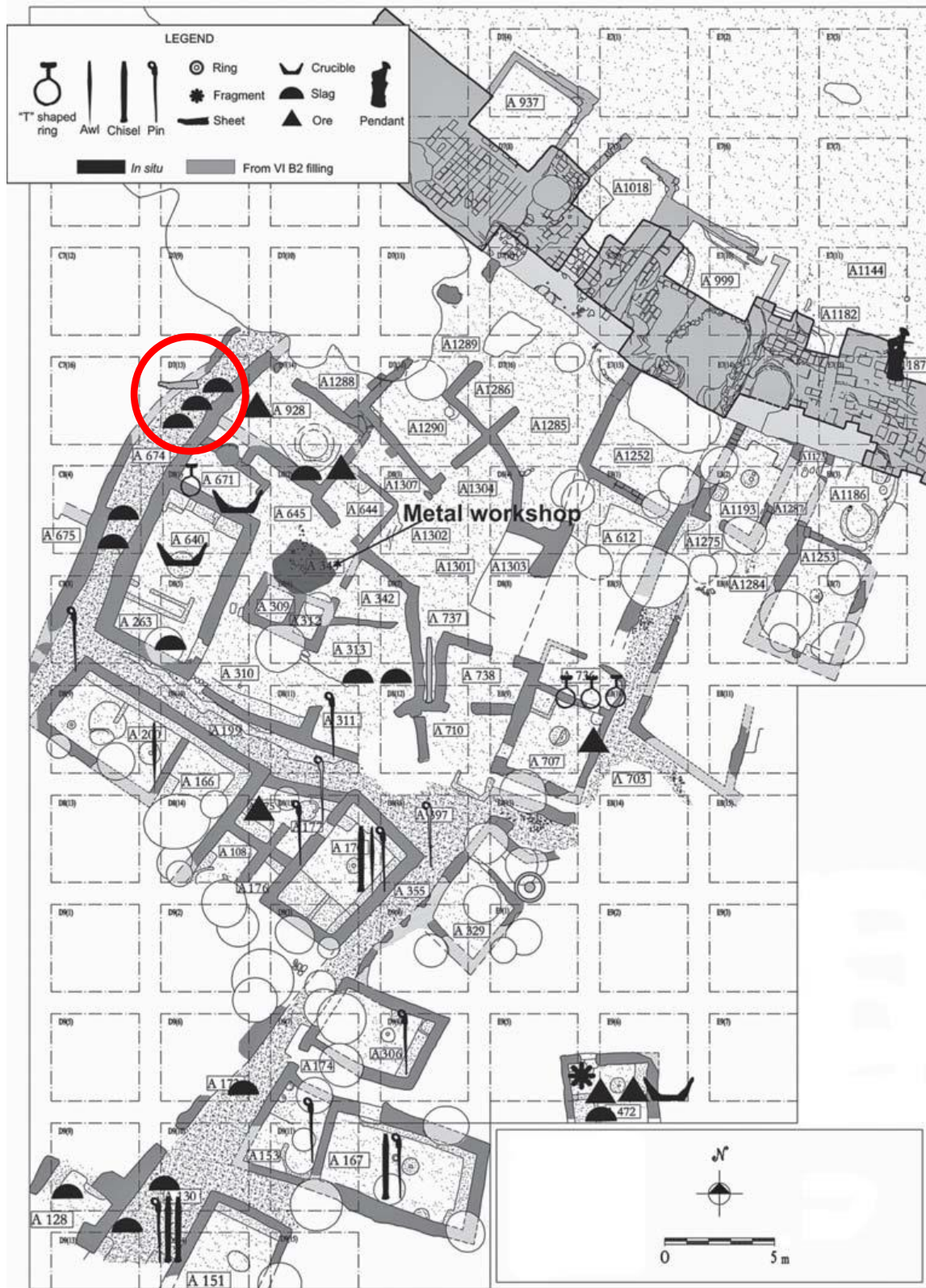


Fig. 8: Topographic plan of the settlement of Arslantepe-VI B2 (Early Bronze Age I) showing the distribution of metal objects, crucibles, slag and ores. The finding location of present analyzed slag samples marked in a red circle. (taken from *Di Nocera*, 2013:126)

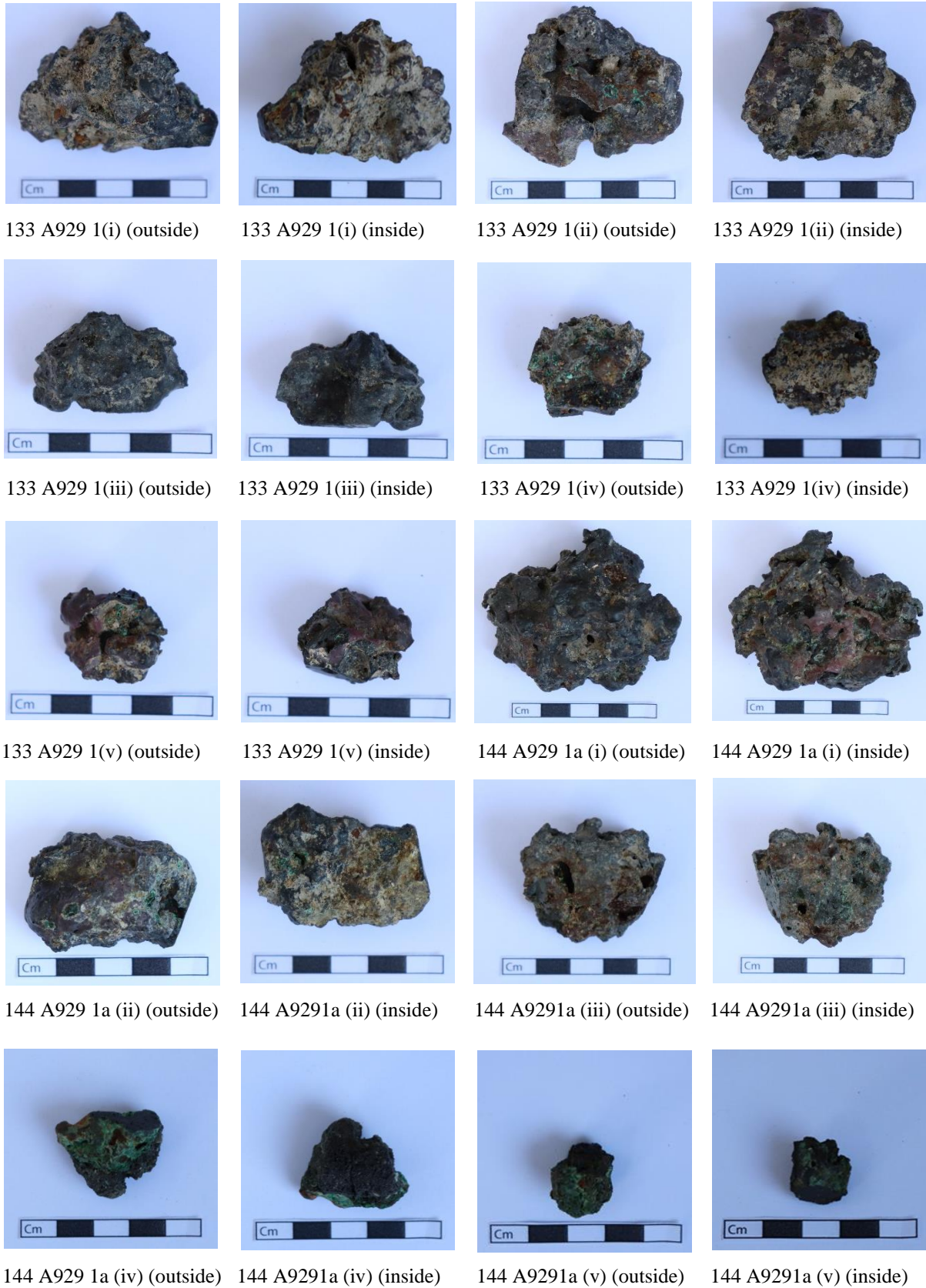


Fig. 9a: Photographic images of analyzed slag samples

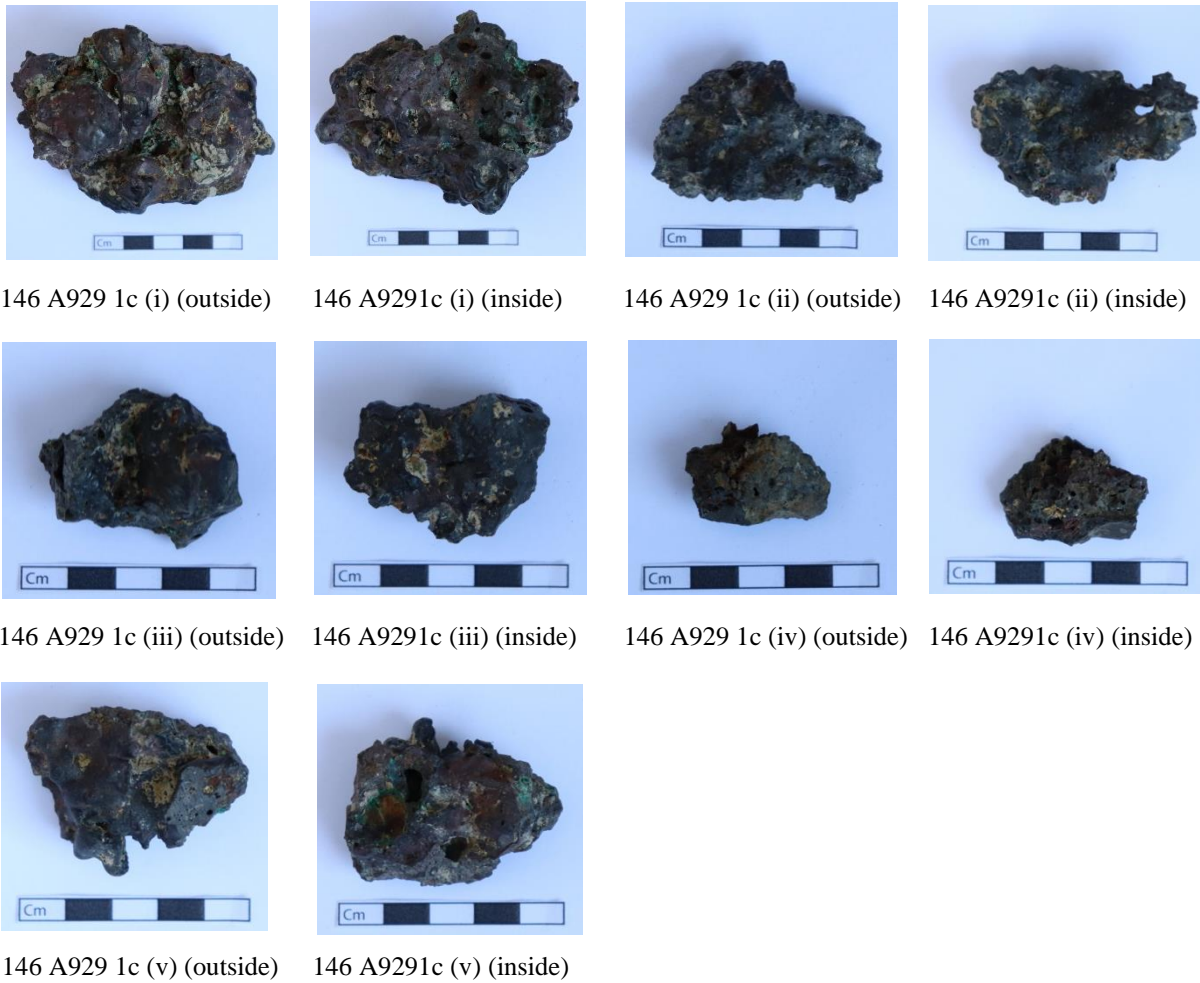


Fig. 9b: Photographic images of analyzed slag samples

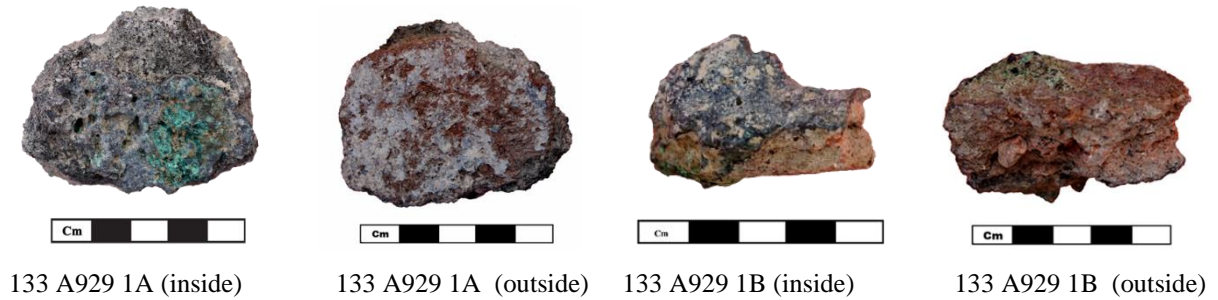


Fig. 10a: Photographic images of analyzed crucible fragments

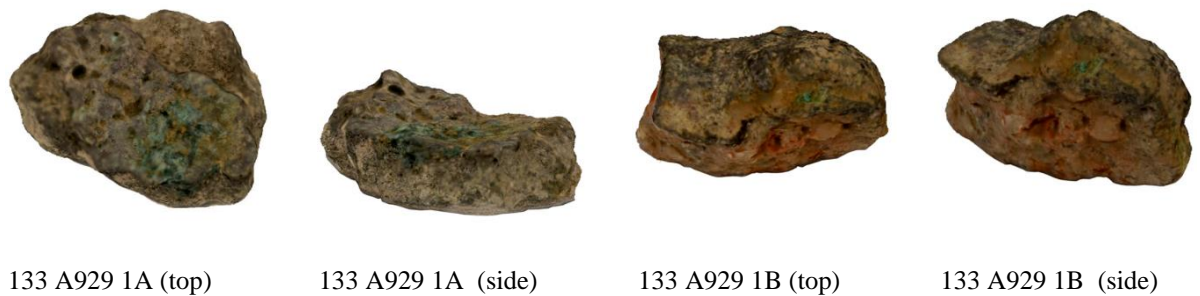


Fig. 10b: 3D images of analyzed crucible fragments

4.2 X-ray fluorescence (XRF) spectroscopy for chemical characterization

4.2.1 Working principle

The study of slag is a complicated and specialized issue which necessarily demands much sophisticated and sensitive analytical techniques. For the elemental analysis of this kind of material, X-ray fluorescence (XRF) is probably one of the earliest and most widely used archaeometric techniques.

XRF principle is based on the emission of secondary or characteristic (photons) from a material that was bombarded by a high energy X-rays (primary radiation). When a sample is excited with a primary X-radiation, the electrons from inner electron shells are knocked and, in the process, electrons from outer electron shells fill the resultant voids emitting fluorescence radiation that is characteristics in its energy distribution for a particular material. This fluorescence radiation is evaluated by a detector. The generation of the X-ray fluorescence radiation is shown simplified in fig.11. Since, fluorescence X-rays possess energies that are characteristic of each type of element, by using Moseley's law it is possible to obtain qualitative information on the elemental composition of the sample. Moreover, by using the intensity of the fluorescence radiation (number of photons) at each characteristics X-ray energy it is possible to perform a quantitative analysis (Pollard *et al.*, 2007, Shackley, 2011).

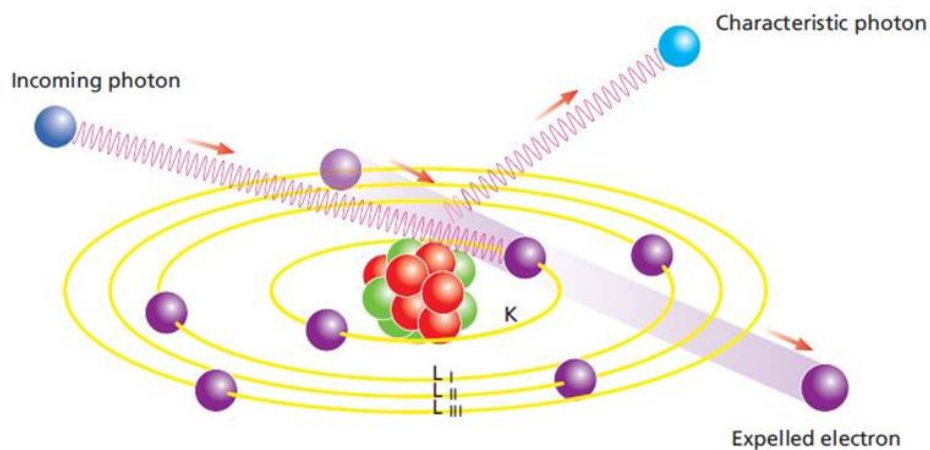


Fig. 11: Production of characteristic radiation (after Brouwer, 2011:18)

There are two types of XRF spectrometers, one is the energy dispersive (EDXRF), the other is the wavelength dispersive (WDXRF). In present research, EDXRF is used for the elemental analysis of slag samples. However, there are some disadvantage of EDXRF for slag analysis. The main disadvantage of the method is the surface nature of the analysis, as the X-ray beam cannot penetrate the sample more than some tens of micrometers (Carter, 1978, Pollard *et al.*,

2007). Consequently, the results of the analysis are not very quantitatively reliable, especially in the presence of surface enrichment or depletion phenomena (ion migration processes, patina and so on), which are very common in archaeological slags. For that reason, the slag sample must be cut in order to analyze their core. Moreover, the XRF results need to be correlated with results obtained with other techniques, like SEM-EDS which is more powerful in this particular field of application.

4.2.2 Analytical parameters

The EDXRF analysis of 15 slag samples and 2 crucible fragments was performed under the supervision of Professor Anna Candida Felici at the LANDA laboratory, Department of Basic and Applied Sciences for Engineering, Sapienza University of Rome. The equipment used for the characterization is an X-ray fluorescence spectrometer that consists of an X-ray generator (Amptek MiniX) with an anode target of rhodium and a beryllium window of 127 μm of thickness. The detector is a Peltier cooled silicon drift with integrated amplifier and multi-channel analyzer (Amptek 123-SDD). The detector has a surface of 25 mm^2 , a thickness of 450 μm , a beryllium window of 12.5 μm of thickness and its energy resolution is 140 eV, full width half maximum at 5.9 keV. The incident and the revealed beams form an angle of 45° with respect to the surface of the sample. The analysed surface is distant 3 cm from the X-ray generator anode and 3.5 cm from the detector surface. The X-ray generator was equipped with a 2 mm diameter collimator and was powered with an accelerating potential difference of 38 kV and an electronic current of 100 μA . The acquisition time was 200 s. Before the analysis a small part was cut from each slag sample using a wet steel bench saw to obtain flat profile sections. For each slag samples, three different points have been selected to collect the EDXRF results. Crucible fragments were analyzed without any sample preparation.

4.3. X-Ray Diffraction (XRD) for mineralogical identification

4.3.1. Working principle

X-Ray Diffraction (XRD) is one of the reliable archaeometry techniques for identifying the mineral phases present within the slag sample. This data will supplement the XRF-analyses that only provide the semi-quantitative amount of the individual chemical elements present, but no information on the minerals. X-ray diffraction is based on constructive interference of monochromatic X-rays interacting with a crystalline sample. These X-rays are generated by a cathode ray tube, filtered to produce monochromatic radiation, collimated to concentrate, and

directed toward the sample. The interaction of the incident rays with the sample produces constructive interference (and a diffracted ray) when conditions satisfy Bragg's Law;

$$2d \sin \theta = n \lambda,$$

where d is the distance between the planes, θ is the angle between the plane and the incident rays, n is a whole number and λ is the wavelength of the X-ray (Fig.12) (Pollard et al, 2008)

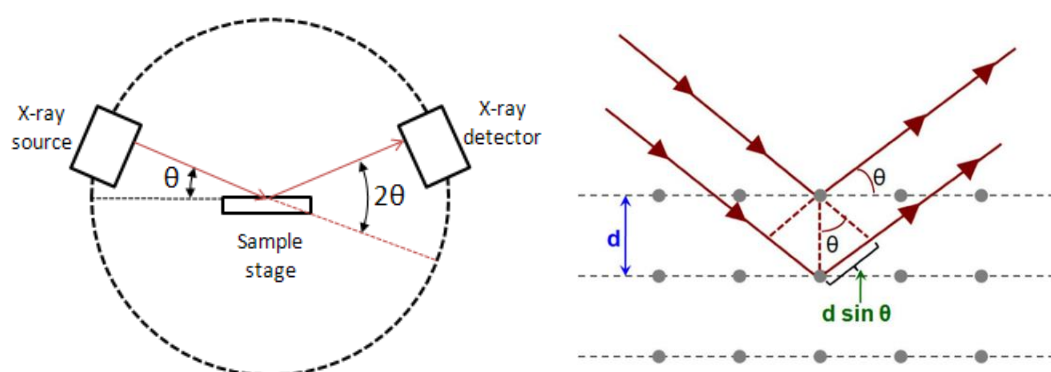


Fig. 12. Schematic diagram of XRD (left) and Bragg's law (right) (retrieved from <http://reference.iucr.org/dictionary>)

The Bragg's law relates the wavelength of electromagnetic radiation to the diffraction angle and the lattice spacing in a crystalline sample. These diffracted X-rays are then detected, processed and counted. In most modern diffractometers the detector rotates slowly around the sample, with the $\theta - 2\theta$ relationship maintained. This allows the angle of diffraction to be known and the detector records the intensity of the diffracted X-rays. The combination of these two pieces of information allows calculation of the d -spacings and, since each mineral has a set of unique d -spacings, this allows the identification of the minerals present in the sample. Typically, this is achieved by comparison of d -spacings with standard reference patterns.

In XRD two main methods can be distinguish: micro X-ray diffraction and powder X-ray diffraction. Micro X-ray diffraction (μ XRD) allows the examination of very small areas of a sample, focusing the incident beam on a certain spot (several micrometers) on a sample surface, providing the knowledge of crystalline structure of material. On the other hand, powder X-ray diffraction method is ideally suited for characterization and identification of polycrystalline phases and it is the most effective method for identifying minerals in a slag sample. Crushing the sample to powder ensures (except in the case of platy crystals like micas) a random

alignment of crystal lattices and these guarantees that all peaks for a given mineral will be present in the spectrum. This makes identification of crystalline compounds more certain than when only some of the peaks are represented, as it happens with single crystals. On the other hand, there are some disadvantages of using powder diffraction method, such as the fact that this technique requires a few grams of powder, which may be too much for small archaeological samples and that it cannot identify minerals that are poorly crystallized (cryptocrystalline) ((Pollard et al, 2008). However, in the present study to identify the mineralogical phases the powder X-ray diffraction method has been applied.

3.2 Analytical parameters

Powder X-ray diffraction analysis was done under the guidance of Professor Jose Mirao and Professor Nick Schiavon at Hercules Laboratory, University of Evora, Portugal. To identify the crystalline phases of copper slags, powder X-ray diffraction was performed on selected 9 slag samples and for this previously cutted small part of each slag samples was grounded with an agate mortar. The XRD patterns were recorded with a Bruker D8 Discover diffractometer (Bruker AXS GmbH, Karlsruhe, Germany) using Cu K α radiation, operating at a 2 θ angular range of 3-75 $^{\circ}$, step size of 0.05 $^{\circ}$ and a step time of 2 s and with a LYNXEYE linear detector, acting as 192 individual detectors. The identification of crystalline phases was performed using the DIFFRAC.EVA software (EVA, Bruker AXS GmbH, Karlsruhe, Germany) and the ICDD PDF-2 database (ICDD, Newtown Square, PA, USA).

4.4 Scanning electron microscope with EDS for microstructure Study

4.4.1 Working principle

Scanning electron microscope coupled with energy dispersive X-ray spectrometer (SEM-EDS) is one of the most effective archaeometry technique to investigate the microstructure and the chemical elemental composition of a slag sample. The principle of this technique is based on the interaction between an electron beam and the surface of a sample. A very narrow beam of electrons is generated by heating a wire filament (as in a light bulb) to a high temperature under a strong electrical potential. This beam passes throughout a cylindrical *column*, around which there is a series of electromagnetic *lenses*, which allow the beam to be focused and moved. At the base of the column, the electrons hit the sample and generate a number of different types of secondary signal (Fig. 13). These signals can be converted electronically to provide an image of the sample.

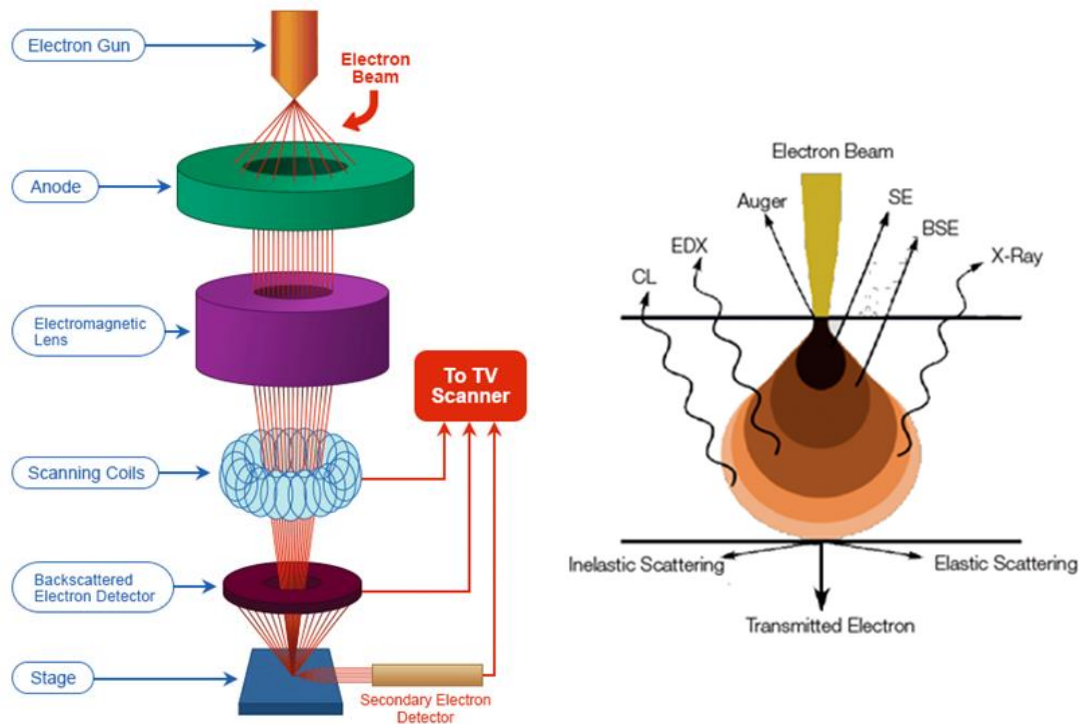


Fig. 13: Schematic diagram of a scanning electron microscope (left) and electron-matter interaction (right) (retrieved from <https://www.nanoimages.com/sem-technology-overview/>)

The secondary products that are most commonly used for creating images are secondary electrons (SE) and backscattered electrons (BSE). Secondary electrons are emitted by the atoms in the sample as a result of the inelastic scattering of the primary electrons. Their energy is low (less than 50 eV). The contrast of the image created with secondary electrons depends on the morphology of the sample. Backscattered electrons are the electrons of the primary beams that in the interactions with the sample have been elastically scattered. They come from regions deeper than the ones in which are originates the secondary electrons. They have a high energy (>50 KV). The contrast of BSE images depends on the chemical composition of the sample.

The most important feature of SEM is the three-dimensional appearance of its images because of its large depth of field. SEM is capable of magnifying objects in the order of 100,000 times and thus produces detailed three-dimensional images (Watt, 2007). Furthermore, a SEM coupled with an energy dispersive X-ray spectrometer (EDS) is capable to provide information on the elemental composition of the sample (Pollard *et al*, 2008). When the surface of the sample is irradiated with a high-energy electron beam, as it is in SEM, characteristic X-rays are emitted. These photons are collected by the EDS photon detector (usually Si (Li) diode), separated according to their energies and counted (Freestone, 1985).

The advantages of SEM-EDS include the high spatial resolution and the ability to analyse small sample areas. On the other hand, SEM-EDS have a poor sensitivity for trace elements and for elements with an atomic number lower than 11 (Na). The detection limits of SEM-EDS are approximately 0.1 wt.%, depending on the atomic number and the matrix composition (Watt, 1997).

4.4.2 Analytical parameters

SEM-EDS analysis was achieved with the help of Sara Valadas and Ana Cardoso at Hercules Laboratory, University of Evora, Portugal. For this analysis 5 slag samples were selected to check the chemical compositions of particular phases (point microanalysis). All analyses were done using a Scanning Electron Microscope (Phenom-World). The EDS was set up at an accelerating voltage of 15kV, using a Backscattered electrons detector. For the analysis a small cutting part of each sample was used, and minimum three or more different points have been selected to collect the SEM-EDS results. In Table 3, the type of analysis undertaken for each sample is shown.

Table 3: Summary of the analytical methods used for the samples' characterization.

Sample Number	Types	EDXRF	Powder XRD	SEM-EDS
133 A929 1(i)	Slag	x	x	x
133 A929 1(ii)	Slag	x	x	
133 A929 1(iii)	Slag	x	x	
133 A929 1(iv)	Slag	x	x	x
133 A929 1(v)	Slag	x	x	
144 A929 1a(i)	Slag	x	x	
144 A929 1a(ii)	Slag	x	x	
144 A929 1a(iii)	Slag	x		x
144 A929 1a(iv)	Slag	x		x
144 A929 1a(v)	Slag	x		
146 A929 1c(i)	Slag	x	x	x
146 A929 1c(ii)	Slag	x		
146 A929 1c(iii)	Slag	x		
146 A929 1c(iv)	Slag	x	x	
146 A929 1c(v)	Slag	x		
133 A929 1A	Fragment of Crucible	x		
133 A929 1B	Fragment of Crucible	x		
Total		17	9	5

CHAPTER 5: RESULTS

5.1 EDXRF analysis: Chemical composition

EDXRF analysis ascertain the presence of 20 elements in the analyzed 15 slag samples: iron (Fe), silicon (Si), aluminum (Al), copper (Cu), calcium (Ca), sulphur (S), potassium (K), titanium (Ti), vanadium (V), chromium (Cr), manganese (Mn), zinc (Zn), molybdenum (Mo), strontium (Sr), phosphorus (P), nickel (Ni), arsenic (As), tin (Sn), antimony (Sb), lead (Pb). However, the compositional analysis confirms the presence of iron, silicon and aluminum as the significant elements with the modest level of copper and calcium (Fig.14, 15).

Other elements e.g., potassium, titanium, vanadium, chromium, manganese, zinc, molybdenum and strontium are present with the lower level of concentrations. Phosphorus is present in only two sample (133 A929 1(ii) and 133 A929 1(iv)), while nickel, arsenic, tin, antimony and lead are presents in a few samples with very low concentrations. The presence of low concentration of sulphur in each sample is very significant (Fig.16). Therefore, the chemical compositions of the slag confirm the ferrous nature of the slag.

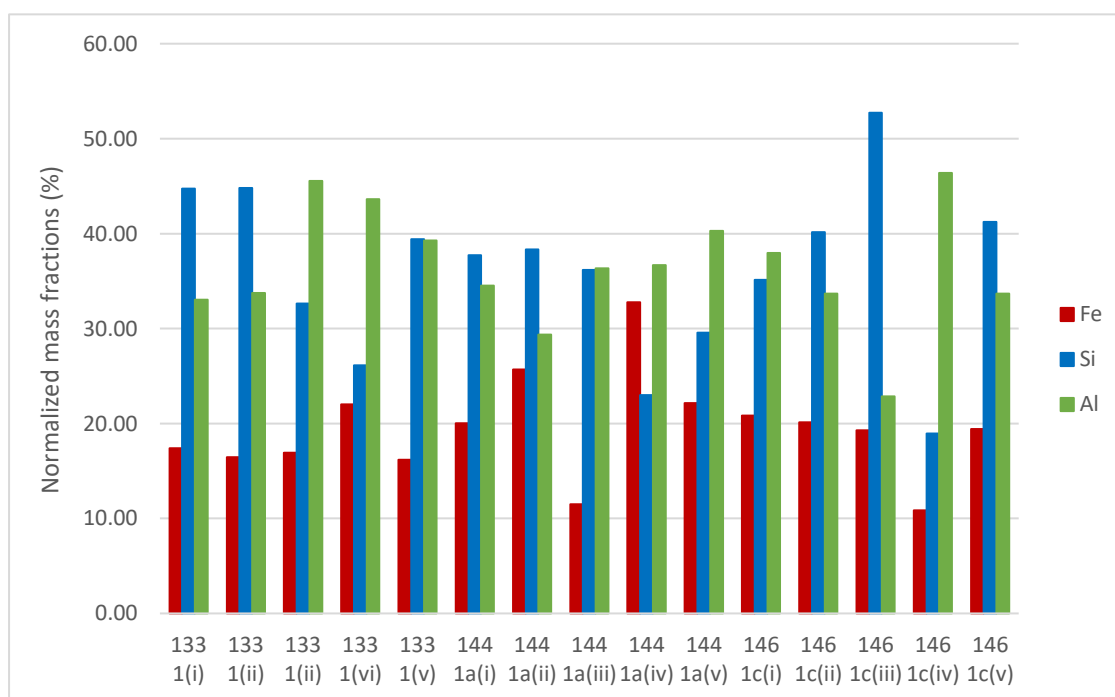


Fig. 14: The EDXRF results for iron, silicon and aluminum contents in analyzed slag samples, results are presented as normalized mass fractions (%).

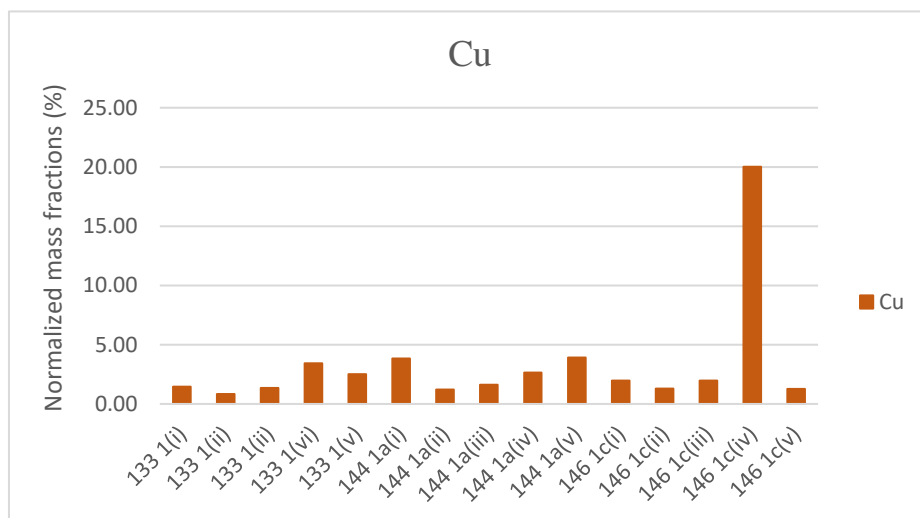


Fig. 15: The EDXRF results for copper content in analyzed slag samples, results are presented as normalized mass fractions (%).

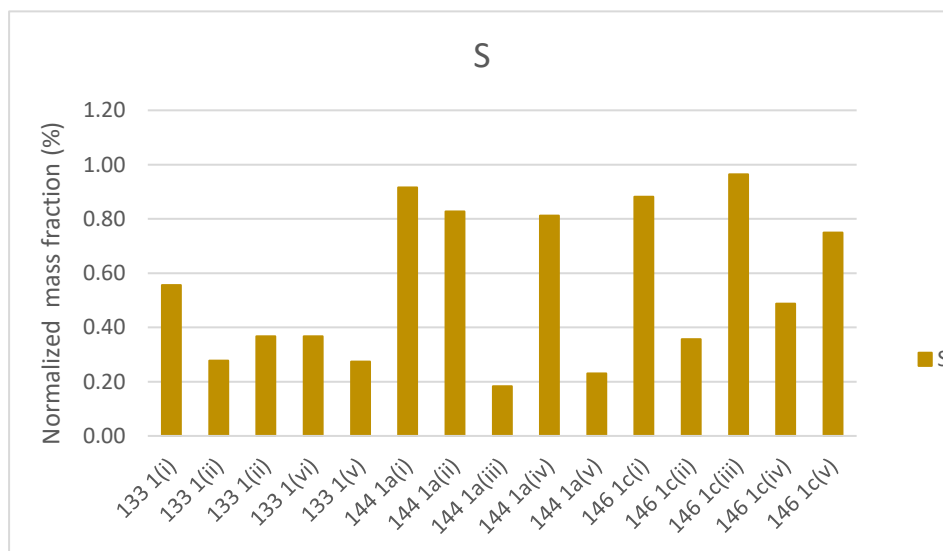


Fig. 16: The EDXRF results for sulphur content in analyzed slag samples, results are presented as normalized mass fractions (%).

In Table 4, EDXRF elemental analysis of 15 slags samples are reported. Here the results are presented as averages values of normalized mass fractions (%). The values of the mass fractions obtained analyzing the spectra with the PyMca software were normalized to 100% (normalized mass fractions). In the table, the dispersion values of normalized mass fractions of each element are also added. These values were calculated as one half of the difference between the maximum and the minimum values of normalized mass fractions of each element, obtained from three-point analyses of each sample. However, it should be mention that the results are obtained from a semiquantitative analysis. Besides, due to the limits of EDXRF spectroscopy, some elements present in the sample, such as oxygen and magnesium are not detected. For the

reasons, normalized mass fractions cannot be truly representative of the real concentrations. In any case, they could be used for a rough comparison between the samples. Moreover, analyses were done on small cutted part of each slag samples, not on the core and due to the degradation of slags in the buried soil, the external part of the slags was completely changed. Hence, EDXRF results may not completely represent the composition of the slags itself, but also that of the degradation products present in the slags.

Table 4: EDXRF elemental analysis of 15 slags samples. Results are presented as averages values of normalized mass fractions (%) with dispersion values.

Sample ID	Al	Si	P	S	K	Ca	Ti	V	Cr	Mn	Fe	Ni	Cu	Zn	As	Sr	Mo	Sn	Sb	Pb
133 A929 1(i)	33.02	44.74	0.00	0.56	0.15	2.34	0.05	0.02	0.06	0.08	17.41	0.00	1.46	0.03	0.01	0.01	0.02	0.01	0.00	0.05
	± 10.08	± 13.17	± 0.00	± 0.64	± 0.06	± 1.35	± 0.02	± 0.01	± 0.03	± 0.03	± 5.22	± 0.00	± 1.08	± 0.01	± 0.01	± 0.01	± 0.01	± 0.02	± 0.00	± 0.05
133 A929 1(ii)	33.75	44.80	0.36	0.28	0.30	2.84	0.05	0.02	0.05	0.08	16.46	0.01	0.85	0.02	0.00	0.01	0.02	0.01	0.00	0.10
	± 26.37	± 23.25	± 0.54	± 0.04	± 0.26	± 0.97	± 0.02	± 0.02	± 0.02	± 0.04	± 5.93	± 0.01	± 0.38	± 0.00	± 0.00	± 0.00	± 0.00	± 0.02	± 0.00	± 0.05
133 A929 1(iii)	45.54	32.62	0.00	0.37	0.19	2.67	0.04	0.02	0.04	0.07	16.94	0.01	1.35	0.03	0.01	0.01	0.02	0.02	0.00	0.09
	± 14.84	± 7.09	± 0.00	± 0.04	± 0.13	± 1.30	± 0.02	± 0.01	± 0.03	± 0.03	± 8.44	± 0.01	± 0.44	± 0.01	± 0.01	± 0.00	± 0.01	± 0.03	± 0.00	± 0.12
133 A929 1(vi)	43.62	26.11	0.38	0.37	0.37	3.27	0.06	0.05	0.06	0.08	22.02	0.00	3.44	0.04	0.02	0.01	0.02	0.10	0.03	0.07
	± 2.93	± 2.61	± 0.75	± 0.19	± 0.25	± 1.75	± 0.02	± 0.05	± 0.01	± 0.01	± 2.55	± 0.00	± 2.17	± 0.04	± 0.05	± 0.01	± 0.02	± 0.11	± 0.06	± 0.08
133 A929 1(v)	39.29	39.43	0.00	0.27	0.17	1.78	0.04	0.01	0.04	0.08	16.17	0.01	2.52	0.06	0.01	0.02	0.04	0.00	0.00	0.04
	± 18.12	± 20.99	± 0.00	± 0.19	± 0.20	± 1.25	± 0.02	± 0.01	± 0.01	± 0.02	± 1.28	± 0.01	± 2.85	± 0.06	± 0.02	± 0.03	± 0.04	± 0.00	± 0.00	± 0.04
144 A929 1a(i)	34.51	37.73	0.00	0.92	0.15	2.37	0.06	0.01	0.12	0.10	20.02	0.00	3.84	0.07	0.01	0.01	0.03	0.05	0.00	0.06
	± 4.85	± 4.72	± 0.00	± 0.55	± 0.01	± 0.40	± 0.02	± 0.01	± 0.09	± 0.02	± 4.45	± 0.00	± 2.30	± 0.04	± 0.01	± 0.01	± 0.01	± 0.08	± 0.00	± 0.02

144 A929 1a(ii)	29.37 ± 3.25	38.32 ± 3.94	0.00 ± 0.00	0.83 ± 0.40	0.25 ± 0.13	3.86 ± 0.06	0.06 ± 0.00	0.05 ± 0.00	0.08 ± 0.01	0.13 ± 0.00	25.69 ± 0.26	0.00 ± 0.00	1.22 ± 0.54	0.05 ± 0.01	0.00 ± 0.00	0.02 ± 0.00	0.03 ± 0.00	0.00 ± 0.00	0.00 ± 0.00	0.03 ± 0.00
144 A929 1a(iii)	36.33 ± 6.44	36.16 ± 4.15	0.00 ± 0.00	0.18 ± 0.11	0.51 ± 0.14	13.28 ± 0.98	0.08 ± 0.01	0.02 ± 0.01	0.05 ± 0.01	0.07 ± 0.02	11.50 ± 1.49	0.01 ± 0.01	1.61 ± 1.10	0.04 ± 0.01	0.01 ± 0.02	0.09 ± 0.02	0.02 ± 0.00	0.00 ± 0.00	0.00 ± 0.00	0.03 ± 0.03
144 A929 1a(iv)	36.69 ± 4.68	22.99 ± 2.91	0.00 ± 0.00	0.81 ± 0.45	0.13 ± 0.02	3.61 ± 0.45	0.03 ± 0.00	0.03 ± 0.01	0.10 ± 0.02	0.13 ± 0.02	32.76 ± 0.78	0.00 ± 0.00	2.64 ± 0.77	0.02 ± 0.01	0.00 ± 0.00	0.00 ± 0.00	0.02 ± 0.00	0.00 ± 0.00	0.00 ± 0.00	0.04 ± 0.01
144 A929 1a(v)	40.27 ± 0.23	29.55 ± 6.76	0.00 ± 0.00	0.23 ± 0.11	0.23 ± 0.04	3.19 ± 1.33	0.10 ± 0.02	0.03 ± 0.01	0.07 ± 0.01	0.12 ± 0.04	22.15 ± 5.98	0.03 ± 0.01	3.91 ± 0.61	0.03 ± 0.01	0.00 ± 0.00	0.01 ± 0.01	0.02 ± 0.00	0.00 ± 0.00	0.00 ± 0.00	0.07 ± 0.02
146 A929 1c(i)	37.97 ± 13.42	35.12 ± 9.42	0.00 ± 0.00	0.88 ± 0.68	0.11 ± 0.02	2.70 ± 0.31	0.05 ± 0.01	0.02 ± 0.00	0.14 ± 0.13	0.09 ± 0.01	20.83 ± 1.37	0.00 ± 0.00	1.98 ± 1.82	0.03 ± 0.01	0.01 ± 0.01	0.01 ± 0.00	0.02 ± 0.01	0.00 ± 0.00	0.00 ± 0.00	0.03 ± 0.04
146 A929 1c(ii)	33.67 ± 2.59	40.15 ± 3.37	0.00 ± 0.00	0.36 ± 0.04	0.16 ± 0.07	3.89 ± 0.23	0.05 ± 0.00	0.03 ± 0.01	0.05 ± 0.01	0.10 ± 0.01	20.11 ± 2.48	0.00 ± 0.01	1.29 ± 0.66	0.04 ± 0.01	0.00 ± 0.00	0.02 ± 0.00	0.03 ± 0.00	0.11 ± 0.08	0.00 ± ±0.00	0.05 ± 0.02
146 A929 1c(iii)	22.87 ± 18.56	52.71 ± 15.57	0.00 ± 0.00	0.96 ± 0.35	0.09 ± 0.09	1.72 ± 1.23	0.05 ± 0.04	0.02 ± 0.01	0.06 ± 0.03	0.09 ± 0.04	19.28 ± 7.90	0.01 ± 0.01	1.97 ± 0.60	0.06 ± 0.05	0.01 ± 0.01	0.01 ± 0.01	0.03 ± 0.01	0.07 ± 0.13	0.00 ± 0.00	0.05 ± 0.07
146 A929 1c(iv)	46.39 ± 6.98	18.96 ± 4.31	0.00 ± 0.00	0.49 ± 0.15	0.24 ± 0.07	2.70 ± 0.14	0.05 ± 0.01	0.01 ± 0.01	0.04 ± 0.01	0.07 ± 0.01	10.85 ± 3.00	0.04 ± 0.01	20.01 ± 4.34	0.08 ± 0.03	0.00 ± 0.00	0.00 ± 0.00	0.01 ± 0.00	0.05 ± 0.01	0.01 ± 0.02	0.06 ± 0.01
146 A929 1c(v)	33.69 ± 3.99	41.24 ± 9.05	0.00 ± 0.00	0.75 ± 0.17	0.13 ± 0.06	3.13 ± 0.93	0.04 ± 0.01	0.03 ± 0.02	0.06 ± 0.04	0.09 ± 0.03	19.41 ± 5.63	0.01 ± 0.01	1.27 ± 0.49	0.09 ± 0.02	0.01 ± 0.01	0.01 ± 0.00	0.02 ± 0.00	0.01 ± 0.02	0.00 ± 0.00	0.03 ± 0.03

5.2 Powder X-ray diffraction analysis: Mineralogical phases

5.2.1 133 A929 1(i)

The XRD diffractogram shows that this slag sample is mainly composed by quartz, together with minor percentage of fayalite. Scarce amounts of cristobalite low, maghemite-C, syn and gypsum co-exist with trace amount of magnetite, syn and pentlandite.

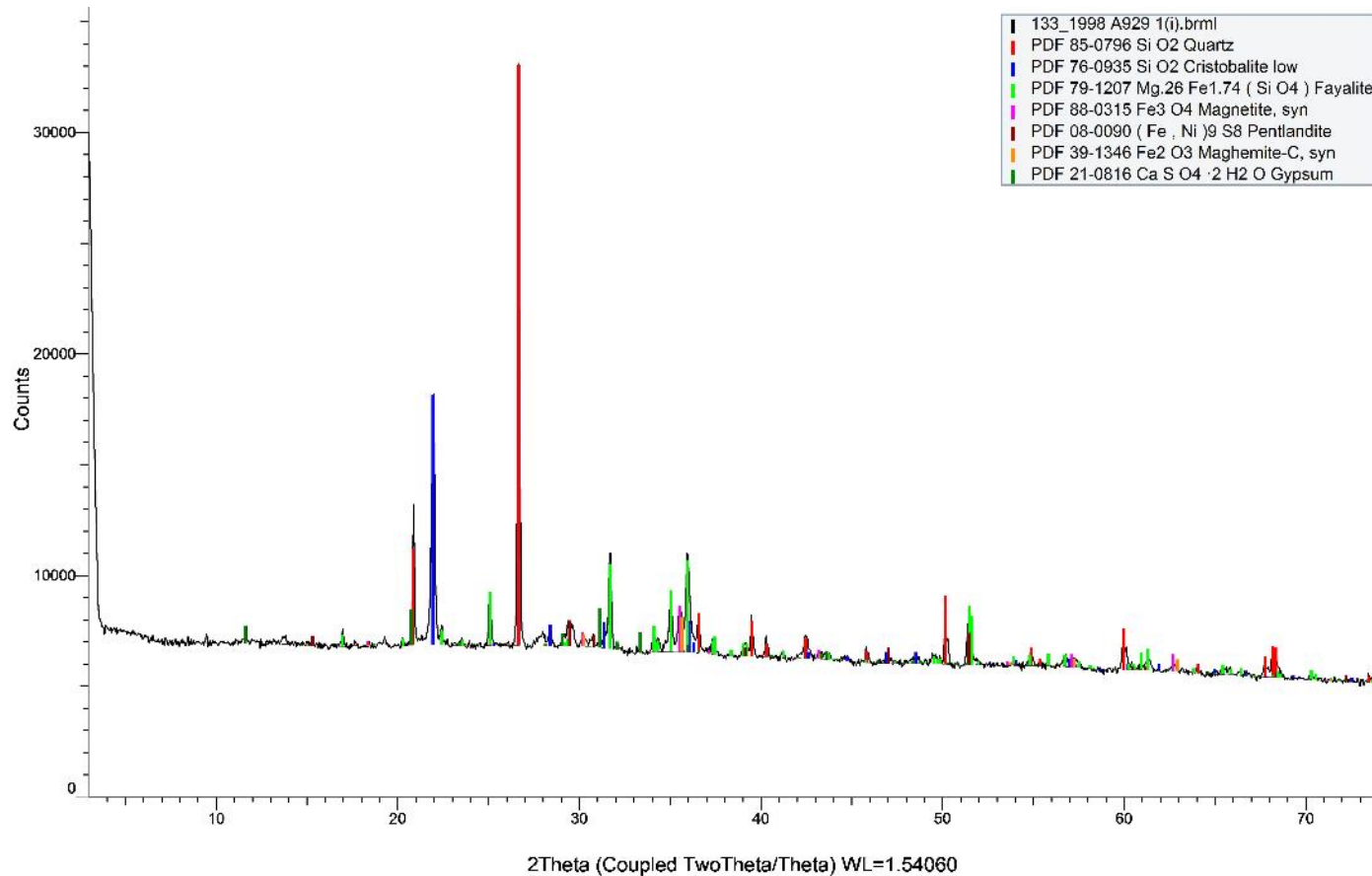


Fig. 17: X-ray diffraction (XRD) patterns of slag sample 133 A929 1(i)

5.2.2 133 A929 1(ii)

The XRD diffractogram reveals that in this slag sample the most abundant mineral is quartz, followed by a minor percentage of fayalite and maghemite-C, syn. Cristobalite low is less abundant. There are also traces of magnetite, syn, pentlandite and gypsum.

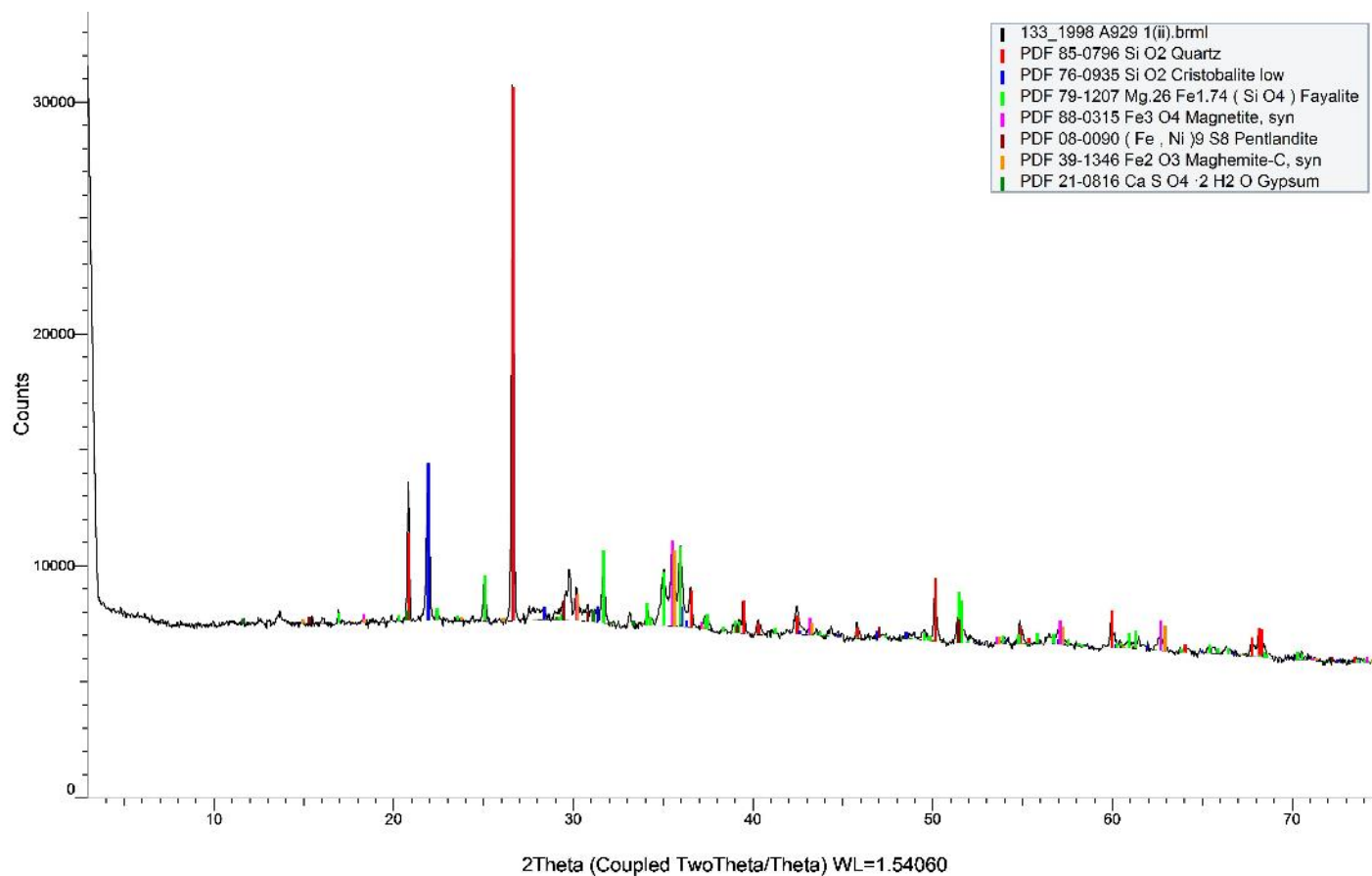


Fig. 18: X-ray diffraction (XRD) patterns of slag sample 133 A929 1(ii)

5.2.3 133 A929 1(iii)

The XRD diffractogram shows that quartz is very abundant in this slag sample. Fayalite is also present. Scarce amounts of cristobalite low and maghemite-C, syn appear along with trace amount of magnetite, syn and pentlandite and gypsum.

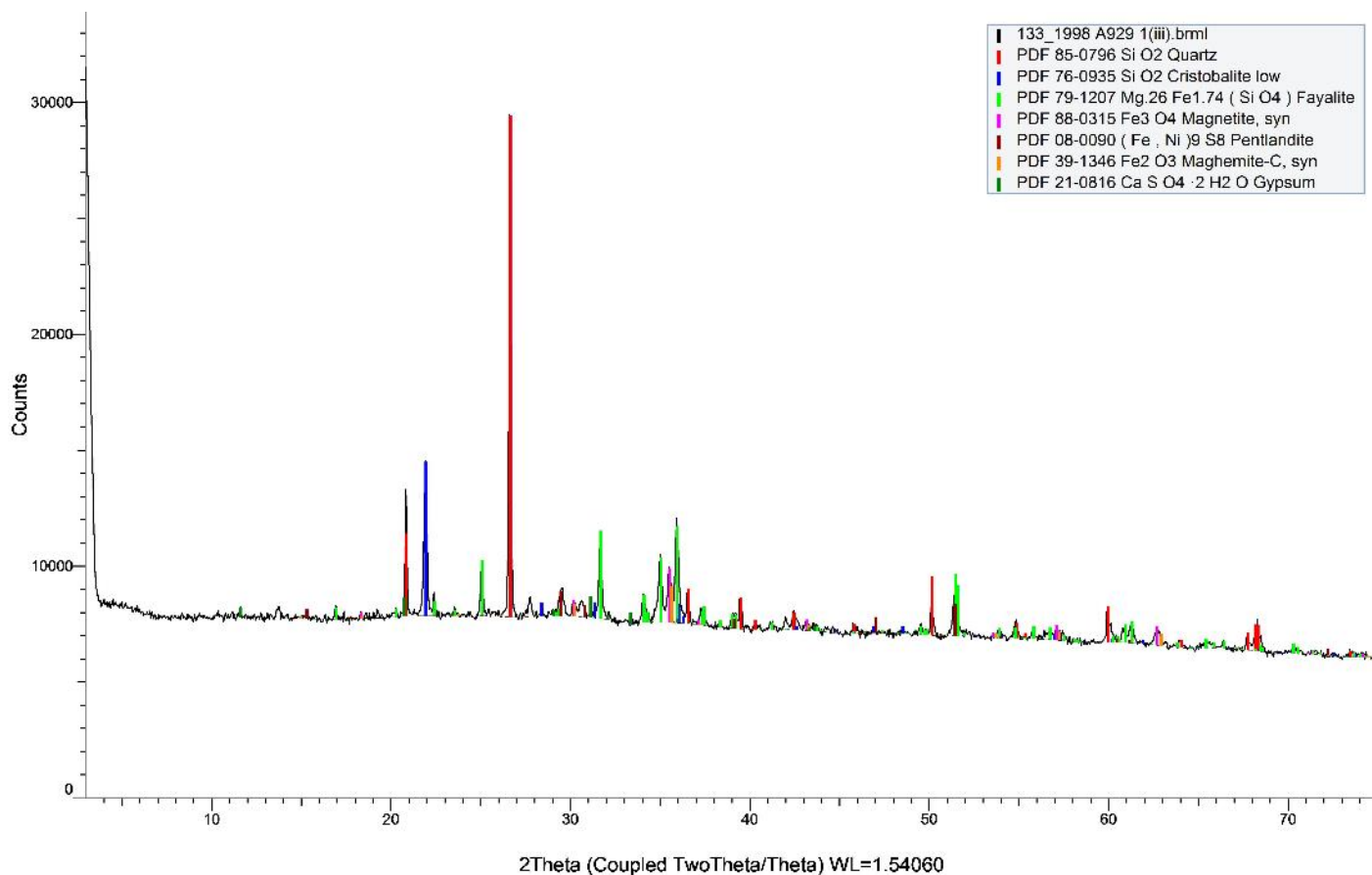


Fig. 19: X-ray diffraction (XRD) patterns of slag sample 133 A929 1(iii)

5.2.4 133 A929 1(iv)

The XRD diffractogram reveals that fayalite predominates in the mineral composition of this slag sample while maghemite-C, syn is less abundant. Scarce amounts of quartz and magnetite, syn were also detected.

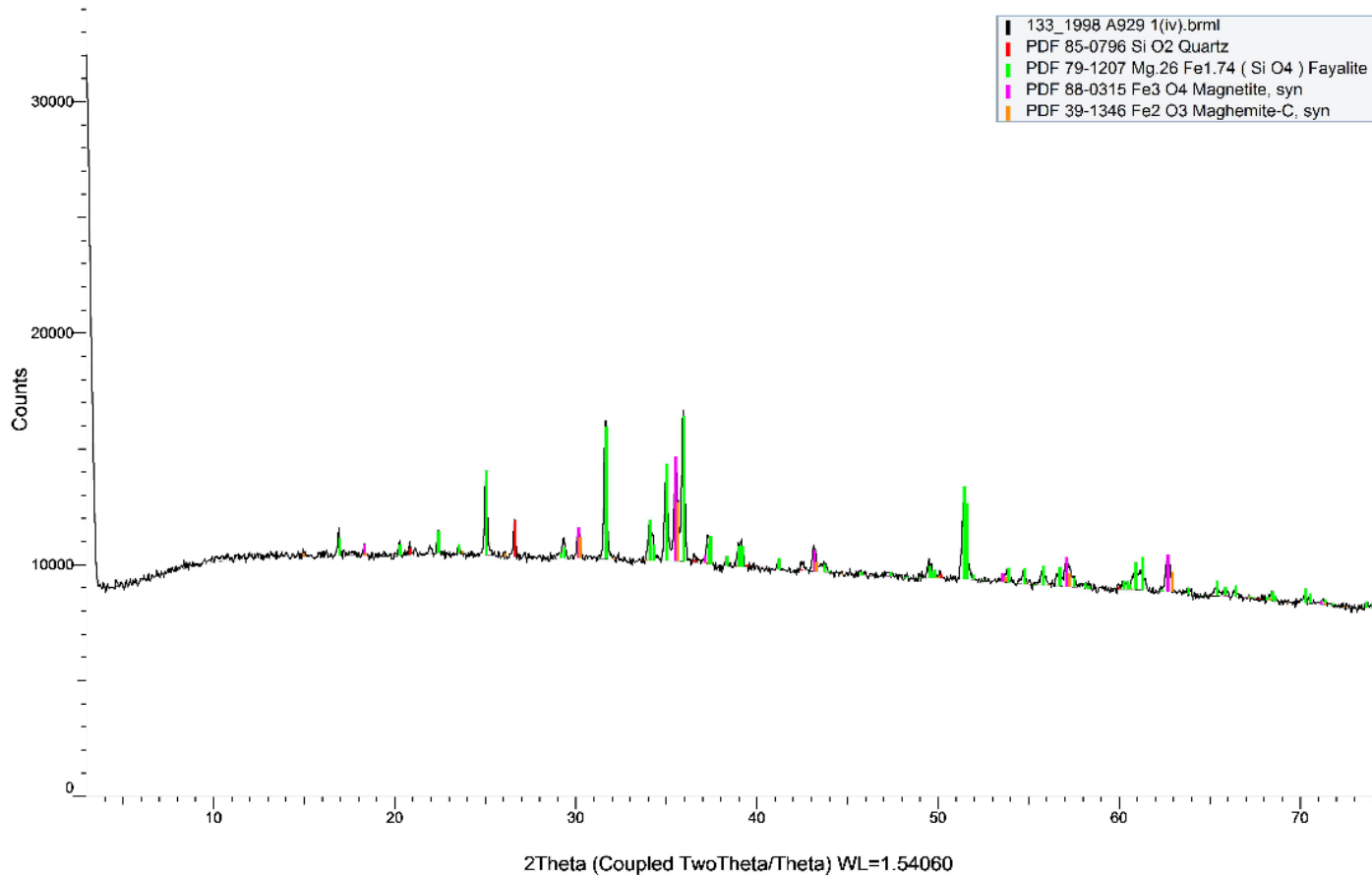


Fig. 20: X-ray diffraction (XRD) patterns of slag sample 133 A929 1(iv)

5.2.5 133 A929 1(v)

The XRD diffractogram reveals that this slag sample is mainly composed by fayalite, together with minor percentage of maghemite-C, syn. Scarce amount of quartz and magnetite, syn co-exists with trace amount of cristobalite low.

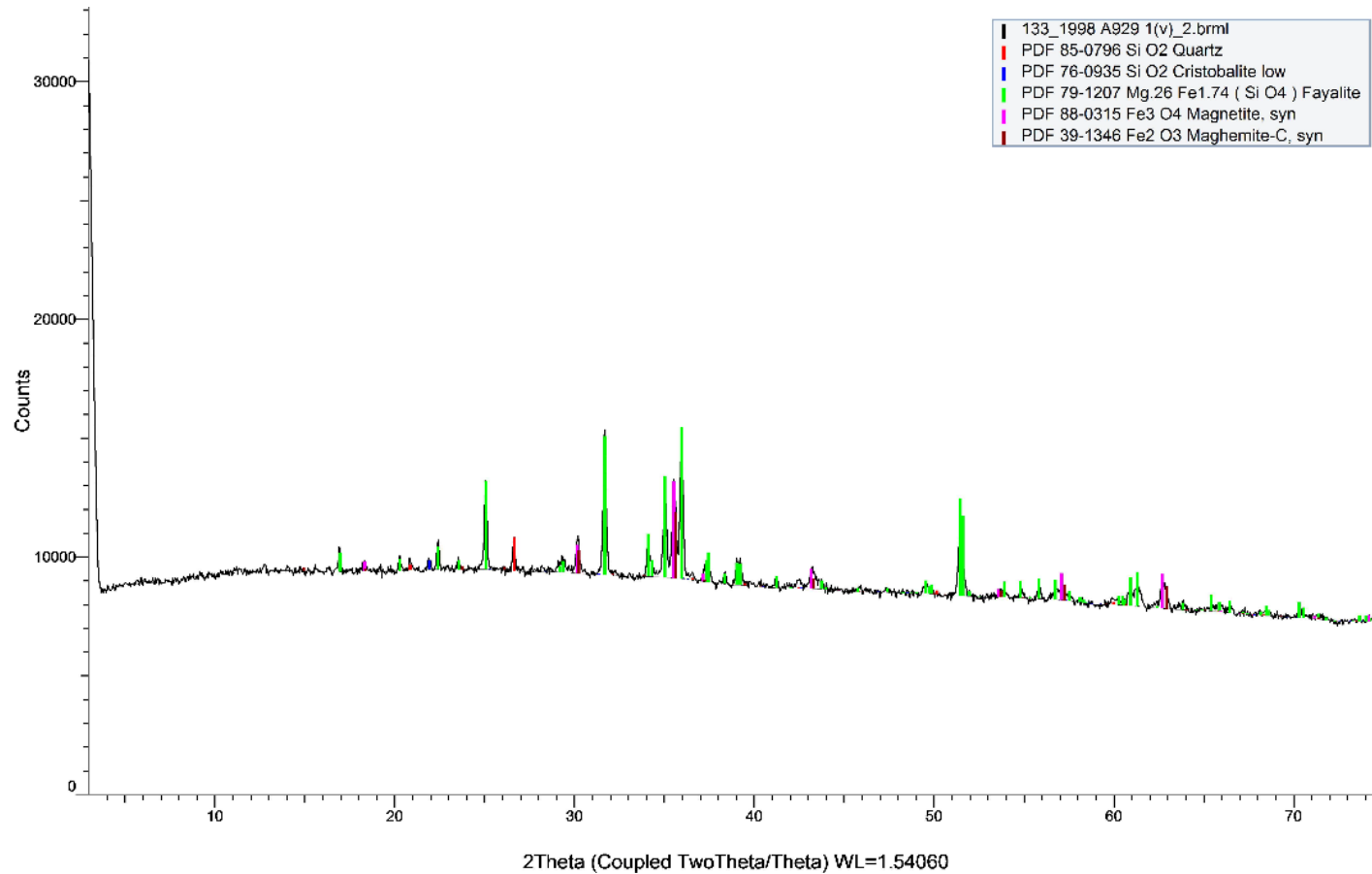


Fig. 21: X-ray diffraction (XRD) patterns of slag sample 133 A929 1(v)

5.2.6 144 A929 1a(i)

The XRD diffractogram shows that in this slag sample the most abundant mineral is fayalite, followed by a minor percentage of maghemite-C, syn and gypsum. Scarce amount of quartz and magnetite, syn also appear along with trace amount of cristobalite low and magnetite, syn.

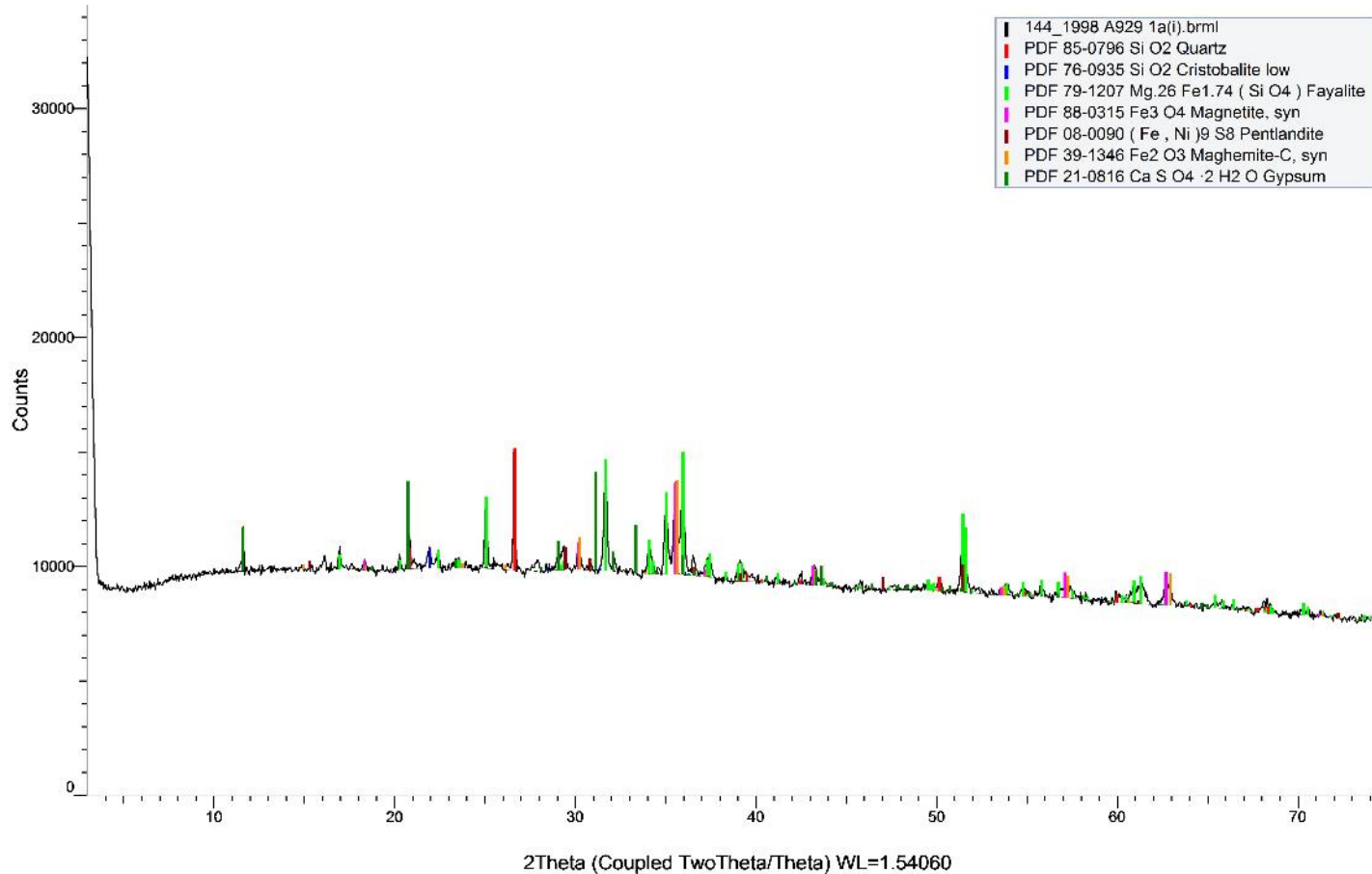


Fig. 22: X-ray diffraction (XRD) patterns of slag sample 144 A929 1a(i)

5.2.7 144 A929 1a(ii)

The XRD diffractogram reveals that quartz is abundant in this slag sample. Fayalite and maghemite-C, syn are also present. Scarce gypsum appears along with trace amount of cristobalite low, magnetite, syn and pentlandite.

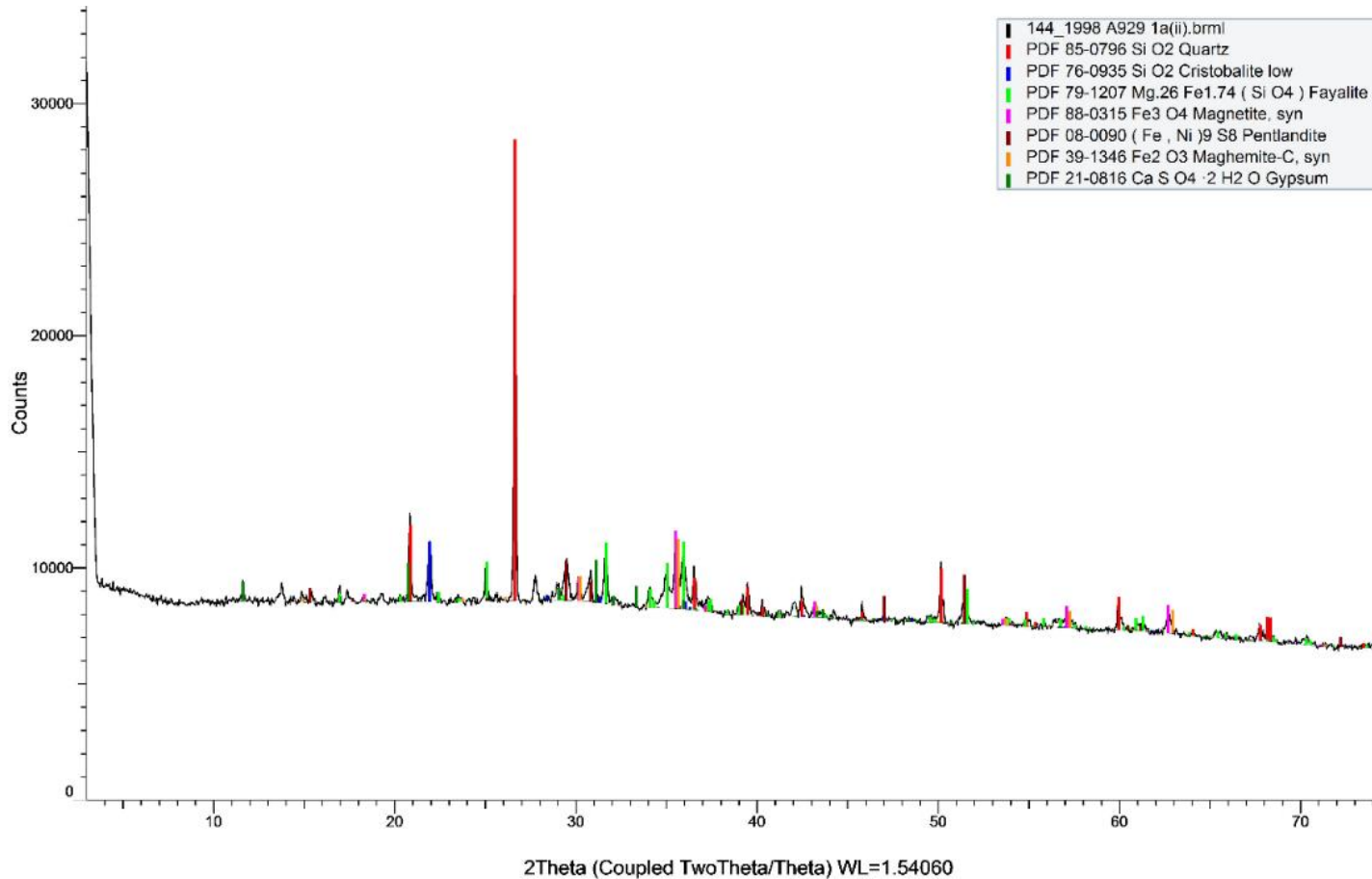


Fig. 23: X-ray diffraction (XRD) patterns of slag sample 144 A929 1a(ii)

5.2.8 146 A929 1c(i)

The XRD diffractogram shows that fayalite predominates in the mineral composition of this sample, while maghemite-C, syn is less abundant. Scarce amounts of quartz and magnetite, syn, along with cristobalite low, pentlandite and gypsum were also detected.

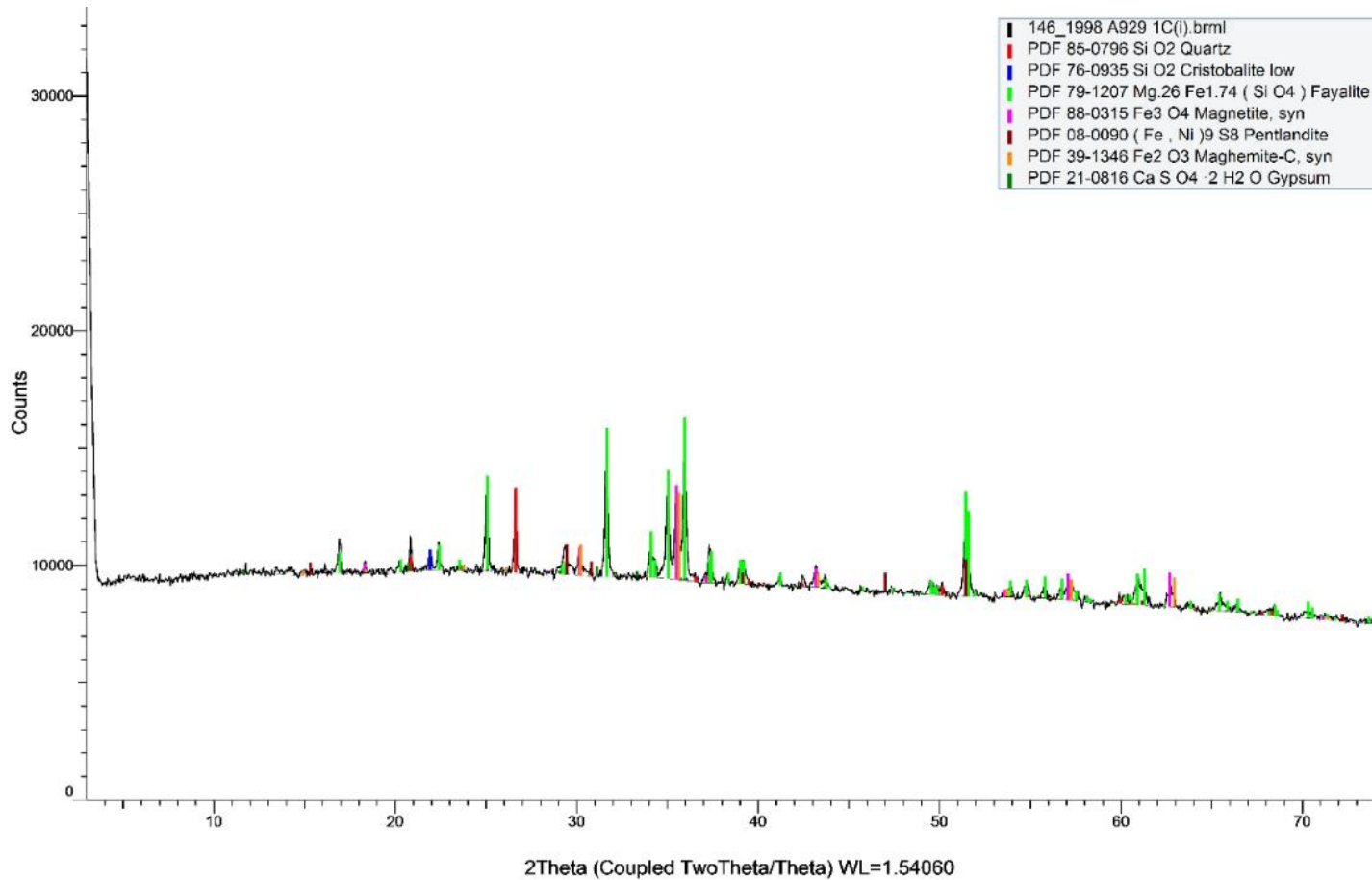


Fig. 24: X-ray diffraction (XRD) patterns of slag sample 146 A929 1c(i)

5.2.9 146 A929 1c(iv)

The XRD diffractogram shows that this slag sample is mainly composed by quartz. Fayalite is also present. Scarce amounts of cristobalite low and maghemite-C, syn co-exist with trace amount of magnetite, syn, pentlandite and gypsum.

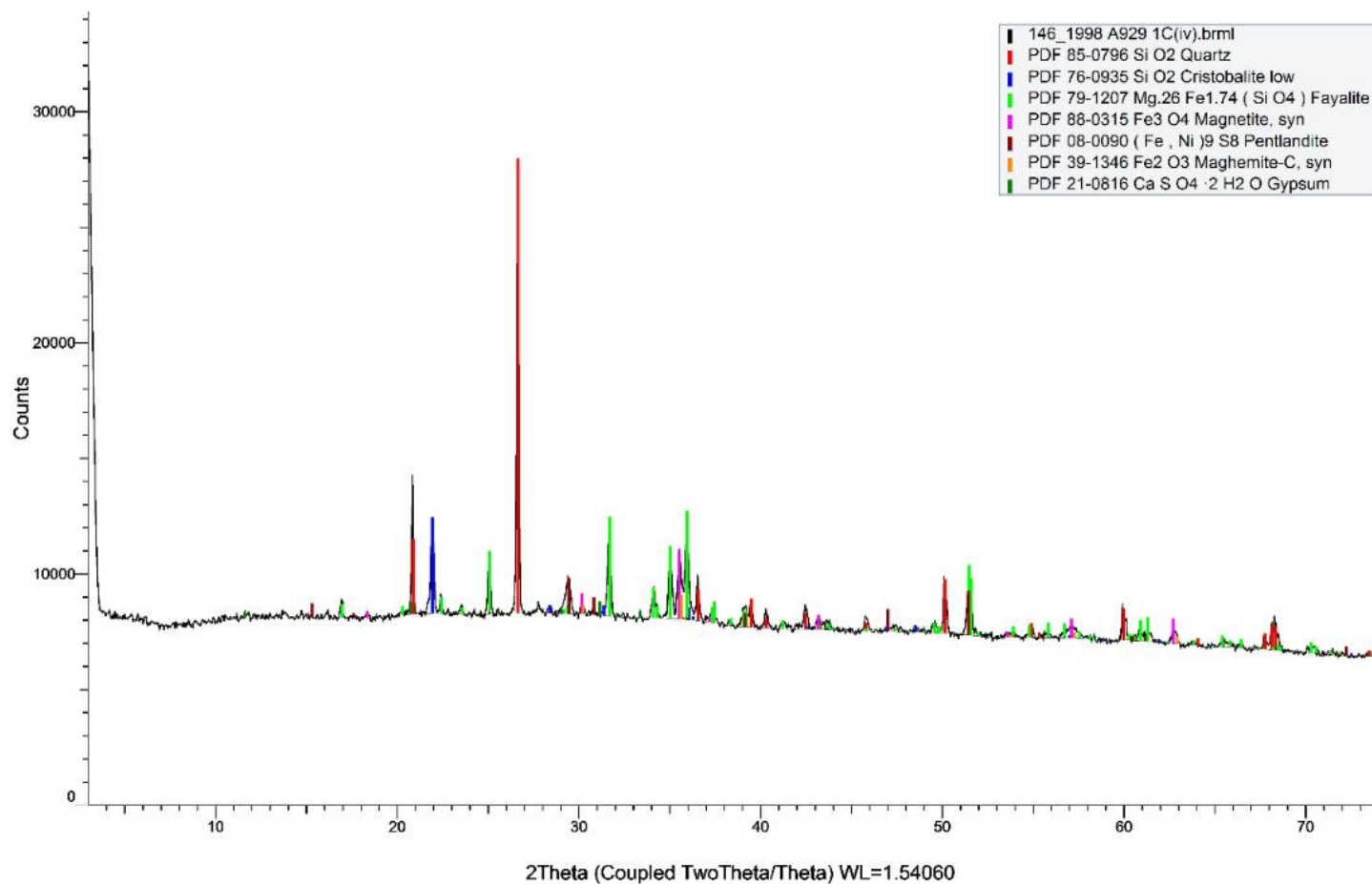


Fig. 25: X-ray diffraction (XRD) patterns of slag sample 146 A929 1c(iv)

Table 5: XRD results of analyzed slag samples

Sample ID	SiO ₂ Quartz	SiO ₂ Cristobalite low	Mg.26 Fe _{1.74} (SiO ₄) Fayalite	Fe ₃ O ₄ Magnetite, syn	(Fe, Ni) 9S ₈ Pentlandite	Fe ₂ O ₃ Maghemite- C, syn	CaSO ₄ .2H ₂ O Gypsum
133 A929 1(i)	++++	+	++	tr	tr	+	+
133 A929 1(ii)	++++	+	++	tr	tr	++	tr
133 A929 1(iii)	++++	+	++	tr	tr	+	tr
133 A929 1(iv)	+	-	++++	+	-	++	-
133 A929 1(v)	+	Tr	++++	+	-	++	-
144 A929 1a(i)	+	Tr	+++	+	tr	++	++
144 A929 1a(ii)	+++	Tr	++	tr	tr	++	+
146 A929 1c(i)	+	Tr	+++	+	tr	++	tr
146 A929 1c(iv)	++++	+	++	tr	tr	+	tr

(++++ very abundant 70-50%, +++ abundant 50-30%, ++present 30-15%, +scarce 15-5%, Traces <5%)

XRD analysis shows the presence of 7 minerals in the analyzed 9 slag samples (Table 5). However, quartz (SiO₂), and fayalite Mg_{2.6} Fe_{1.74} (SiO₄) were the major crystalline phases identified in the slag samples. The relative abundance of quartz and fayalite varied greatly among slag samples (fig. 26). Besides these two minerals, cristobalite low (SiO₂) and magnetite, syn (Fe₃O₄) were also identified as minor mineral phases along with pentlandite (Fe, Ni) 9S₈, maghemite-C, syn (Fe₂O₃) and gypsum (CaSO₄.2H₂O).

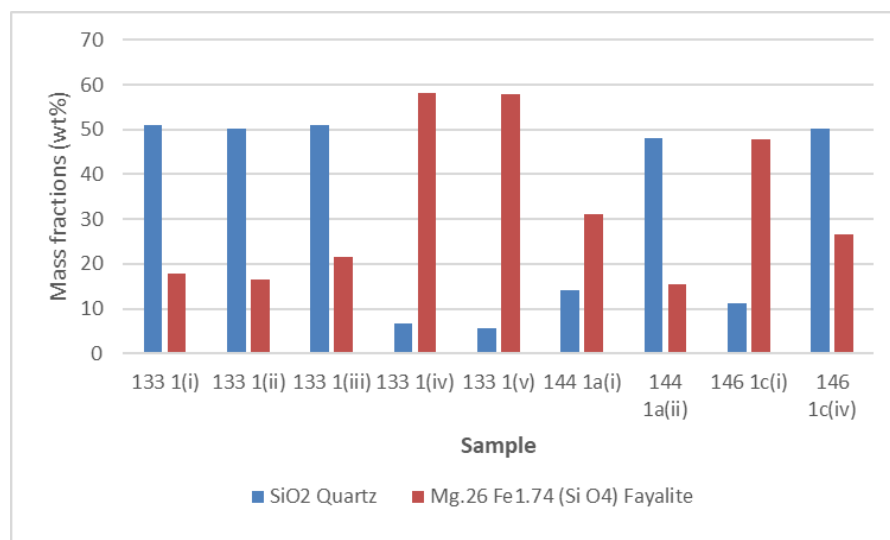
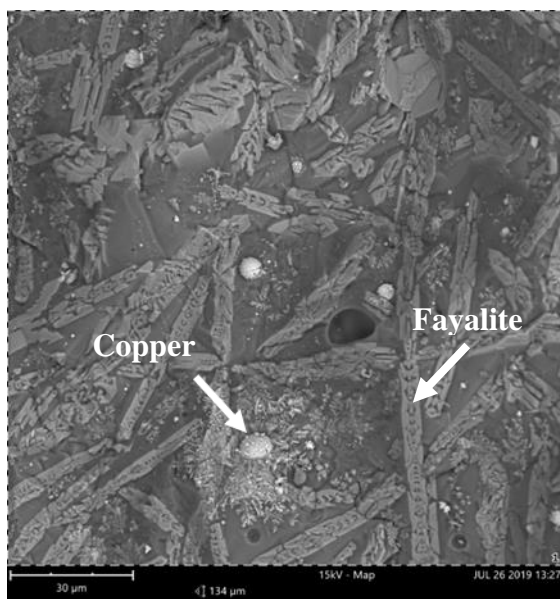


Fig. 26: Mass fraction (wt%) of quartz and fayalite in analyzed 9 slag samples.

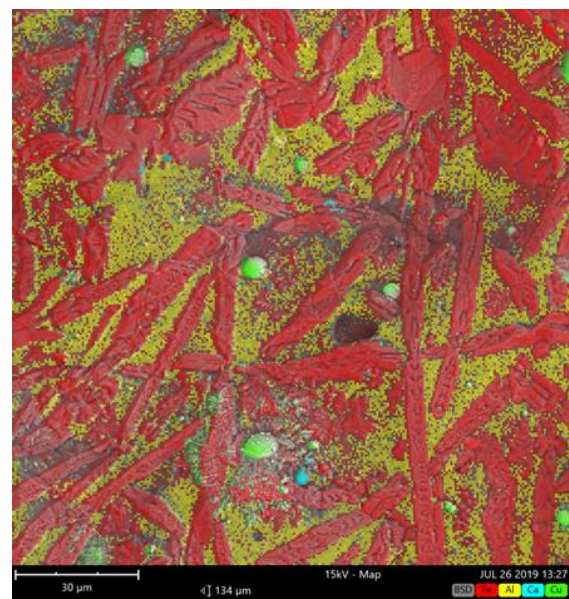
5.3 SEM-EDS analysis: Microstructure

5.3.1 133 A929 1(i)

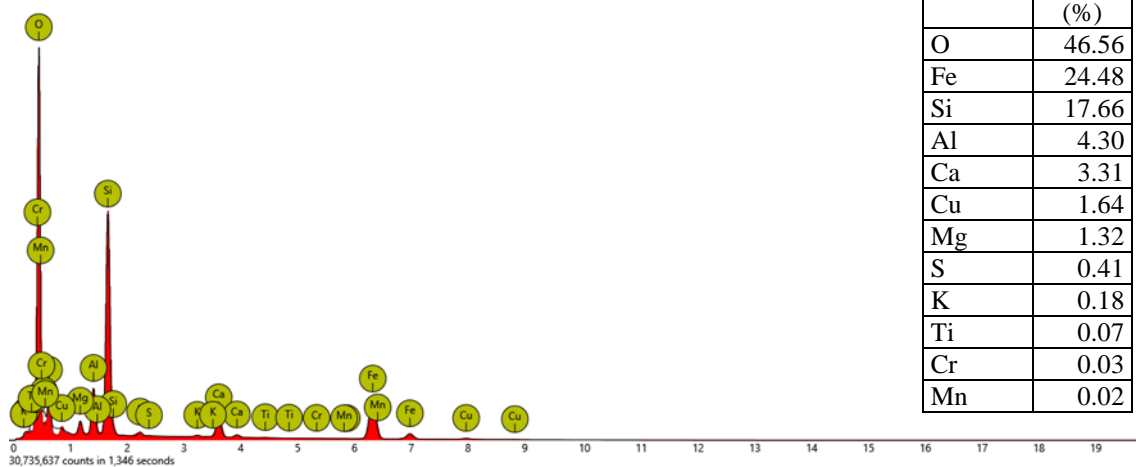
In this sample, SEM-EDS shows the presence of elongated fayalite crystals, which correspond to the lighter grey phase in black scattered (BS) image, and of copper droplets, seen as a white phase (fig 27a). However, the presence of fayalite as a major phase in slag microstructure is very significant and highlights the type of slag's origin. In the SEM-EDS elemental maps (fig.28), it is possible to observe that copper droplets are associate with sulphur. This might be due to the nature of the ore, in which were probably present some mineral containing copper sulfide.



a



b



c

Fig. 27: SEM-EDS backscattered image (a), combined map (b), and EDS spectrum (c) of sample 133 A929 1(i).

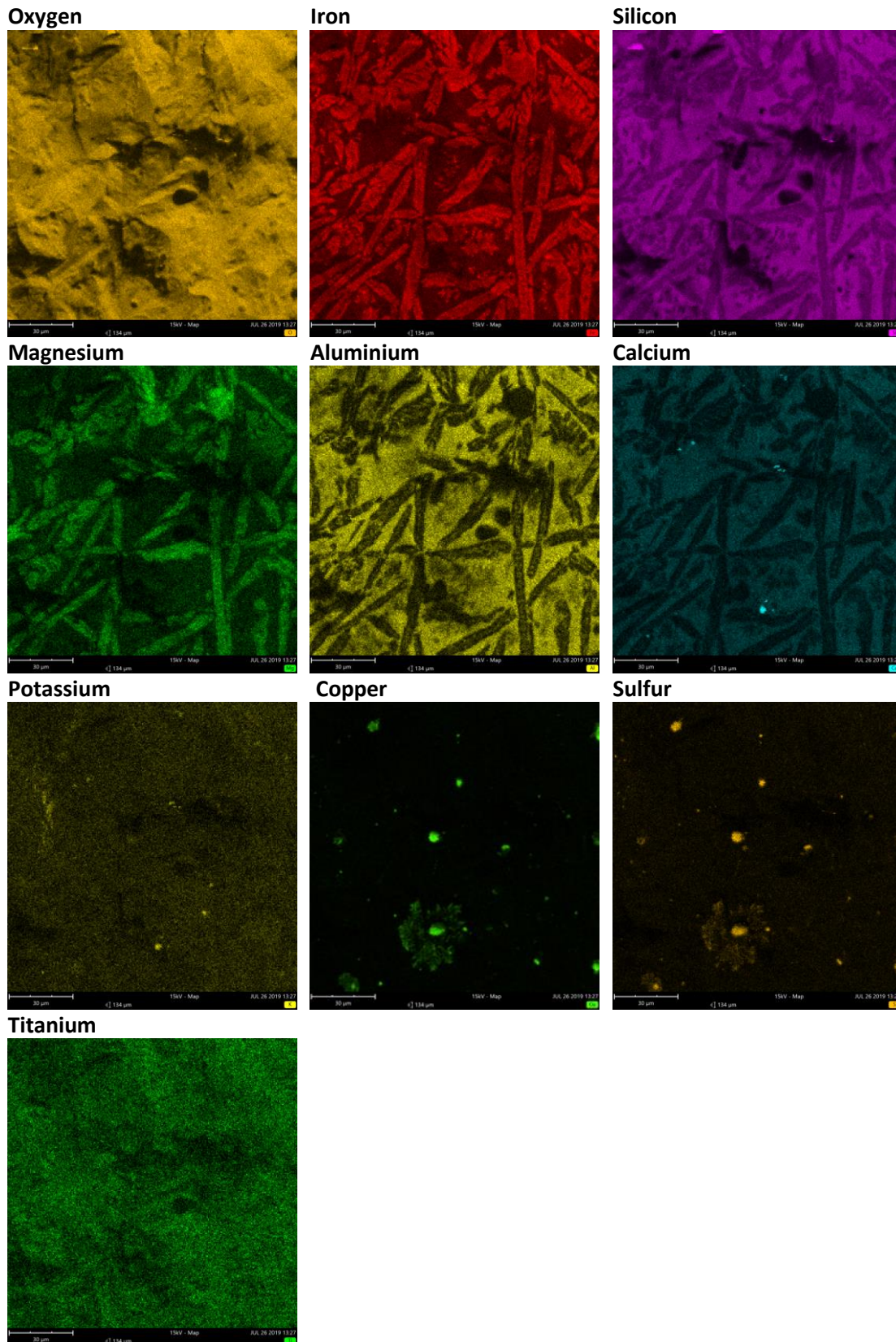


Fig. 28: SEM-EDS elemental maps of sample 133 A929 1(i).

5.3.2 133 A929 1(iv)

In this sample, SEM-EDS reveals the presence of elongated fayalite crystals as a major phase, seen in light grey phase in BS image (fig.26a), and of tiny copper droplets, seen as green spots in the combined map (fig 29b). It is worthy to mention that XRD powder analysis also reveal the presence of fayalite as a major mineral phase in this slag sample. Like in the previous sample, in the elemental maps, it is visible the association of copper with sulphur (fig 30). In the elemental maps, calcium is also seen as droplets (fig.30).

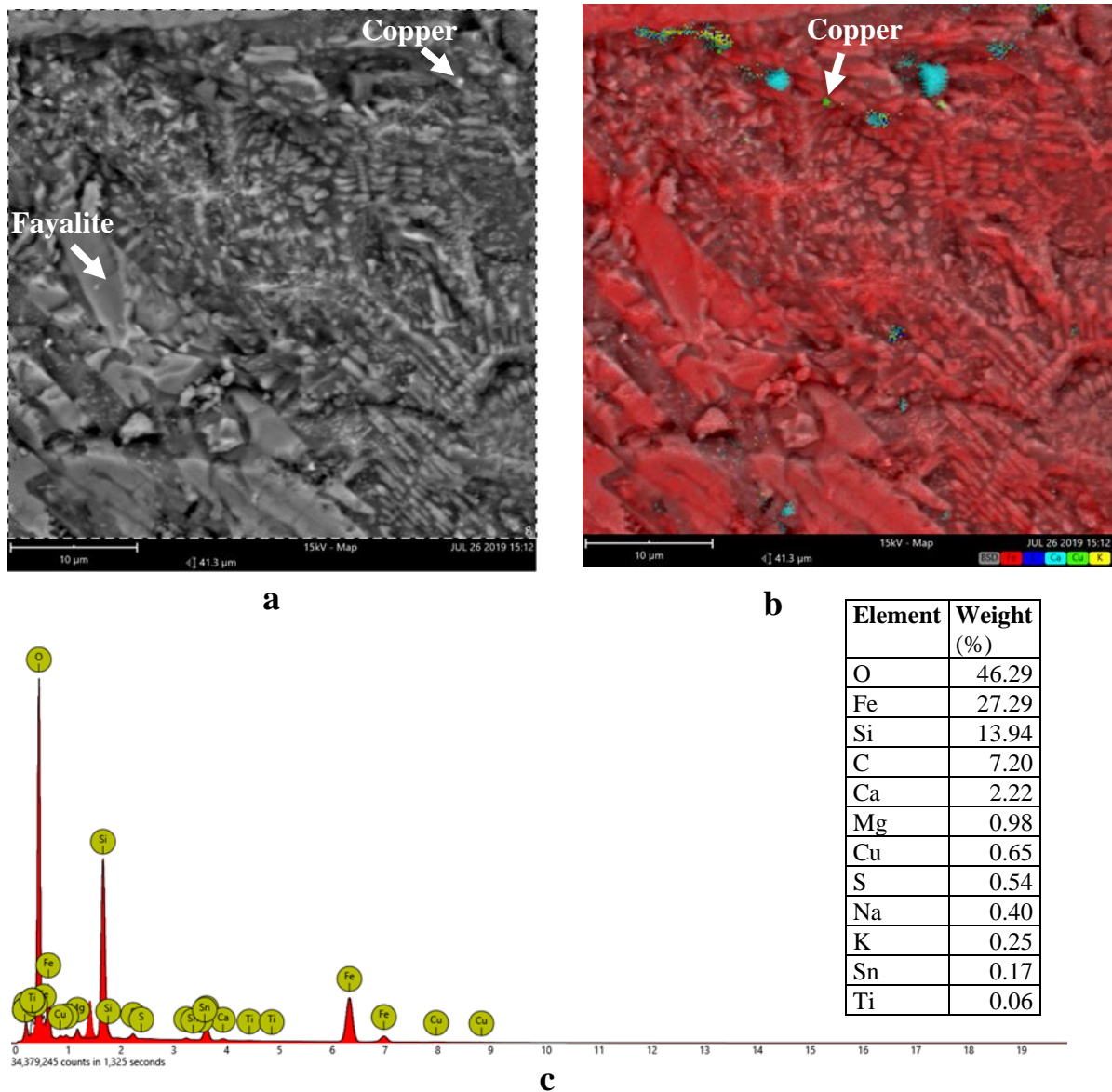


Fig. 29: SEM-EDS backscattered image (a), combined map (b), and EDS spectrum (c) of sample 133 A929 1(iv)

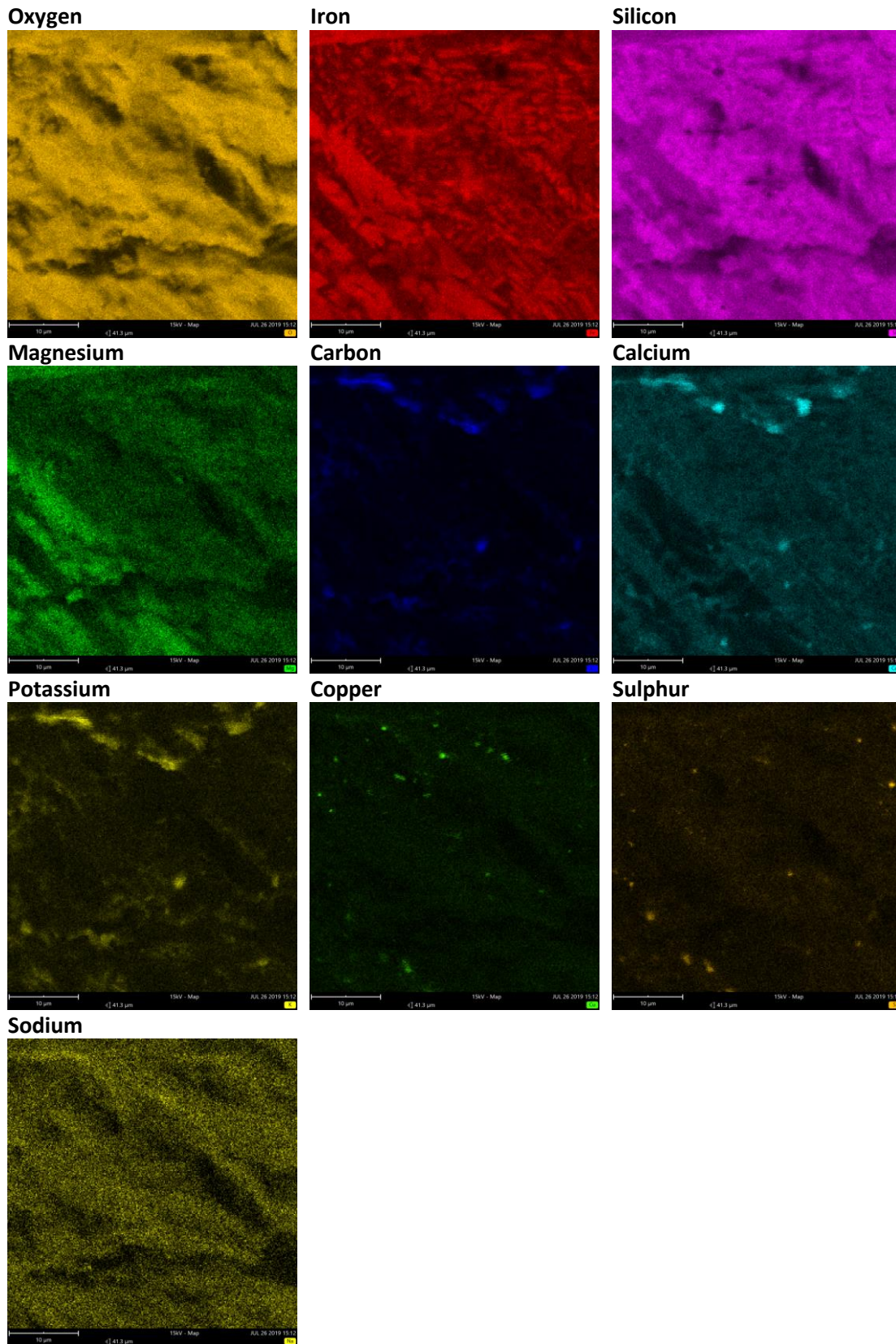
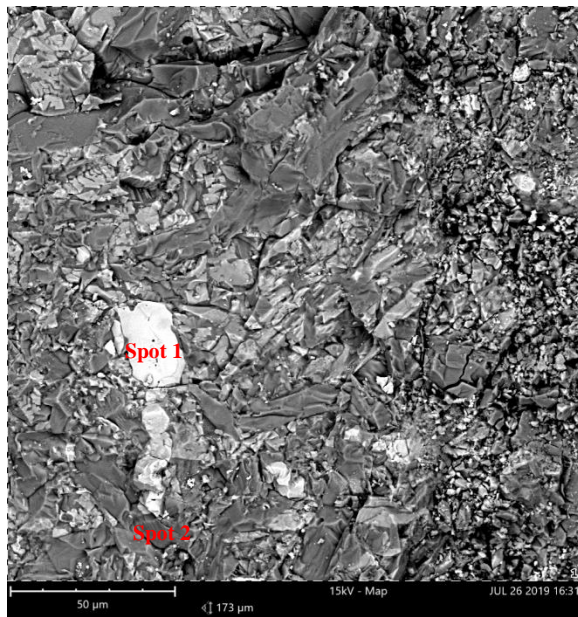


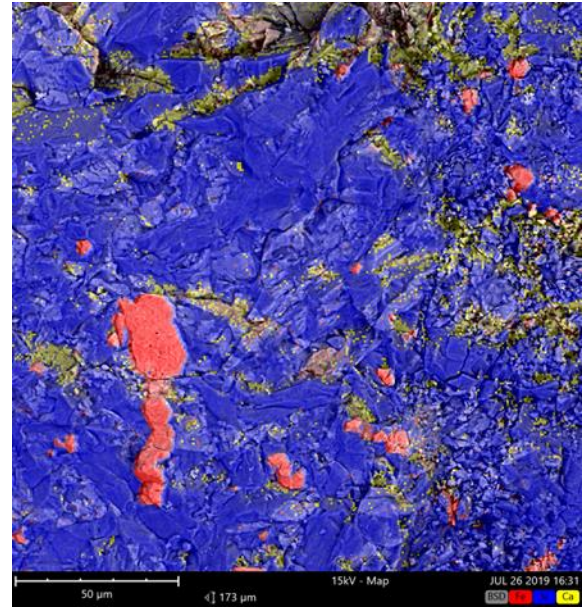
Fig. 30: SEM-EDS elemental maps of sample 133 A929 1(iv).

5.3.3 144 A929 1a(iii)

In this SEM-EDS image, iron nodules and droplets are seen as white phase in BS image (fig.31a, spot 1), while the Si-Ca-Fe-Mg matrix is seen as light grey phase (fig. 31b, spot 2). In the elemental maps, it is possible to observe the association of iron nodules with silicon, aluminum, and calcium (fig. 32). Some copper droplets are also seen in the elemental maps (fig.32). However, no sulphur is observed in the elemental maps.



a



b

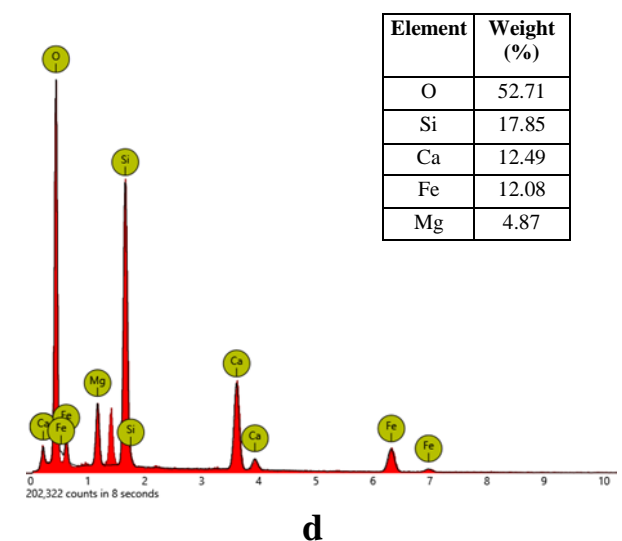
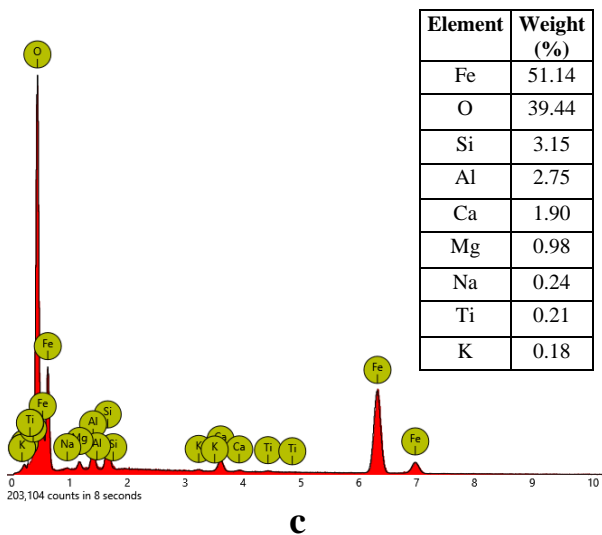


Fig. 31: SEM-EDS backscattered image (a), combined map (b) and EDS spectrum of spot 1(c), EDS spectrum of spot 2 (d) of sample 144 A929 1a(iii).

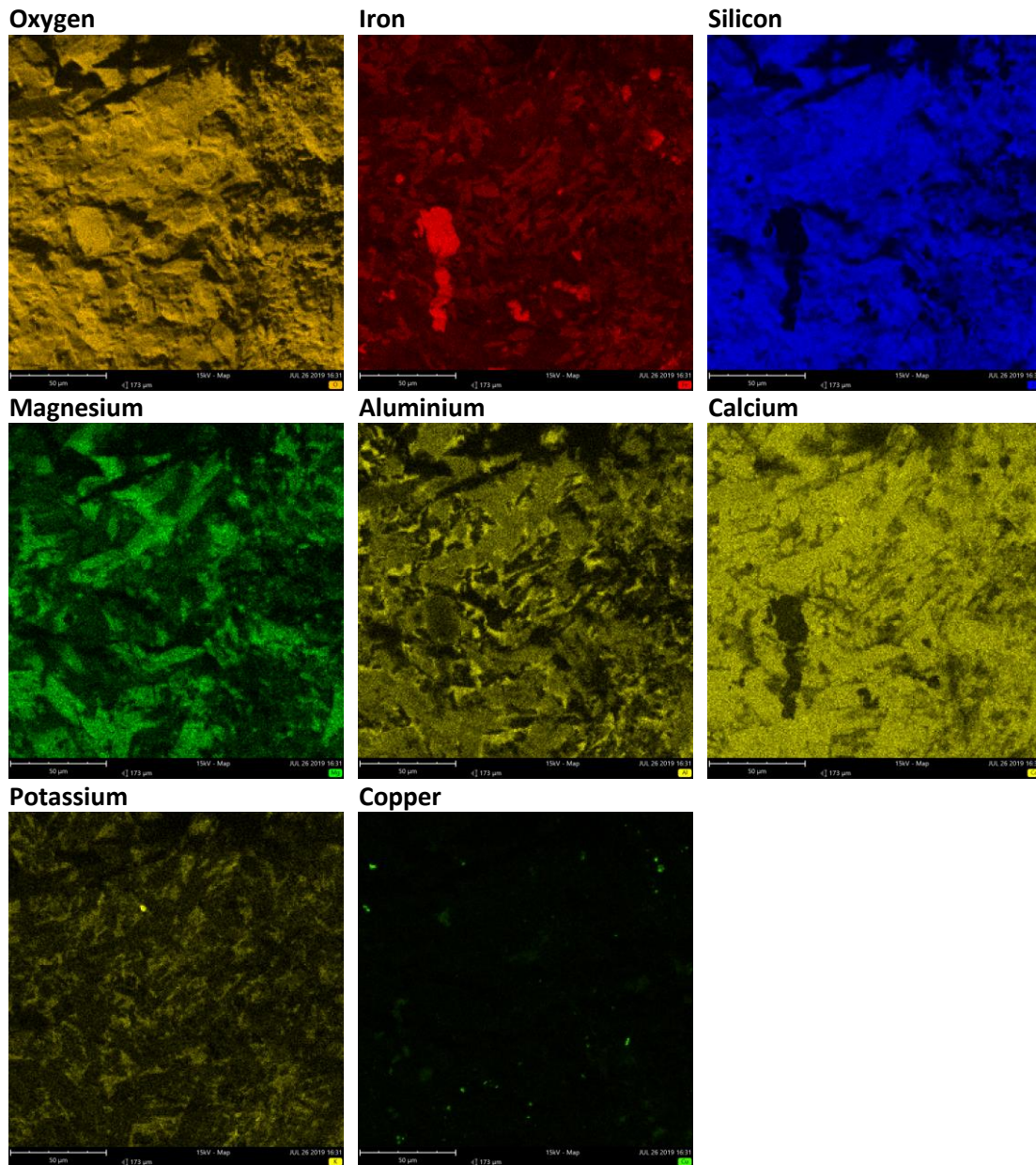


Fig. 32: SEM-EDS elemental maps of sample 144 A929 1a(iii).

5.3.4 144 A929 1a(iv)

In this sample, SEM-EDS reveals the presence of large irregularly shaped magnetite crystals as a major phase, seen in light grey in the BS image (fig.33a), and the tiny copper droplets, seen as grey colored phase in the combine map (fig. 33b). Tiny copper droplets are associated with sulphur while the bigger piece of copper to chlorine. In the elemental maps, it is observed the association of copper with sulphur (fig.34). The presence of chlorine associated with copper might be due to the deterioration of slag in the soil.

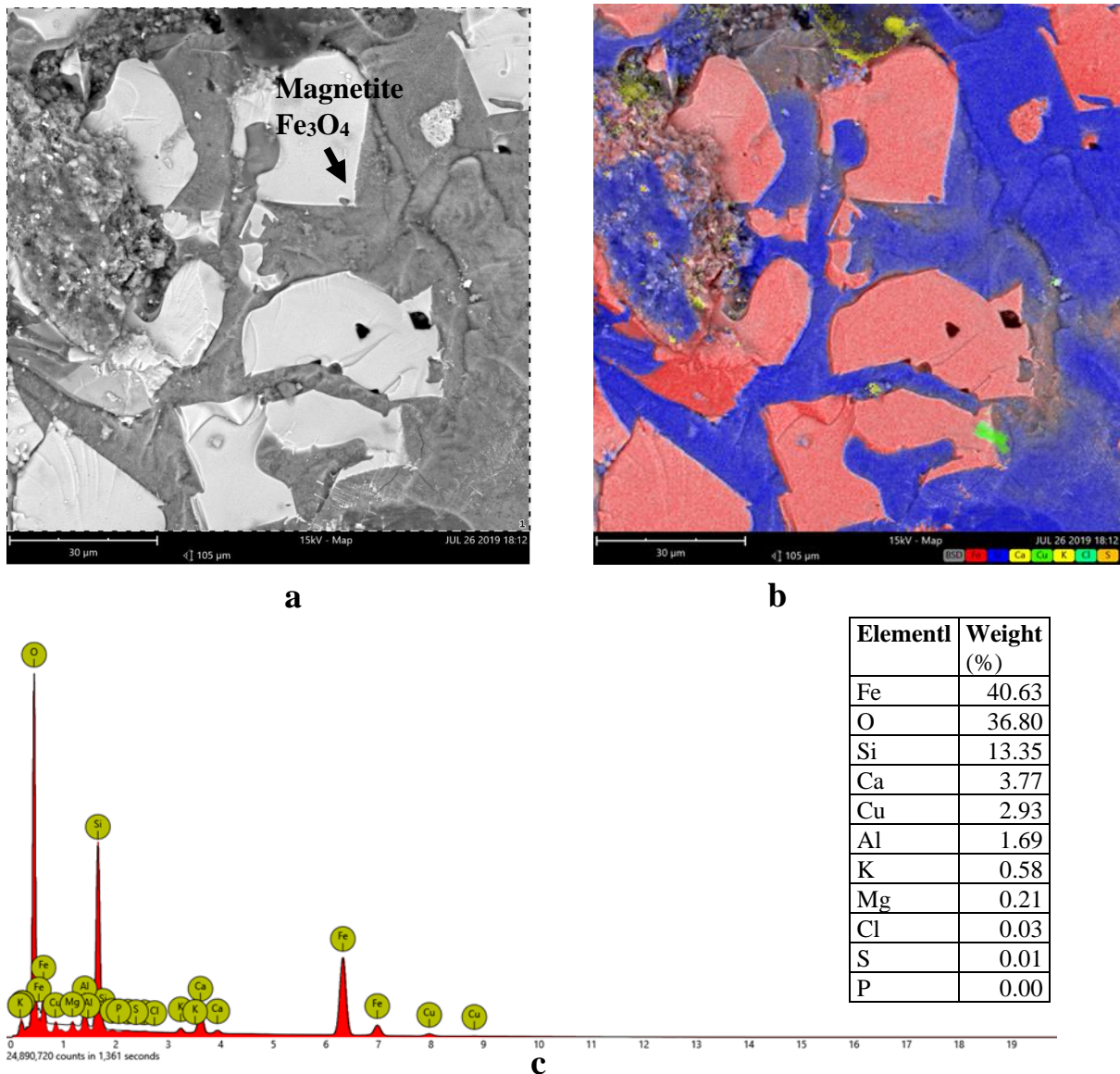


Fig. 33: SEM-EDS backscattered image (a), combined map (b), and EDS spectrum (c) of sample 144 A929 1a(iv)

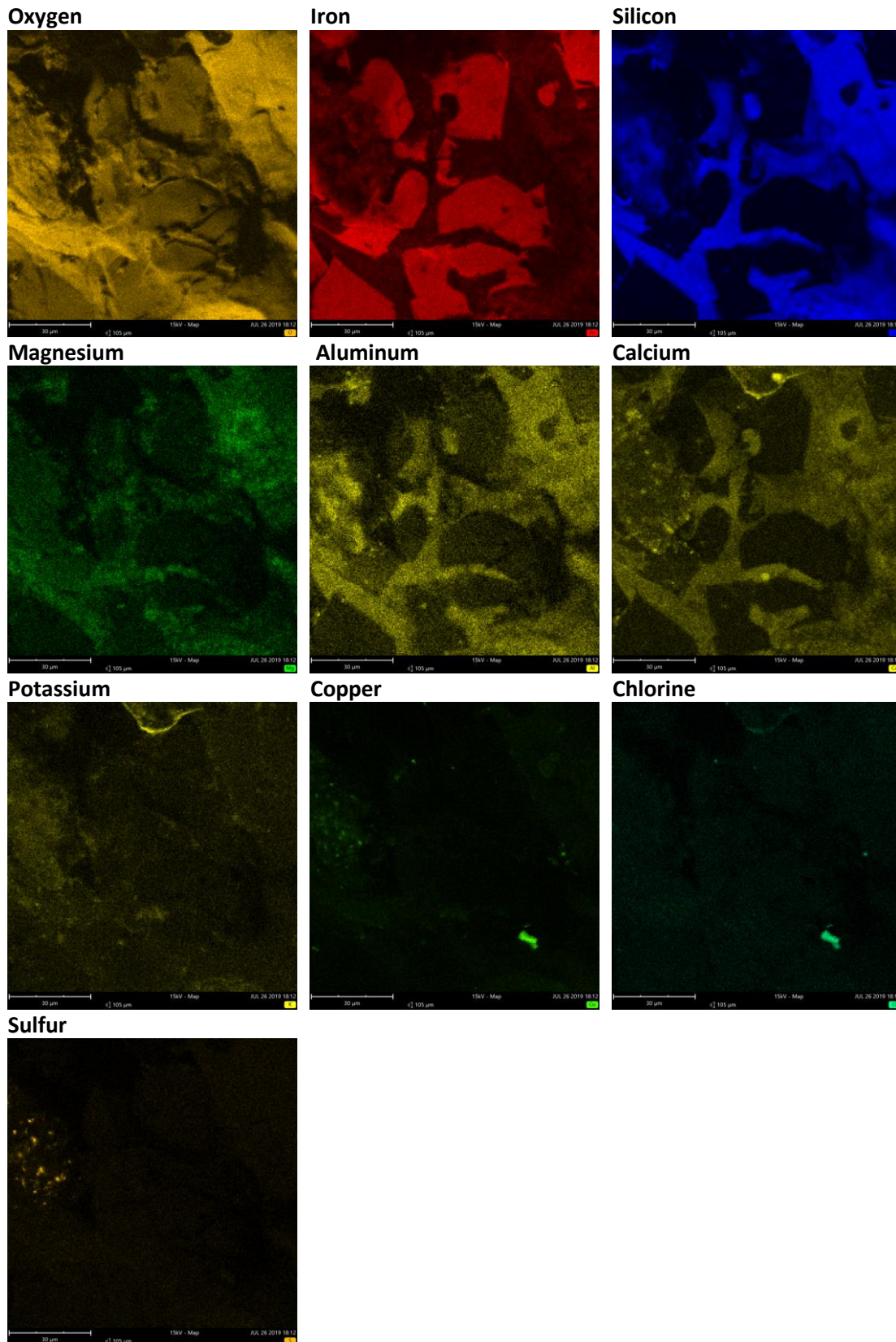


Fig. 34: SEM-EDS elemental maps of sample144 A929 1a(iv).

5.3.5 146 A929 1c(i)

In this SEM-ED image, fayalite crystals are not easily recognized under the backscattered detector, though XRD powder analysis of this sample reveals the fayalite as a major mineralogical phase. However, in the elemental map they are quite visible (fig. 36). In the elemental maps, tiny copper and sulphur droplets are seen, but the association of copper and sulphur is not clear as in the previous samples (fig. 36). There are many sulphur droplets that don't correspond to copper. Sodium droplets are also seen in the elemental maps and they are also not highly correlated to copper like the previous one (fig.36).

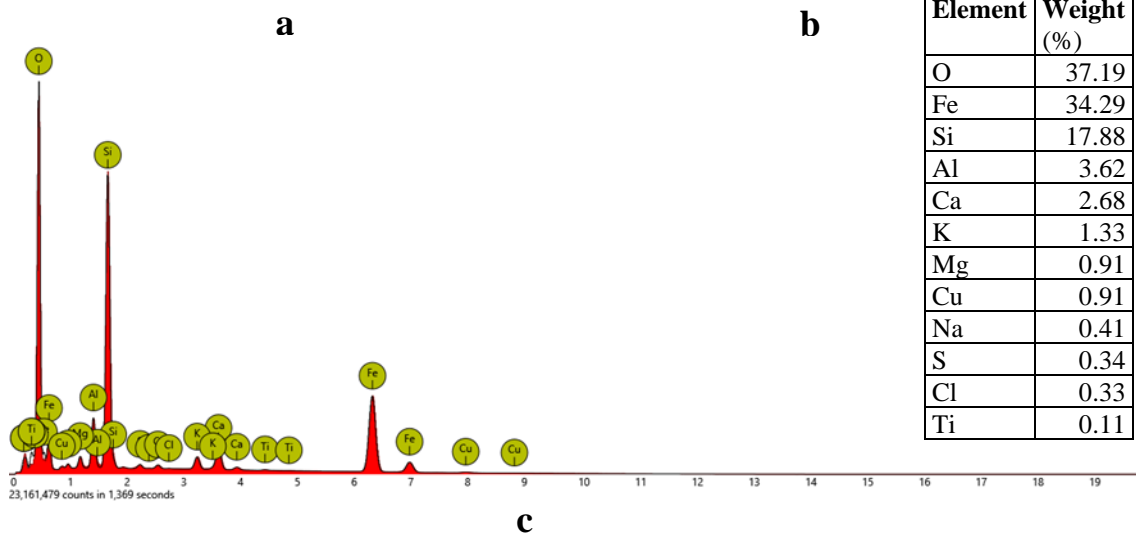
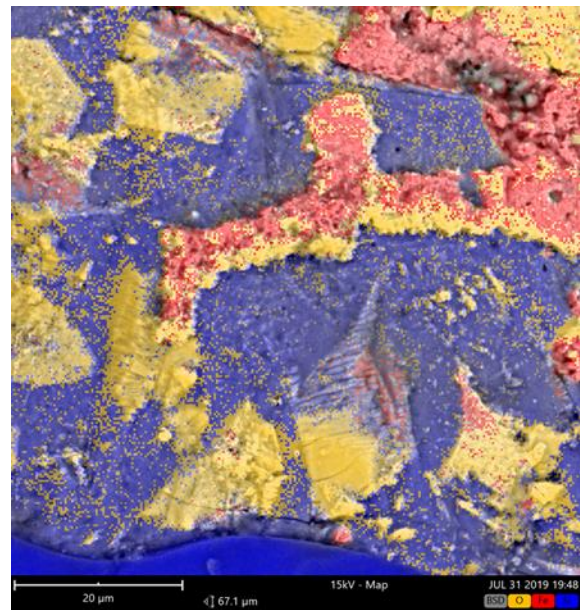
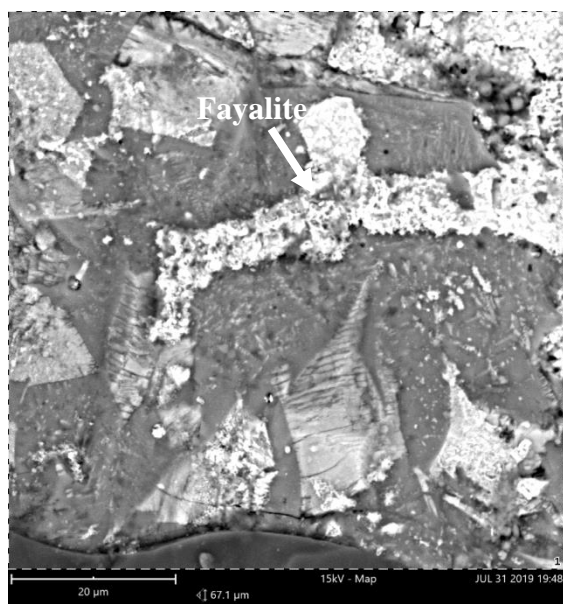


Fig. 35: SEM-EDS backscattered image (a), combined map (b), and EDS spectrum (c) of sample 146 A929 1c(i)

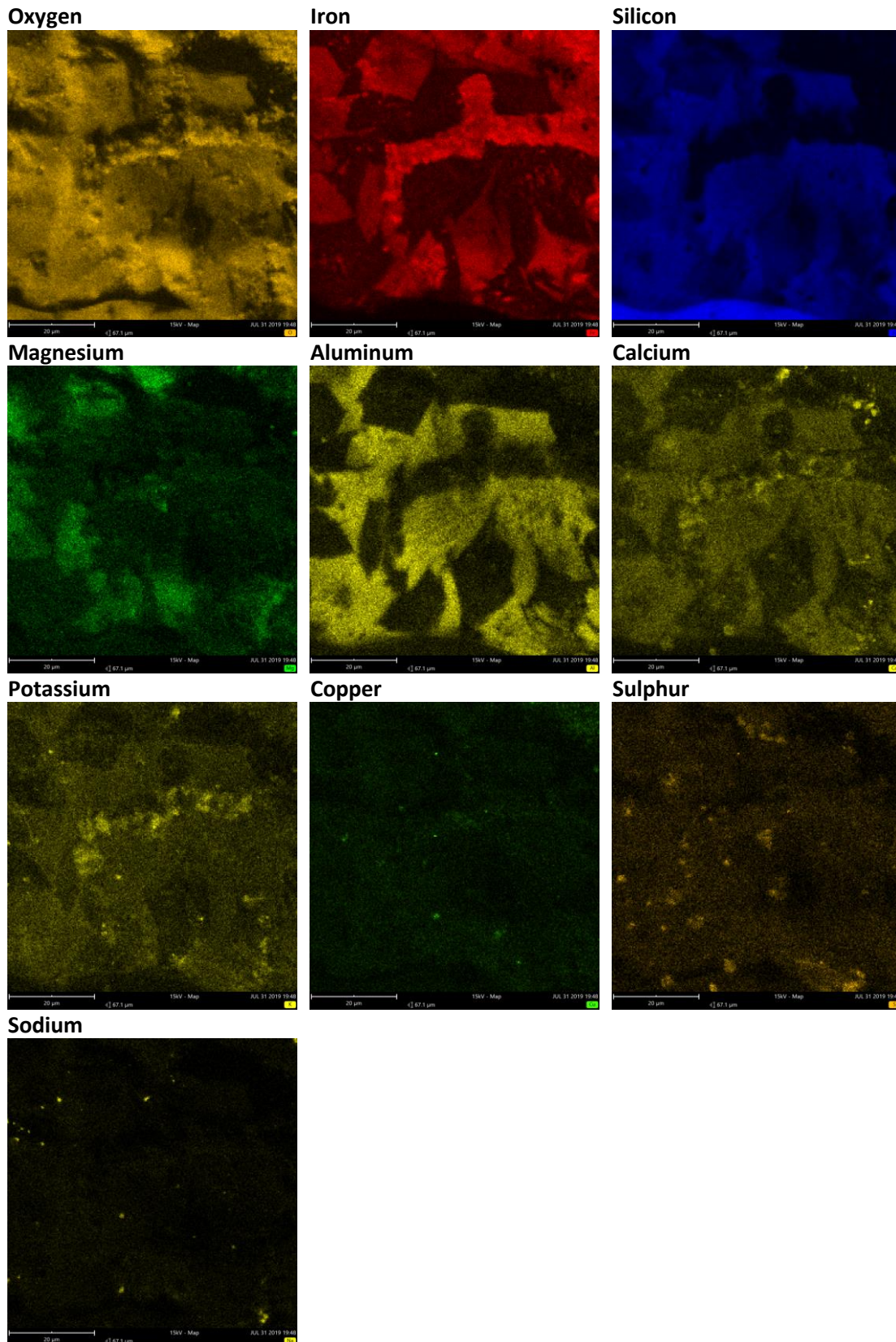


Fig. 36: SEM-EDS elemental maps of sample146 A929 1c(i)

CHAPTER 6: DISCUSSIONS

6.1 Type of slags and relevant metallurgical processes

For the study of ancient slags, it is very crucial and fundamental to identify the nature of metallurgical process that produced them. As discussed in chapter 2, the slags can be formed by a wide range of activities, e.g. by smelting ores or by melting metal (e.g., by casting, alloying, or refining processes) within the metallurgical *chaîne opératoire* system (Haughton, 2014:92) and therefore, copper slag can be divided into two main groups: smelting slags and crucible slags (melting/refining/casting slags) (Bachmann, 1982). Smelting slags and crucible slags are completely different. The first ones are the result of high technological level process, because only advanced metallurgist can be able to transform mineral into metal. On the other hand, the second type of slags are formed during the works of metalsmith. By identifying the type of the slags, it is possible not only to infer about the metallurgical process that occurred within the site but also to infer about the technological level achieved by the ancient metal workers.

However, to differentiate the different types of copper slags, along with the chemical composition the study of micro-structure is very important. In the present study, EDXRF analyses of the 15 slag samples show high Fe, Si and Al content and XRD analyses reveal the presence of quartz and fayalite as the two major mineralogical phases. Moreover, SEM-EDS analyses on selected slag samples also confirm the presence of fayalite phase, for example; in sample 133 A929 1(i) well-formed elongated crystals of fayalite have been seen. Fayalite is a silicate of iron which is very typical in the smelting slags and that is produced during the smelting process, especially in reducing environment (Haughton, 2014). Some copper droplets are also observed. These droplets of metallic copper are generally achieved during the decreasing of temperature, therefore probably achieved during the transformation of minerals ore into copper. Thus, based on the chemical and mineralogical characterization and SEM-EDS microstructure it can be assumed that some of these slags might be obtained during the primary transformation of minerals into copper metal, which is a significant evidence of the smelting activities associated with the site.

Here it is interesting to note that, in some previous research on Arslantepe EBI metal artifacts, researchers found the evidence of use of arsenical copper (Palmieri & Frangipane 1994-1995), but during the present study EDXRF analysis only shows the presence of As in only 9 samples

out of 15 with very low concentrations (.01-.02 % as normalized mass fraction), while SEM-EDS analyses of selected 5 samples do not show any presence of this element. Therefore, the results obtained from the present study could not evident the production of arsenical copper.

6.2 Nature of the thermodynamics

From the study of the micro-chemical and structural characteristics of the slag it is possible to define the technological and scientific-empirical level reached by an ancient community. In general, the chemical microstructure of the slag is closely linked to the specific conditions of pyrometallurgical process which transforms the mineral into metal, to the type of minerals used in the process, to any additives suitable to satisfy the pyrometallurgical requirements of a furnace. Moreover, the complex chemical micro-structure of a slag composed of different phases in equilibrium between them, provides a detailed and permanent reminder of the thermal and chemical conditions present in the furnace. The results of the micro-structural and micro-chemical investigations can therefore clarify their nature (of primary production and post-processing) and help to determine the level of technological competence achieved during the complex chemical-physical processes that are at the base of obtaining metals or alloys.

The reactions that are at the base of the formation of the slag, between silica and silicates with the iron oxides, both contained in the fissure rocks, and any intentionally added substances, had to lead to the formation of metallurgically active waste and able to satisfy the requirements of the process and produce good quality metal. Only a profound knowledge, even if empirical, of the genesis and properties of the slag could allow the effective conduction of the different phases and reactions of the pyro-metallurgical process and its optimal control.

In fact, to improve the separation of the slag from the solid metal copper a controlled excess of iron oxides was used, which formed with the high-melting silica part contained in the metal-bearing rocks, a fayalitic phase (Fe_2SiO_4) characterized by melting points varying from 1150°C at 1200°C, the typical process temperatures of the ancient furnaces (Bachmann 1982; Hauptmann 2007). The skill of the metallurgist consisted, therefore, in calibrating and guiding these reactions and using the least possible amount of iron oxides to maximize the metal produced.

Here, it should be noted that, fayalite (Fe_2SiO_4) is very rare in nature, but common in man-made metallurgy, especially in early copper and iron smelting slags (Bachmann 1982; Hauptmann 2007; Rehren *et al*, 2016). It is the iron-rich end-member of the olivine solid-

solution series, generally forms solid solution with the magnesium olivine endmember forsterite (Mg_2SiO_4) and also with the manganese rich olivine endmember tephroite (Mn_2SiO_4) (fig. 37a & b) (Smyth, 1975). Therefore, the presence of fayalite crystals in a copper slag indicate strongly reducing conditions with an equilibrium between both ferric and ferrous iron oxide, diagnostic for the conditions required to reduce copper oxide to copper metal (Rehren *et al*, 2016).

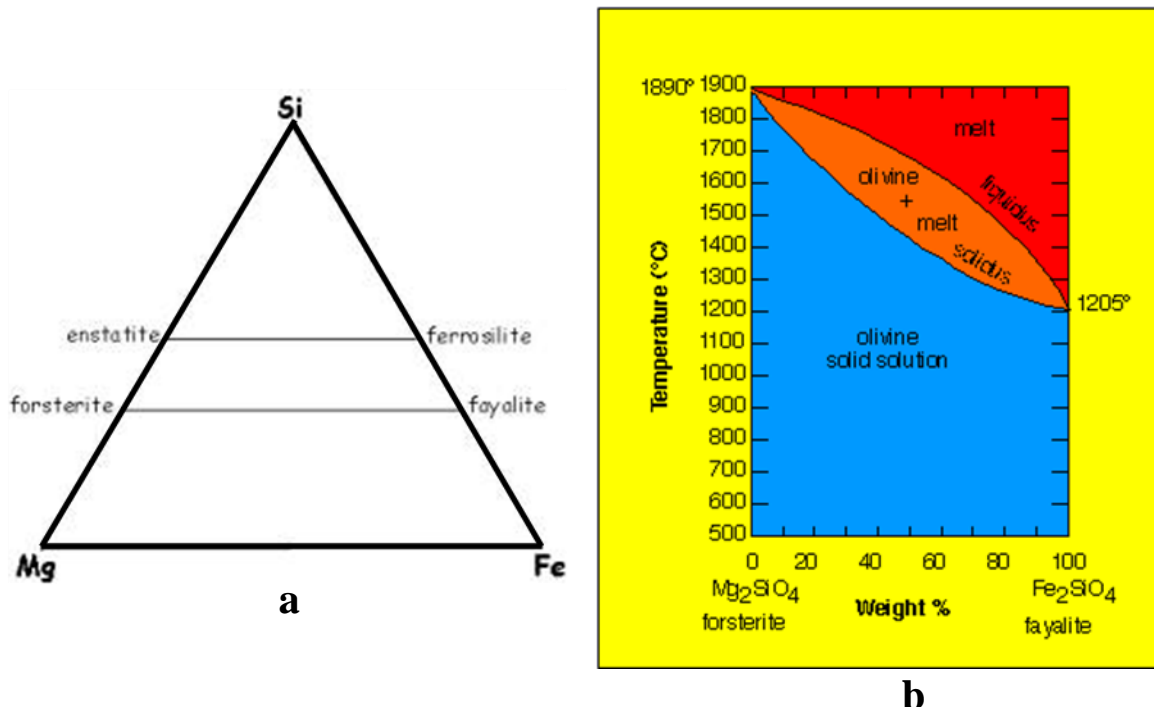


Fig. 37: (a) Ternary diagram of Si-Fe-Mg. Here FeO-SiO₂ binary are shown on one side of the triangle, and an analogous MgO-SiO₂ binary on the other side of the triangle. The solid solution series between the olivine and pyroxene end members form horizontal lines parallel to the base of the triangle. (b) Phase diagram for the components forsterite and fayalite. Here are graphically represented the equilibrium relationships governed by the laws of thermodynamics between these two minerals. (retrieved from <http://clay.uga.edu/courses/8550/olivinephase.gif>)

In the present study, the results of XRD powder analysis and SEM-EDS microstructure demonstrate the existence of a metallurgical activity aimed at the transformation of copper ore into metal and its subsequent processing. The process was conducted by metallurgist skilled in controlling the transformation processes of minerals in order to produce both the metal and a liquid slag that could easily separate from the solid metal copper and whose melting temperature was about 1150° C. The process led to the formation of well-formed fayalite crystals, surrounded by an amorphous gray glassy phase composed of calcium and iron-silico-aluminate. For example, SEM-EDS image of 133 A929(i) shows that the fayalite is well

crystallized and evidence of an optimal thermodynamic and kinetic control of the process and of a solidification occurred inside the furnace with a slow cooling.

The presence of quartz, cristobalite low and magnetite, syn as mineral phases in analyzed slag samples are also very significant to understand the related thermodynamics system. X-ray powder diffraction analyses reveal that hexagonal quartz phase is present in the analyzed samples. Hexagonal quartz also known as beta-quartz, which is a high-temperature ($> \sim 573^{\circ}\text{C}$) polymorph of silica with a very similar crystal structure of quartz (quartz-trigonal, Beta quartz-hexagonal) (Heaney,1994). This is usually unstable at room temperature and cannot be quenched from high temperature. The phase transition is at about 573°C at ambient pressures. When heated quickly, beta-quartz melts at about 1550°C , otherwise it will turn into beta-cristobalite at around 1050°C . The temperature of the phase transition from quartz to beta-quartz increases with pressure (fig.38).

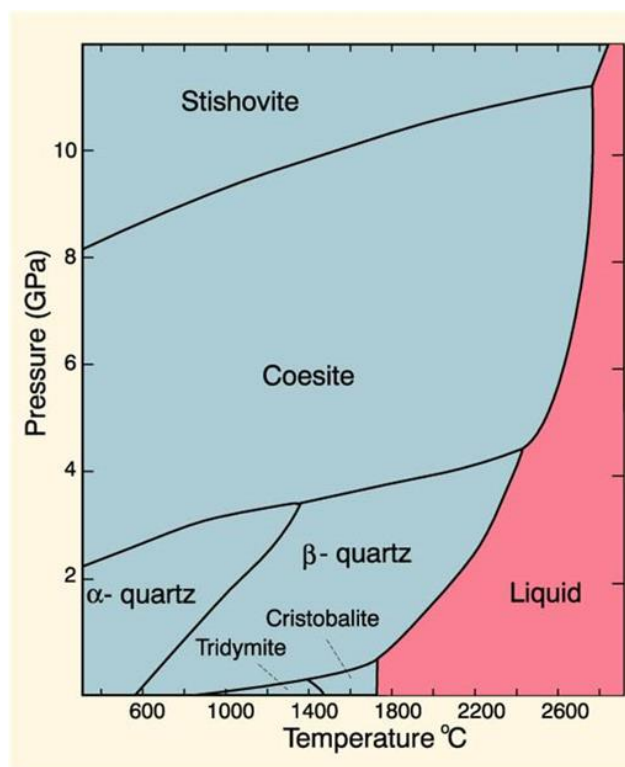


Fig. 38: The phase diagram for SiO₂ (retrieved from https://serc.carleton.edu/research_education/equilibria/simplephasediagrams.html)

However, beta quartz and cristobalite low share a significant relationship. Cristobalite is a silica polymorph that is thermodynamically stable only at temperatures above 1470°C , up to the melting point at 1705°C , at atmospheric pressures (Bath, 1932). Cristobalite has two modifications: low-cristobalite (also known as α cristobalite), which occurs naturally up to

268° C (514° F) but is not stable; and high cristobalite also known as β cristobalite), which occurs above 268° C but is only stable above 1,470° C. The presence of cristobalite low indicates that reducing temperature in which beta quartz turns into cristobalite. Magnetite is another characteristic phase that is formed during a smelting process under just slightly reducing conditions, ie. under a low cover charcoal and allowing for the access of air. Therefore, the presence magnetite phase in a copper slag also indicate a reducing environment during the smelting activities (Hauptman, *et al*, 2003b).

6.3 Nature of the ore

Based on the archaeometric results, it can be assumed that ancient metal workers might be exploiting copper ore from the polymetallic sulfide deposits of the eastern Anatolia, where chalcopyrite is the dominant copper-bearing mineral. This is aptly demonstrated by the presence of sulphur. Here it is needed to mention that, type of the ore is one of the key factors related to the formation of slags, the purer the ore, the less slag will be formed (Bachmann, 1982, Bourgarit, 2007). Refining processes, like crucible melting can reduce the noticeable amount of slag and sometimes left none at all, perhaps only some dross or a slagging ('glazing', vitrification) of the ceramic material of the crucible used for the operation (Bachmann, 1982).

In the present study, EDXRF and SEM-EDS analyses showed the presence of sulphur in all slag samples, though in very low concentration, this is very important and crucial information regarding the nature of the ore. This indicates that the smelted ore contained a significant amount of sulphide minerals and was not a pure oxidic copper ore such as malachite or azurite. The analyzed slag types must have been the result of the processing of copper-rich sulphidic ores such as chalcopyrite (CuFeS_2), the dominating ore type available in Eastern Anatolia.

6.4 Crucible properties

In the present study, along with the slags, two crucible fragments were analyzed by using only EDXRF techniques. Due to the availability of instrument, XRD and SEM-EDS analyses were not done on these crucible samples. However, chemical composition of crucible samples was almost same to the slag samples. Based on the result it can be assumed that both fragments were a part of crucible which might be related to the copper smelting or copper related activities. Besides, presence of green particles and highly vitrified area (fig. 39 A1, and B1) also evident that these fragments were might be a part of specialized activities related to copper metallurgy.

It is interesting to note that both fragments are highly vitrified in terms of inside but outside they are not vitrified (fig.39A1, A2, A3, B1, B2, and B3). In many experimental reconstructions of archaeometallurgical process, it is proven that the early bronze age crucibles were not heated from the outside, they are heated in inside (Rehren, 2004). In case of present samples, it is also evident that they might be heated from the top or from inside, not the outside which might cause the internal part to transform into highly vitrified area. Unfortunately, both analyzed samples are body fragments, hence, any idea regarding their shape could not be determined.

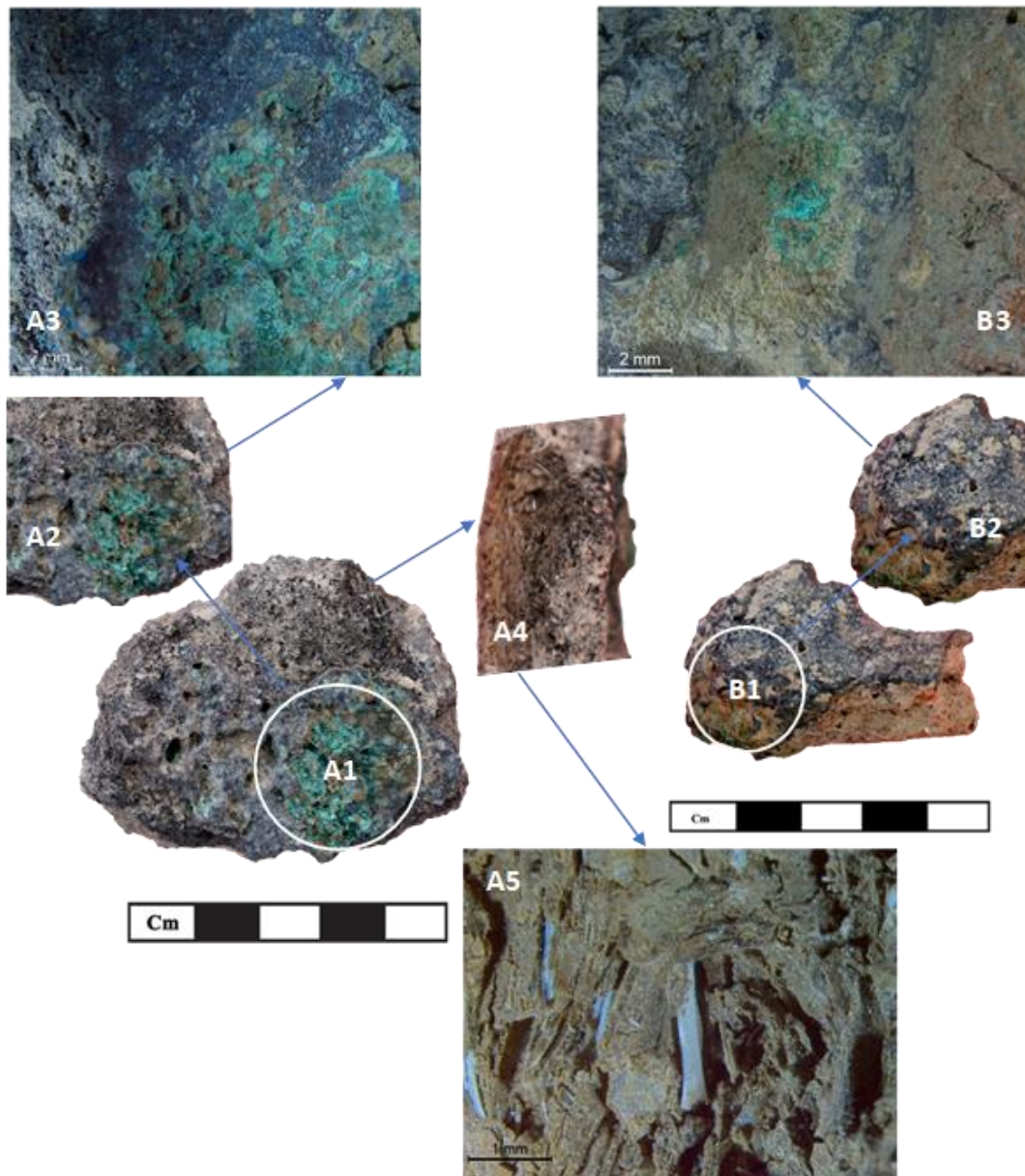


Fig. 39: (A1) Slag and vitrified area of crucible sample 133 A929 1A, (A2) magnified detail of the same area, (A3) stereomicroscope image of the same area, (A4) A core area of the crucible sample 133 A929 1A, (A5) stereomicroscope image of the unidentified white inclusion in the same core area, (B1) slag and vitrified area of crucible sample 133 A929 1B, (B2) magnified detail of the same area , (B3) stereomicroscope image of the same area.

While conducting the studies on these two crucible fragments, an interesting query was developed regarding the tempered materials used to them. In sample 133 A929 1A, some white inclusions were visible in the core, these inclusions were also observed under a Leica M205C stereo microscope, but not possible to identified (fig 39 A4, A5). From the thermomechanical point of view crucibles must be strong enough to absorb the heat and to hold the liquid metal, otherwise they will be broken during the work. Some researches show that in ancient times to improve the crucible properties, clay is modified by adding quartz, whose melting points is about 3000°C, and that increased the refractories features. The early bronze age crucible qualities were also improved by adding the organic tempers (Rehren, 2004, 2011). In the present study it was not possible to determine whether these crucible fragments were truly refractories in nature, or their qualities were modified by intentional adding of organic temper materials. In future, optical microscopic and SEM-EDS analyses can provide more significant inside regarding this issue.

6.5 Weathering phenomenon

One of the interesting aspects of the present study is that the results of EDXRF and X-ray powder diffraction analysis of each slag samples show very consistent chemical and mineralogical composition. These homogenous composition of analyzed slag samples suggests that either these samples were produced in a very similar manner in terms of the methodological approach to technology and the ingredients used, or theses might be due to the long-time deterioration process under the same weathering conditions. In case of this study, the later seems more convenient than the former one.

In generals, slags are considered as a highly resistant materials (Bachmann, 1982; Hauptmann, 2014), but it would be also wise to count their post depositional and burial conditions. In the present research, all analyzed slags and crucibles fragments come from Arslantepe early bronze age Ib (3100-2900BC), which means all analyzed samples going through a some short of deterioration processes over 5000 years, and these could have transformed completely the external parts of the samples. Besides, same burial conditions might be play an important role also. This degradation trend is easily visible by the presence of green particle in the outer part of the slag and crucible samples, which might be degraded products of copper. However, SEM-EDS analyses show some evidence of degradation processes, for example, in SEM-EDS elemental maps of sample 144 A929 1b (iv), copper droplets were seen in association with

chlorine. This association might be due to the burial condition, which accelerate the transformation of metallic copper into copper chloride.

Moreover, X-ray powder diffraction analyses also evidence the deterioration processes of analyzed samples. For example, scarce amount of maghemite, sync was found in almost all analyzed 9 slag samples. It is worthy to mention that maghemite ($\gamma\text{-Fe}_2\text{O}_3$) is a ferric oxide with similar cubic spinel crystal structure and ferrimagnetic properties to magnetite. It is an unstable mineral and generally forms by weathering or low temperature oxidation of magnetite (Anthony, et al,1997) (fig.40). Based on the overall features of analyzed samples it can be assumed that these analyzed samples are going through a degradation process, where ferrous nature of slag and the presence of oxygen and the chlorine content of soil might be played a vital role.

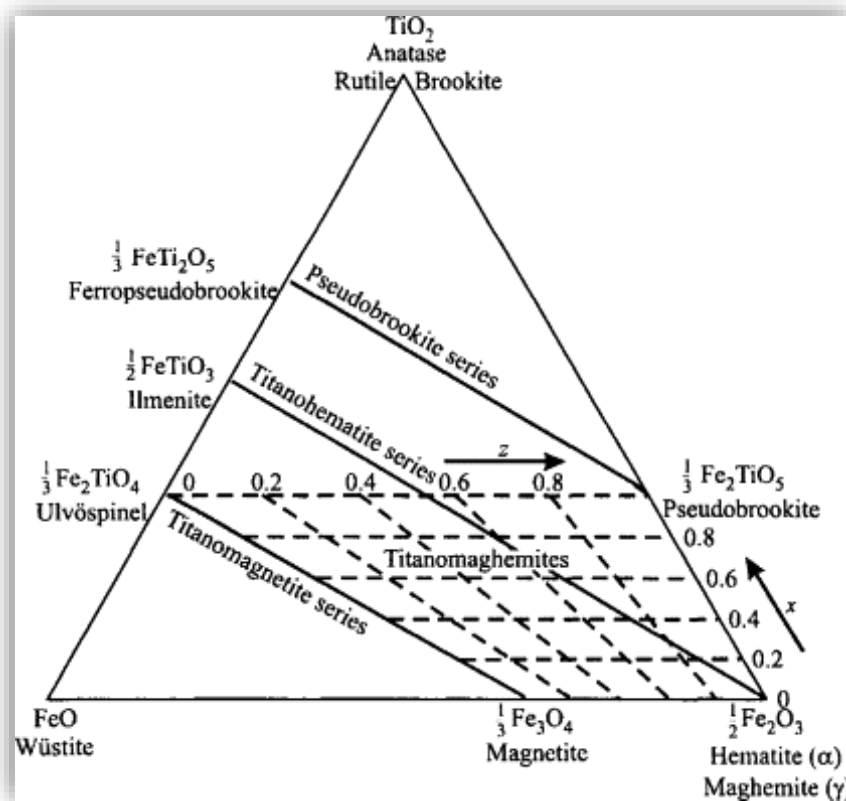


Fig. 40: Ternary compositional diagram of iron-titanium-oxide solid solution magnetic minerals. During low temperature oxidation, the bulk composition follows the horizontal dashed lines, where z is the oxidation parameter and x is the titanomagnetite composition parameter. (retrieved from <https://www.sciencedirect.com/topics/earth-and-planetary-sciences/maghemite>)

CHAPTER 7: FINAL REMARKS

7.1 Research findings

The aim of this research was to determine the chemical and mineralogical characterization and the micro structure study of slag and crucible samples from the village of Early Bronze Age I (VI B2 period, 3100-2900 BC) at Arslantepe. This work provides a significant insight into the nature of slags and the metallurgical processes relevant to them. Interestingly, EDXRF and powder XRD analysis of each slag samples showed that all analyzed slags are highly homogenous in terms of chemical and mineralogical composition. Iron (Fe), silicon (Si) and aluminum (Al) are predominate in all samples. Relatively low amount of copper (Cu) and calcium (Ca) are present in all samples along with lesser concentrations of other elements e.g., potassium (K), titanium (Ti), vanadium (V), chromium (Cr), manganese (Mn), zinc (Zn), molybdenum (Mo) and strontium (Sr). Phosphorus (P) is present in only two sample (133 A929 1(ii) and 133 A929 1(iv)), while nickel (Ni), arsenic (As), tin (Sn), antimony (Sb) and lead (Pb) were not detected in all samples. However, the element sulphur is present in all analyzed slag samples with very low concentration. From the presence of sulphur, it can be assumed that the early bronze age metal workers might have exploited some minerals to transform metal in which sulphide minerals were also associated.

Regarding the mineralogical composition, quartz and fayalite were identified as a major mineralogical phase along with the magnetite as minor phase in all analyzed slag samples. Due to the availability of the instrument, among the 15 slag samples, only 5 samples were selected for the micro structure studies. SEM-EDS analyses of slag sample 133 A929 1(i) and 133 A 929 1(iv) show the presence of well-formed elongated fayalite crystals as a major phase along with the metallic copper droplets. The SEM-EDS images of sample 144 A929 1b(iii), 144 A929 1b(iv) and 146A929 1c (i) do not show the well grown fayalite crystals.

The overall features of analyzed samples indicate that some of them were produced during the primary smelting process and some of them might be formed during the works of metal. Hence, it can be assumed that both copper smelting and melting activities were attested at Arslantepe in period VIB2 which correspondent to Early bronze age Ib. All samples have very similar chemical compositions, and this suggests that either these samples were produced in a very similar manner in terms of the methodological approach to technology and the ingredients used, or that these might be due to the long-time deterioration process under the same weathering

conditions. The micro structure of some slag samples, e.g. 133 A929 1(i) shows the presence of elongated fayalite crystals. It can be assumed that these fayalite crystals might be produced in a slow cooling system which demonstrate that at Arslantepe in period VIB2 early bronze age metal workers already achieved a significant level of skilled to control the smelting environment.

Overall, chemical composition of the slags demonstrates the capacity to balance the starting constituents of the furnace charge, further, the presence of well crystallised fayalite and the low presence of “lost copper” finely dispersed in the slag (not recoverable) demonstrate the good skill of the metalsmiths.

7.2 Research contributions and prospects for future research

The findings of this research will reflect the benefit of archaeometric research and will be a contribution to the field of Early Bronze Age metallurgy and Ancient Near Eastern studies. Moreover, it can be also a reference for a detailed understanding of the technological advancement and the consequent impact on the socio-economic structure and the cultural diversity.

Furthermore, several opportunities for future research can be emerged from this present work to investigate the Early Bronze Age copper smelting and the related thermodynamics. For example, experimental research will provide answers to questions about prehistoric smelting furnace and thermal treatment. Such experiments will provide valuable information on the advantages and disadvantages of the use of different type of ores and the role of crucible in metallurgical processes. Linking these slags to possible ore sources can be another important subject for the future study. Future research can also look into prehistoric firing strategies in order to answer questions about the efficiency of extraction and the fuel resources that were available to early bronze age metal workers at Arslantepe.

7.3 Limitations

Every scientific research is associated with lot of limitations from the beginning to the end and it is essential to minimize the limitations for a better outcome. This research was not an exception in terms of limitations. However, this research is often directed by the available means, being expertise, analytical techniques and equipment. For example, instead of WDXRF, EDXRF analyses were done for the chemical characterization of slag and crucible samples, though former one is more useful than the later and this was happened due to the availability



of instrument. Besides, analysis was done on small cutting part of each slag sample not on the core and due to the degradation of slags in the soil, the external part of the slag was completely changed. Hence, EDXRF results may not completely represents the composition of the slag itself, but also the degradation products present in the slags, Moreover, due to the availability of the instrument, SEM-EDS analyses could not performed for each samples which limited the microstructure study of all slag samples and also restricted the precise description of the metallurgical process relevant to them.

REFERENCES

- Adriaens, A., Yener, K. A. & Adams, F. (1999). An analytical study using electron and ion microscopy of thin-walled crucibles from Göltepe, Turkey. *Journal of Archaeological Science*, 26(8), 1069–1073.
- Anthony, John W.; Bideaux, Richard A.; Bladh, Kenneth W.; Nichols, Monte C., eds. (1997). "Maghemite". *Handbook of Mineralogy (PDF). III (Halides, Hydroxides, Oxides)*. Chantilly, VA, US: Mineralogical Society of America. ISBN 0962209732.
- Bachmann, H. G. (1982). *The Identification of Slags from Archaeological Sites*. Institute of Archaeology, University of London, Occasional Papers 6.
- Barth, T.F.W. (1932). The cristobalite structures: II. Low cristobalite. *American Journal of Science*: 24: 97-110.
- Bayley, J., & Rehren, Th. (2007). Towards a functional and typological classification of crucibles. In S. LaNiece, D. Hook, & P. Craddock (Eds.), *Metals and Mines—Studies in Archaeometallurgy*, 46–55. London: Archetype.
- Bokonyi, S. (1983). Late Chalcolithic and Early Bronze I animal remains from Arslantepe (Malatya), Turkey: a preliminary report, *Origini*, XII (2), 581-598.
- Bourgarit, D. (2007). Chalcolithic copper smelting. In S. La Niece, D. Hook, & P. T. Craddock (Eds.), *Metals and mines: Studies in archaeometallurgy*, 3–14. London: Archetype Publications.
- Brouwer, P. (2003). *Theory of XRF: Getting acquainted with the principles*, Netherland:PNAalytical BV.
- Caneva, C. and Palmiri, A.M. (1983). Metal work at Arslantepe in Late Chalcolithic and Early Bronze I: the evidence from metal analyses in *Perspectives Protourbanization in Eastern Anatolia, Arslantepe (Malatya)*.
- Carter, G. F. (1978). Precision in the X-ray fluorescence analysis of sixty-one Augustan quadrantes, *Journal of Archaeological Science*, 5, 293–300.
- Castellano, A. Martini, M. and Sibilla, E. (2007). *Elementi di Archeometria. Metodi fisici per I beni culturali*, Second edition.
- Choyke, A. M. (2000). Bronze Age antler and bone manufacturing at Arslantepe (Anatolia). In Mashkour, M. - Choyke, A. M. - Buitenhuis, H. (eds.), *Archaeozoology of the Near East IVA.*,170-183. ARC Publication 32: Groningen.
- Craddock, P. T. (1995). *Early metal mining and production*. Edinburgh: University of Arizona



- Press. de Jesus, P. S. (1980). *The development of prehistoric mining and metallurgy in Anatolia. BAR International Series 74*. Oxford: BAR.
- Craddock, P. T. (2013). Refractories: ceramics with a purpose, *The Old Potter's Almanack*, 18, 9–20.
- Dercksen, J. G. (2005). Metals according to documents from Kültepe-Kanish Dating to the old Assyrian Colony. Period. In Ü.Yalçın (Ed.), *Anatolian Metal III (pp. 17-34)*. *Der Anschnitt 18*. Bochum: Deutsches Bergbau-Museum.
- Delrue, P. (2008). *Archaeometallurgical analyses of pre-Islamic artefacts from ed-Dur (Emirate of Umm al-Qaiwain, U.A.E.)*. Ghent University. Faculty of Arts and Philosophy, Ghent, Belgium.
- Di Nocera, G.M. (2013). Organization of Production and Social Role of Metallurgy in the Prehistoric Sequence of Arslantepe (Turkey). *Origini*, 35, 111-142.
- Frangipane, M. and Palmieri, A. (1983). Cultural Developments at Arslantepe at the Beginning of the Third Millennium BC. *Origini*, 12, 523-575.
- Frangipane, M. (1993). Local components in the development of centralized societies in Syro-Anatolian regions. In Frangipane M, Hauptmann H, Liverani M, Matthiae P, Mellink M (eds) *Between the rivers and over the mountains. Studi in Memoria di Alba Palmieri*, 133–161. Università La Sapienza, Roma.
- Frangipane, M. and Palmieri, A. M. (1994–1995) *Un modello di ricostruzione dello sviluppo della metallurgia antica: il sito di Arslantepe. Scienze dell'Antichità* 8–9, 59–78.
- Frangipane, M. et al. (2002). "New symbols of a new power in a "royal" tomb from 3000 BC Arslantepe, Malatya (Turkey)", *Paleorient* 27/2: 105-139.
- Frangipane, M. (2012). Arslantepe-Malatya: A Prehistoric and Early Historic Center in Eastern Anatolia. *The Oxford Handbook of Ancient Anatolia: (10,000-323 BCE (March)*. <https://doi.org/10.1093/oxfordhb/9780195376142.013.0045>
- Frangipane, M. (2016). The development of centralized societies in Greater Mesopotamia and the foundation of economic inequality. In H. Meller, H.P. Hahn, R. Jung, R. Risch, (eds), *Arm und Reich / Rich and Poor – Competing for Resources in Prehistoric Societies*, 469-489, SN- 978-3-944507-45-3.
- Frangipane, M. (2017). The Role of Metallurgy in Different Types of Early Hierarchical Society in Mesopotamia and Eastern Anatolia. In Stockhammer, P.W., & Maran, J. (eds) *Appropriating innovations entangled knowledge in Eurasia, 5000-1500 BCE*. 172-183. Oxford: Oxbow Books.



- Freestone, I.C. (1985). Scanning electron microscopy and X-ray microanalysis. In Phillips, P (ed) *The Archaeologist and the Laboratory*, 67-68. CBA Research Report 58. Oxford: Council for British Archaeology London.
- Freestone, I. C. (1989). Refractory materials and their procurement, in A. Hauptmann, E Pernicka, and G.Wagner, (eds.), *Old World Archaeometallurgy. Der Anschnitt, Beiheft 7*, 155–162. Bochum: Deutsches Bergbau-Museum.
- Garzanti, E., Al-Juboury, A., *et al.* (2016). The Euphrates-Tigris-Karun river system: Provenance, recycling and dispersal of quartz-poor foreland-basin sediments in arid climate. *Earth-Science Reviews*. 162. 10.1016/j.earscirev.2016.09.009.
- Hauptmann, A., Schmitt-Strecker, S., Begemann F. and Palmieri, A. (2003a). "Chemical Composition and Lead Isotopy of Metal Objects from the Royal Tomb and Other Related Finds at Arslantepe, Eastern Anatolia", *Paleorient* 28:43-70.
- Hauptmann, A., Rehren, Th., & Schmitt-Strecker, S. (2003b). Early Bronze Age copper metallurgy at Shahr-I Sokhta (Iran), reconsidered. In Th. Stöllner, G. Körlin, G. Steffens and J. Cierny (eds), *Man and Mining-studies in honour of Gerd Weisgerber on occasion of his 65th birthday*. 197-214. Bochum.
- Hauptmann, A. (2007). The Archaeometallurgy of copper, Evidence from Faynan, Jordan. In G. A.Wagner, B. Herrmann (Eds.), *Natural Science in Archaeology* (p.270). Heidelberg:Springer.
- Hauptmann, A. (2014). The investigation of archaeometallurgical slag, in B. W. Roberts and C. P. Thornton, (eds.), *Archaeometallurgy in Global Perspective*, 91–105. Springer.
- Heaney, P.J. (1994). Structure and chemistry of the low-pressure silica polymorphs. In: *Reviews in Mineralogy*, Volume 29, Silica - Physical behavior, geochemistry and materials.
- Knapp, A. B. (1998). Social approaches to the archaeology and anthropology of mining. In A. B. Knapp, V. C. Pigott, & E. W. Herbert (Eds.), *Social approaches to an industrial past: The archaeology and anthropology of mining* (pp. 1–23). London: Routledge.
- Lehner, W., Joseph & Yener, K. (2013). Organization and Specialization of Early Mining and Metal Technologies in Anatolia. In B.W. Roberts and C. P. Thornton, eds., *Archaeometallurgy in Global Perspective: Methods and Syntheses*. 529-557. Springer.
- Martinón-Torres, M. and Rehren, Th. (2014). Technical ceramics. In B.W. Roberts and C. P. Thornton, eds., *Archaeometallurgy in Global Perspective: Methods and Syntheses*, 107–131. Springer.



- Manuelli, F. (2013). Arslantepe IX–Late Bronze Age; Hittite Influence and Local Traditional in an Eastern Anatolian Community. Frangipane, M., (Ed). Grafica Cristal S.r.l, Roma.
- Palmieri A.M., Frangipane m., Hauptmann A. and Hess K. (1999). Early metallurgy at Arslantepe during the Late Chalcolithic and the Early Bronze Age 1A-1B periods. In Hauptmann A. et al. (eds), *The Beginnings of Metallurgy. Der Anschnitt Beiheft* :9 141-148. Bochum: Deutsches Bergbau Museum.
- Piccione, P. (2010). The Ceramic containers of period VI B2: food storage, processing and consumption in village community of the Early 3rd Millennium. In M. Frangipane (ed), *Economic centralisation in formative state. The archaeological reconstruction of the economic system in 4th millennium Arslantepe*, 205-230. Roma: Studi di Preistoria Orientale 3.
- Piccione, P., Cristina L. (2012). Vessels, Tools and Space use at Arslantepe in period VI B2. Everyday life in an EB I village, *Origini XXXIV*, 279-29.
- Piccione, P., Alvaro, C., Bartosiewicz, L., Lemorini, C., Masi, A., & Sadori, L. (2015). Distribution of artifacts and ecofacts in an Early Bronze Age house in Eastern Anatolia: Space use and household economy at Arslantepe VI B2 (2900-2750 BCE) *Journal of Archaeological Science: Reports*, 4, 8–22.
<https://doi.org/10.1016/j.jasrep.2015.08.035>
- Pollard A M, Batt C M, Stern B, and Young S M M (2011). *Analytical Chemistry in Archaeology*. Cambridge: Cambridge University Press.
- Rademakers, F. W. and Rehren, Th. (2014). Heterogeneity in the crucible. Some methodological issues for reconstructing ancient crucible metallurgy, Poster presented at the 40th International Symposium on Archaeometry, 19-23 May 2014, Los Angeles, USA.
- Rademakers, F.W. A. (2015). *Into the Crucible: Methodological approaches to reconstructing crucible metallurgy, from New Kingdom Egypt to Late Roman Thrace*, unpublished thesis, University College London. UCL Institute of Archaeology, London, UK.
- Rehren, Th. (2003). Crucibles as reaction vessels in ancient metallurgy. In P. Craddock & J. Lang (Eds.), *Mining and Metal Production through the Ages*, 207–215 and 147–149. London: British Museum.
- Rehren, T. & Thornton C. P, (2009). A truly refractory crucible from fourth millennium Tep Hissar, Northeast Iran, *Journal of Archaeological Science*, 36, 2700–2712.
- Rehren, Th., Leshtakov, P., Penkova, P. (2016). Reconstructing Chalcolithic copper smelting

- at Akladi cheiri, Chernomorets, Bulgaria. In: *Der Schwarzmeerraum vom Neolithikum bis in die Früheisenzeit (6000-600 v.Chr.)* V. Nikolov & W. Schier (eds), *Leidorf*.
- Sadori, L., Susanna, F., & Persiani, C. (2006). Archaeobotanical data and crop storage evidence from an early Bronze Age 2 burnt house at Arslantepe, Malatya, Turkey. *Vegetation History and Archaeobotany*, 15(3), 205–215.
<https://doi.org/10.1007/s003340050029-3>.
- Sadori, L., Susanna, F., Balossi Restelli F. (2008). Collapsed beams and wooden remains from a 3200 BC temple and palace at Arslantepe (Malatya, Turkey). In Fiorentino G, Magri D, eds. *Charcoals from the Past. Cultural and Palaeoenvironmental Implications*, 103-116. Oxford: BAR.
- Shackley, M. S. (2011). An introduction to X-Ray Fluorescence (XRF) analysis in archaeology, in M. S. Shackley, (ed.), *X-Ray Fluorescence Spectrometry (XRF) in Geoarchaeology*, Springer Science, pp. 7–44.
- Smyth, J.R. (1975). High temperature crystal chemistry of fayalite. *American Mineralogist*: 60: 1092-1097.
- Vignola, C., Masi, A., Balossi Restelli, F., *et al.* (2017). $\delta^{13}\text{C}$ and $\delta^{15}\text{N}$ from ^{14}C -AMS dated cereal grains reveal agricultural practices during 4300-2000 BC at Arslantepe (Turkey). *Rev Palaeobot Palyno*, 247,164-174.
- Vignola, C., Masi, A., Balossi, Restelli F., *et al.* (2018). $\delta^{13}\text{C}$ values in archaeological ^{14}C AMS dated charcoals: Assessing mid-Holocene climate fluctuations and human response from a high-resolution isotope record (Arslantepe, Turkey). *Rapid Commun Mass Spectrom*, 32, 1149-1162. <https://doi.org/10.1002/rcm.8137>.
- Vignola, C., Marzaioli, F., *et al.* (2019). Changes in the Near Eastern chronology between the 5th and the 3rd millennium BC: New AMS ^{14}C dates from Arslantepe (Turkey). *Nuclear Instruments and Methods in Physics Research, Section B: Beam Interactions with Materials and Atoms*, 456,276-282.
<https://doi.org/10.1016/j.nimb.2019.01.033>.
- Watt, I. M. (1997) *The Principles and Practice of Electron Microscopy*, Cambridge: Cambridge University Press. <https://doi.org/10.1111/j.1365-2818.1990.tb03026.x>.



APPENDIX

1.1 EDXRF elemental analysis of three different points of each slag samples, results are shown as normalized mass fractions (%)

Element	Sample ID																
	133 A929 1(i)_1	133 A929 1(i)_2	133 A929 1(i)_3	133 A929 1(i)_4	133 A929 1(ii)_1	133 A929 1(ii)_2	133 A929 1(ii)_3	133 A929 1(iii)_1	133 A929 1(iii)_2	133 A929 1(iii)_3	133 A929 1(iv)_1	133 A929 1(iv)_2	133 A929 1(iv)_3	133 A929 1(iv)_4	133 A929 1(v)_1	133 A929 1(v)_2	133 A929 1(v)_3
Al	36.87	27.57	23.75	43.92	12.04	24.43	64.78	62.80	40.71	33.12	42.60	46.93	43.88	41.06	23.87	33.87	60.12
Si	39.25	55.87	54.29	29.54	66.67	47.57	20.17	24.37	38.55	34.93	25.27	25.97	29.21	23.99	59.68	40.90	17.70
P	0.00	0.00	0.00	0.00	0.00	0.00	1.09	0.00	0.00	0.00	0.00	0.00	0.00	1.51	0.00	0.00	0.00
S	0.42	1.35	0.38	0.07	0.25	0.33	0.26	0.38	0.40	0.31	0.22	0.32	0.34	0.60	0.09	0.26	0.47
K	0.12	0.13	0.11	0.24	0.10	0.18	0.61	0.08	0.13	0.34	0.42	0.18	0.22	0.67	0.03	0.07	0.42
Ca	1.57	1.05	2.98	3.75	2.84	3.81	1.88	1.46	2.49	4.06	5.41	1.92	2.40	3.35	0.66	1.54	3.15
Ti	0.06	0.03	0.04	0.06	0.06	0.06	0.03	0.03	0.04	0.06	0.07	0.06	0.04	0.07	0.03	0.04	0.07
V	0.01	0.01	0.03	0.01	0.03	0.04	0.00	0.01	0.02	0.03	0.02	0.02	0.02	0.13	0.02	0.02	0.00
Cr	0.10	0.04	0.04	0.06	0.05	0.06	0.03	0.01	0.03	0.06	0.07	0.05	0.06	0.07	0.02	0.04	0.04
Mn	0.11	0.05	0.08	0.10	0.08	0.12	0.05	0.04	0.07	0.11	0.09	0.07	0.06	0.09	0.06	0.10	0.09
Fe	20.24	11.01	16.95	21.44	16.59	22.33	10.46	9.11	15.71	26.00	24.54	19.45	21.48	22.62	14.53	16.90	17.09
Ni	0.00	0.00	0.00	0.00	0.01	0.00	0.01	0.02	0.00	0.00	0.00	0.00	0.00	0.00	0.02	0.00	0.02
Cu	1.06	2.84	1.27	0.68	1.19	0.93	0.43	1.38	1.77	0.89	1.22	4.97	2.03	5.56	0.92	6.18	0.47
Zn	0.03	0.02	0.02	0.04	0.02	0.02	0.02	0.02	0.02	0.04	0.03	0.03	0.02	0.10	0.01	0.03	0.13
As	0.00	0.02	0.00	0.00	0.00	0.00	0.00	0.00	0.02	0.00	0.00	0.00	0.00	0.09	0.00	0.03	0.00
Sr	0.02	0.01	0.01	0.01	0.01	0.02	0.02	0.01	0.01	0.01	0.01	0.00	0.01	0.02	0.00	0.01	0.05
Mo	0.04	0.02	0.01	0.02	0.02	0.02	0.02	0.03	0.02	0.01	0.01	0.02	0.04	0.02	0.02	0.02	0.09
Sn	0.00	0.00	0.00	0.04	0.00	0.04	0.00	0.06	0.00	0.00	0.00	0.19	0.22	0.00	0.00	0.00	0.00
Sb	0.00	0.00	0.00	0.00	0.00	0.00	0.00	0.00	0.00	0.00	0.00	0.00	0.00	0.12	0.00	0.00	0.00
Pb	0.10	0.00	0.03	0.07	0.06	0.08	0.16	0.24	0.00	0.02	0.02	0.03	0.17	0.05	0.04	0.00	0.09



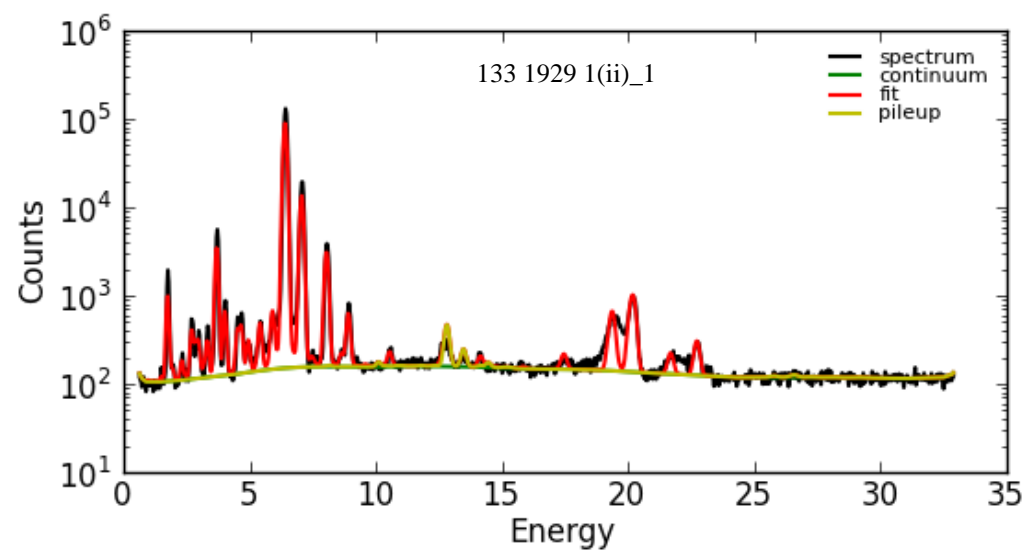
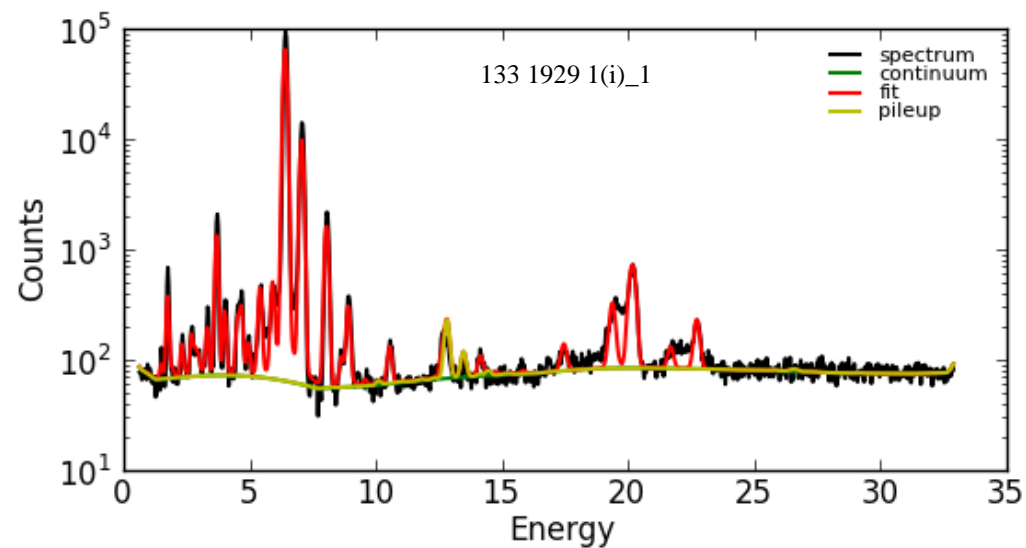
1.2 EDXRF elemental analysis of three different points of each slag samples, results are shown as normalized mass fractions (%)

Element	Sample ID														
	144 A929 1a(i)_1	144 a929 1a(i)_2	144 a929 1a(i)_3	144 A929 1a(ii)_1	144 A929 1a(ii)_2	144 A929 1a(ii)_3	144 A929 1a(iii)_1	144 A929 1a(iii)_2	144 A929 1a(iii)_3	144 A929 1a(iv)_1	144 A929 1a(iv)_2	144 A929 1a(iv)_3	144 A929 1a(v)_1	144 A929 1a(v)_2	144 A929 1a(v)_3
Al	29.35	39.05	35.13	28.56	26.52	33.03	28.28	41.16	39.54	37.14	31.78	41.15	40.04	40.27	40.50
Si	34.10	35.57	43.54	39.23	41.81	33.92	40.79	32.48	35.21	22.00	26.40	20.58	24.79	25.56	38.31
P	0.00	0.00	0.00	0.00	0.00	0.00	0.00	0.00	0.00	0.00	0.00	0.00	0.00	0.00	0.00
S	1.61	0.63	0.51	1.15	0.34	0.99	0.09	0.15	0.31	0.29	0.97	1.18	0.10	0.32	0.27
K	0.15	0.15	0.14	0.14	0.40	0.19	0.45	0.40	0.68	0.15	0.14	0.10	0.21	0.28	0.20
Ca	2.80	2.29	2.00	3.80	3.92	3.87	14.22	12.25	13.35	3.72	4.00	3.09	3.48	4.38	1.72
Ti	0.08	0.04	0.05	0.06	0.07	0.06	0.08	0.07	0.09	0.02	0.03	0.03	0.10	0.12	0.07
V	0.00	0.02	0.02	0.05	0.06	0.05	0.02	0.02	0.01	0.03	0.03	0.02	0.02	0.03	0.04
Cr	0.08	0.05	0.23	0.07	0.08	0.09	0.04	0.05	0.06	0.09	0.08	0.13	0.07	0.08	0.05
Mn	0.12	0.08	0.10	0.13	0.13	0.13	0.10	0.07	0.06	0.13	0.15	0.11	0.15	0.15	0.06
Fe	25.12	18.72	16.22	25.38	25.89	25.80	13.14	11.20	10.17	33.10	33.37	31.82	26.49	25.42	14.53
Ni	0.00	0.00	0.00	0.00	0.00	0.00	0.00	0.01	0.02	0.00	0.00	0.00	0.02	0.03	0.03
Cu	6.46	3.20	1.86	1.29	0.64	1.72	2.54	1.97	0.34	3.26	2.95	1.72	4.43	3.22	4.08
Zn	0.03	0.05	0.12	0.04	0.06	0.05	0.06	0.04	0.04	0.03	0.02	0.02	0.03	0.03	0.02
As	0.00	0.00	0.03	0.00	0.00	0.00	0.00	0.00	0.03	0.00	0.00	0.00	0.00	0.00	0.00
Sr	0.00	0.02	0.01	0.02	0.02	0.02	0.11	0.08	0.09	0.00	0.00	0.00	0.00	0.02	0.01
Mo	0.03	0.03	0.02	0.04	0.03	0.04	0.03	0.02	0.02	0.02	0.02	0.02	0.02	0.02	0.02
Sn	0.00	0.16	0.00	0.00	0.00	0.00	0.00	0.00	0.00	0.00	0.00	0.00	0.00	0.00	0.00
Sb	0.00	0.00	0.00	0.00	0.00	0.00	0.00	0.00	0.00	0.00	0.00	0.00	0.00	0.00	0.00
Pb	0.06	0.08	0.04	0.03	0.03	0.03	0.06	0.04	0.00	0.04	0.04	0.03	0.04	0.07	0.09

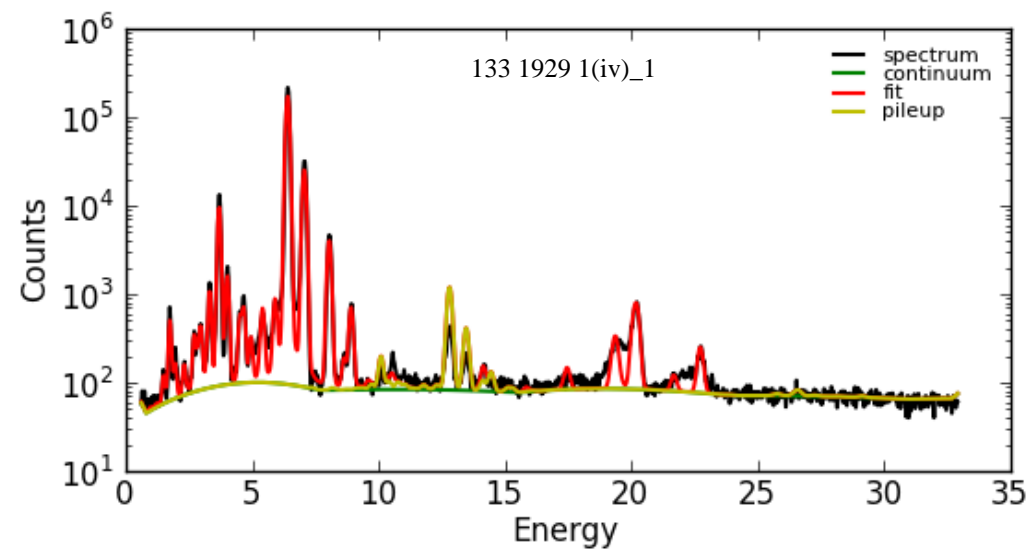
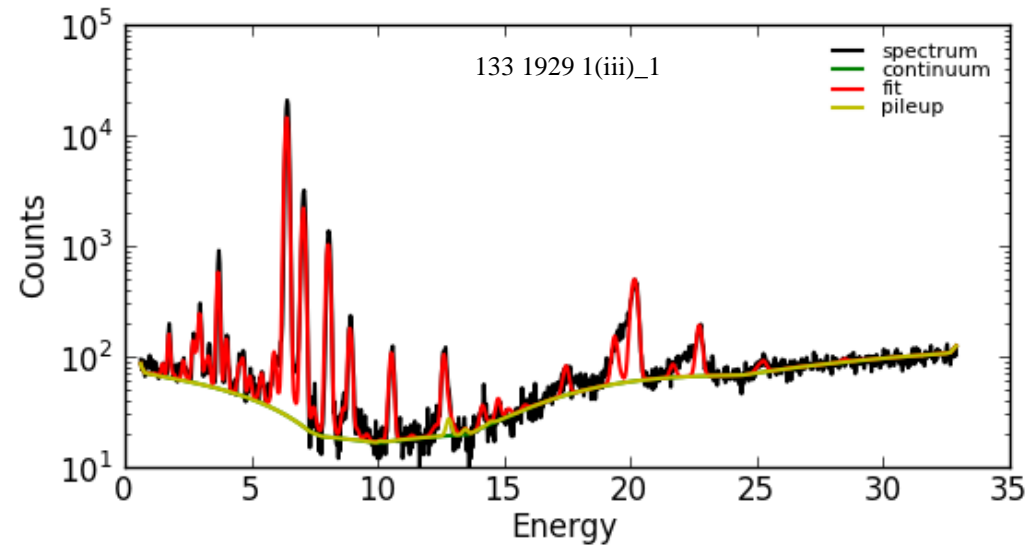
1.3 EDXRF elemental analysis of three different points of each slag samples, results are shown as normalized mass fractions (%)

Element	Sample ID																	
	146 A929 1c(i) 1	146 A929 1c(i) 2	146 A929 1c(i) 3	146 A929 1c(i) 4	146 A929 1c(ii) 1	146 A929 1c(ii) 2	146 A929 1c(ii) 3	146 A929 1c(iii) 1	146 A929 1c(iii) 2	146 A929 1c(iii) 3	146 A929 1c(iii) 4	146 A929 1c(iv) 1	146 A929 1c(iv) 2	146 A929 1c(iv) 3	146 A929 1c(v) 1	146 A929 1c(v) 2	146 A929 1c(v) 3	146 A929 1c(v) 4
Al	25.16	38.84	52.00	35.89	31.49	32.86	36.67	20.10	0.00	37.13	34.26	40.45	54.40	44.32	35.88	30.79	38.03	30.04
Si	43.20	34.74	24.36	38.20	44.42	38.33	37.69	65.85	68.15	37.02	39.83	17.92	15.18	23.79	33.48	44.30	35.61	51.58
P	0.00	0.00	0.00	0.00	0.00	0.00	0.00	0.00	0.00	0.00	0.00	0.00	0.00	0.00	0.00	0.00	0.00	0.00
S	1.89	0.54	0.56	0.53	0.40	0.34	0.33	0.64	1.34	0.88	1.00	0.63	0.50	0.33	0.68	0.95	0.60	0.76
K	0.12	0.14	0.10	0.10	0.12	0.11	0.25	0.00	0.18	0.09	0.10	0.25	0.17	0.30	0.14	0.20	0.11	0.08
Ca	2.84	2.97	2.64	2.35	3.75	3.73	4.19	0.42	0.91	2.68	2.87	2.62	2.88	2.60	3.96	3.02	3.46	2.09
Ti	0.05	0.06	0.05	0.04	0.04	0.05	0.05	0.01	0.08	0.06	0.05	0.05	0.04	0.05	0.06	0.04	0.05	0.03
V	0.02	0.03	0.02	0.02	0.03	0.02	0.03	0.01	0.04	0.01	0.03	0.01	0.00	0.01	0.03	0.05	0.02	0.01
Cr	0.07	0.08	0.07	0.33	0.05	0.06	0.05	0.02	0.08	0.06	0.06	0.06	0.03	0.04	0.07	0.04	0.10	0.02
Mn	0.10	0.10	0.08	0.09	0.09	0.09	0.11	0.06	0.13	0.08	0.10	0.08	0.07	0.06	0.12	0.09	0.09	0.06
Fe	21.85	21.43	19.11	20.94	17.68	22.64	20.01	10.56	26.35	20.67	19.52	13.67	11.19	7.68	24.44	19.21	20.81	13.19
Ni	0.00	0.00	0.00	0.00	0.00	0.00	0.01	0.02	0.00	0.00	0.00	0.05	0.02	0.05	0.00	0.02	0.00	0.02
Cu	4.57	1.00	0.92	1.42	1.77	1.64	0.46	2.22	2.39	1.20	2.08	24.04	15.36	20.65	1.02	1.15	0.96	1.94
Zn	0.03	0.02	0.02	0.02	0.06	0.04	0.03	0.04	0.13	0.04	0.03	0.11	0.08	0.06	0.07	0.08	0.08	0.12
As	0.00	0.02	0.00	0.00	0.00	0.00	0.00	0.02	0.00	0.00	0.02	0.00	0.00	0.00	0.00	0.00	0.00	0.02
Sr	0.02	0.01	0.01	0.01	0.02	0.02	0.02	0.00	0.02	0.01	0.01	0.00	0.01	0.00	0.01	0.01	0.01	0.01
Mo	0.03	0.02	0.02	0.03	0.03	0.03	0.02	0.03	0.04	0.02	0.03	0.01	0.01	0.00	0.02	0.02	0.02	0.01
Sn	0.00	0.00	0.00	0.00	0.15	0.17	0.00	0.00	0.00	0.27	0.00	0.04	0.04	0.06	0.00	0.00	0.04	0.00
Sb	0.00	0.00	0.00	0.00	0.00	0.00	0.00	0.00	0.00	0.00	0.00	0.00	0.00	0.04	0.00	0.00	0.00	0.00
Pb	0.07	0.00	0.03	0.03	0.04	0.04	0.07	0.00	0.15	0.04	0.00	0.06	0.07	0.05	0.02	0.05	0.05	0.00

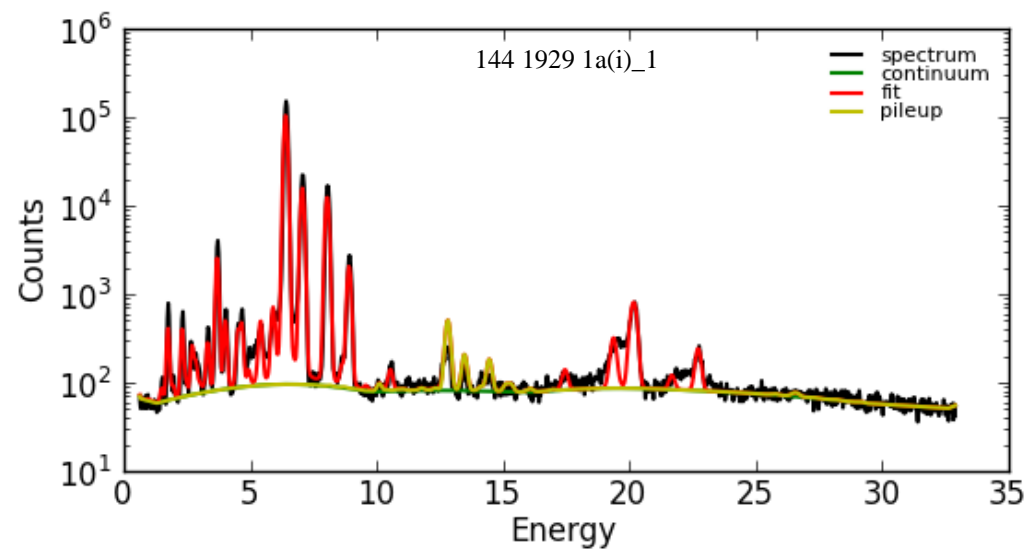
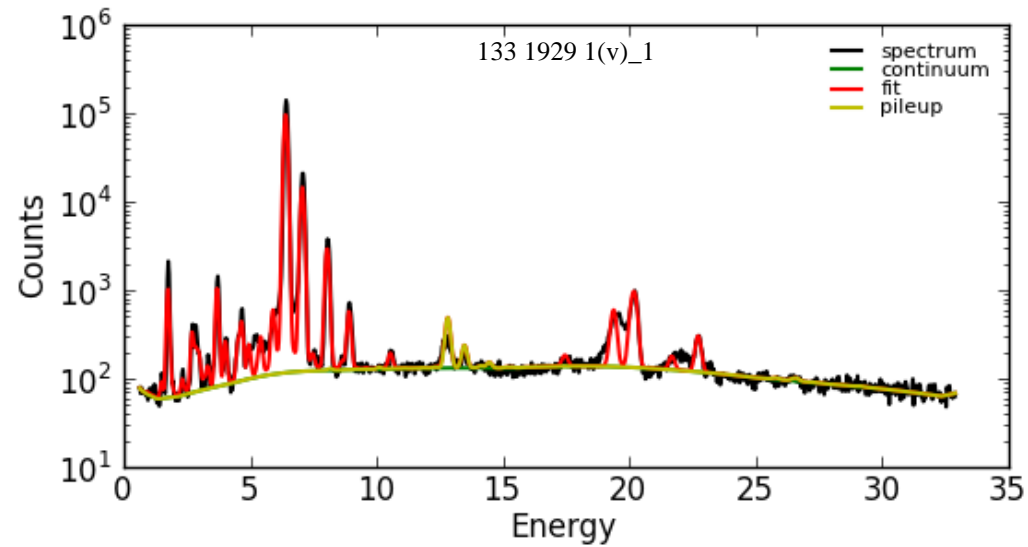
2. 1 Some examples of EDXRF spectrums of analyzed slag samples



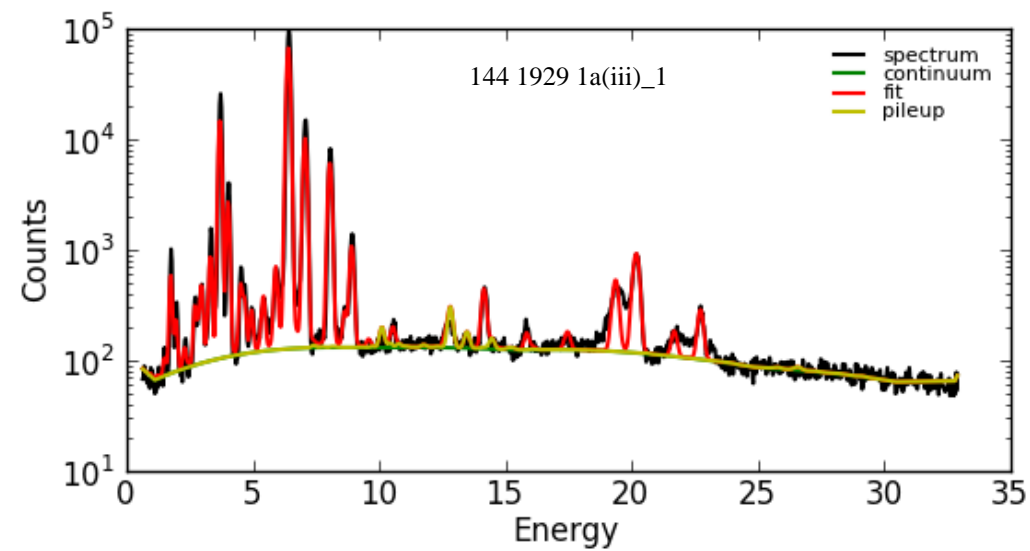
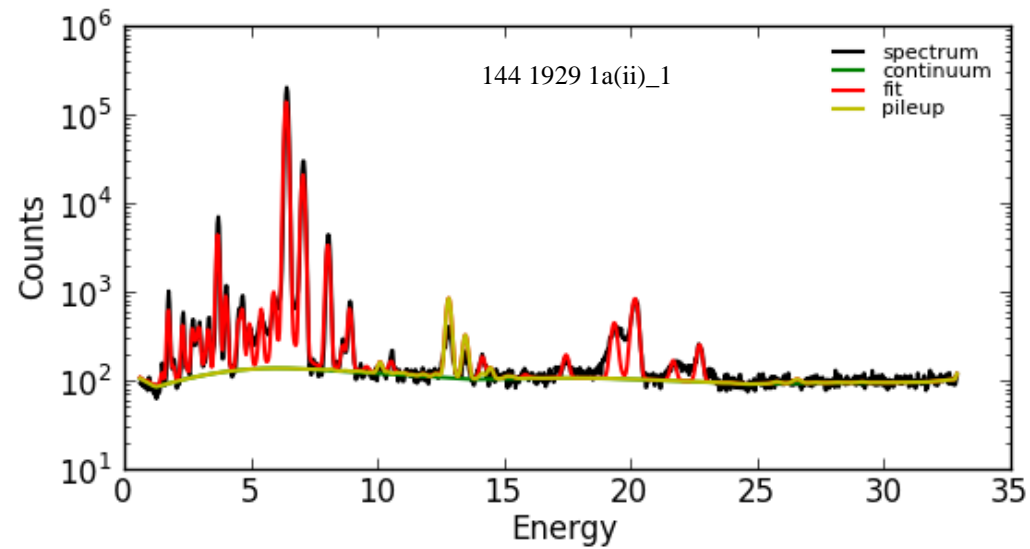
2. 2 Some examples of EDXRF spectrums of analyzed slag samples



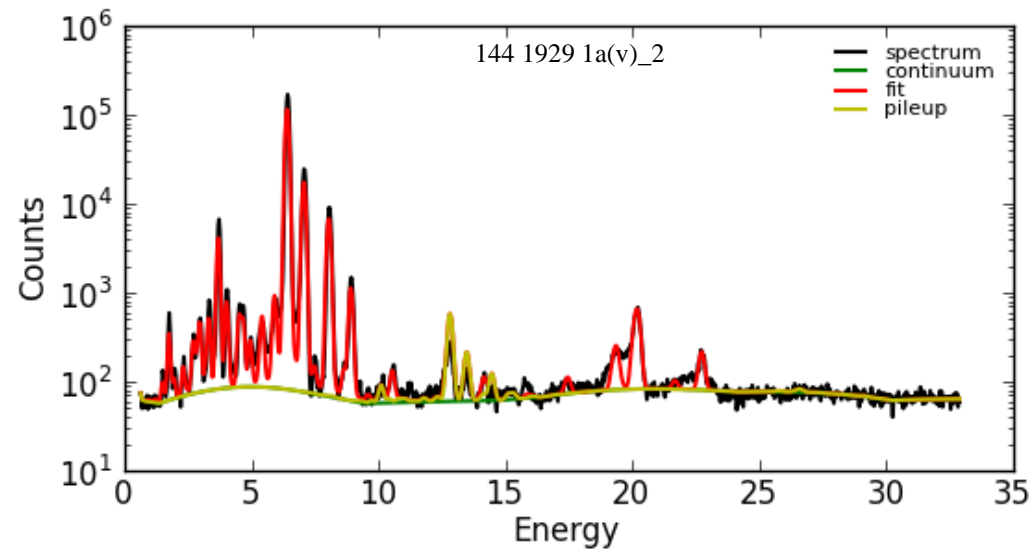
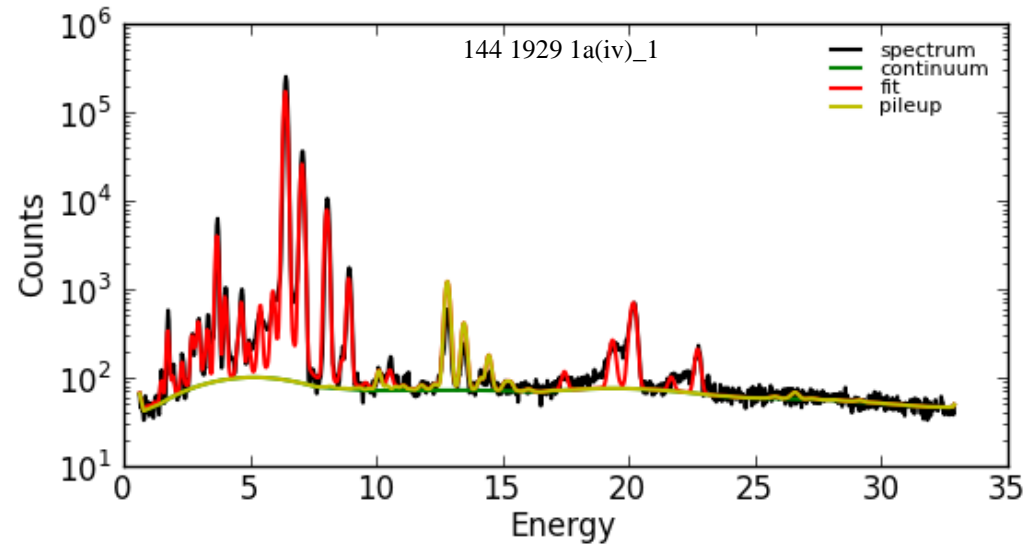
2. 3 Some examples of EDXRF spectrums of analyzed slag samples



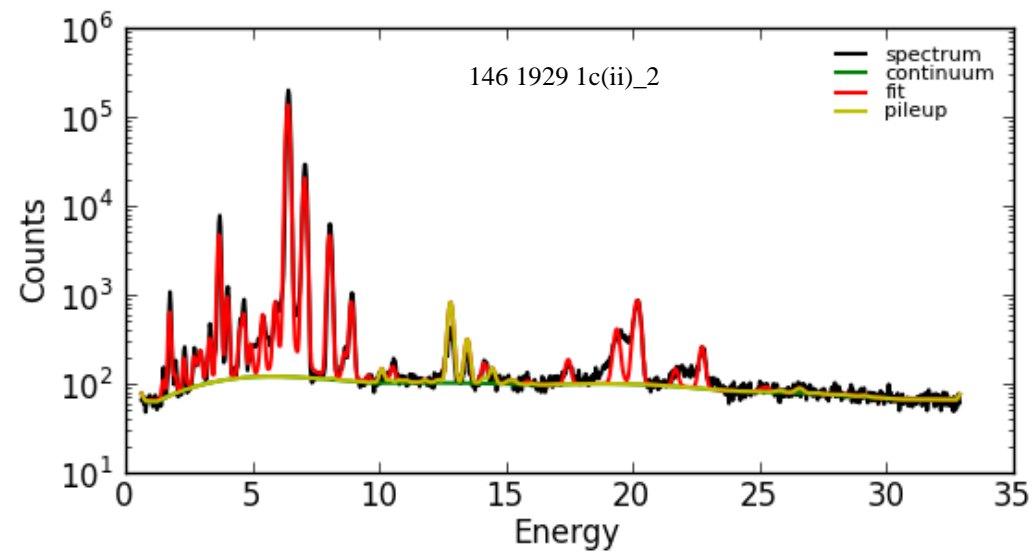
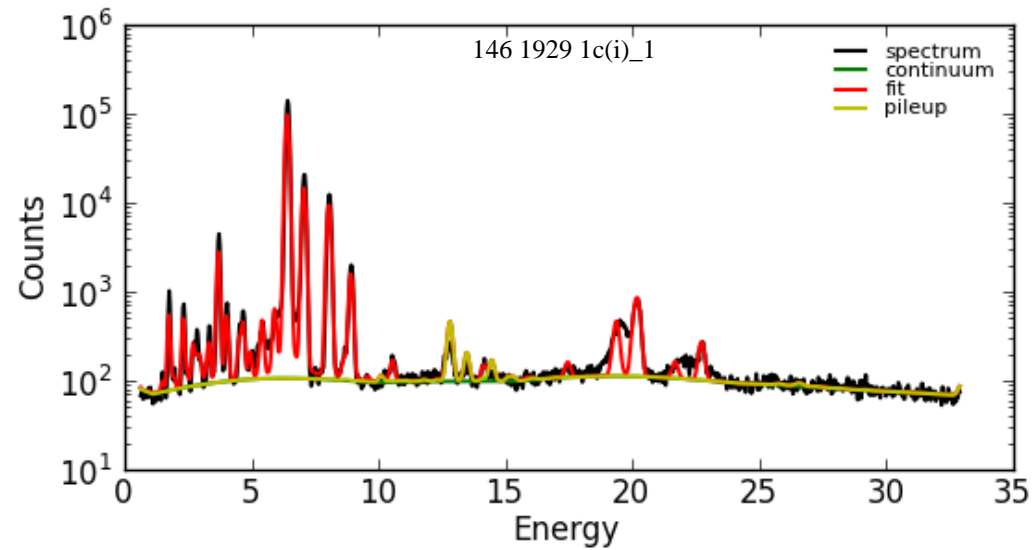
2. 4 Some examples of EDXRF spectrums of analyzed slag samples



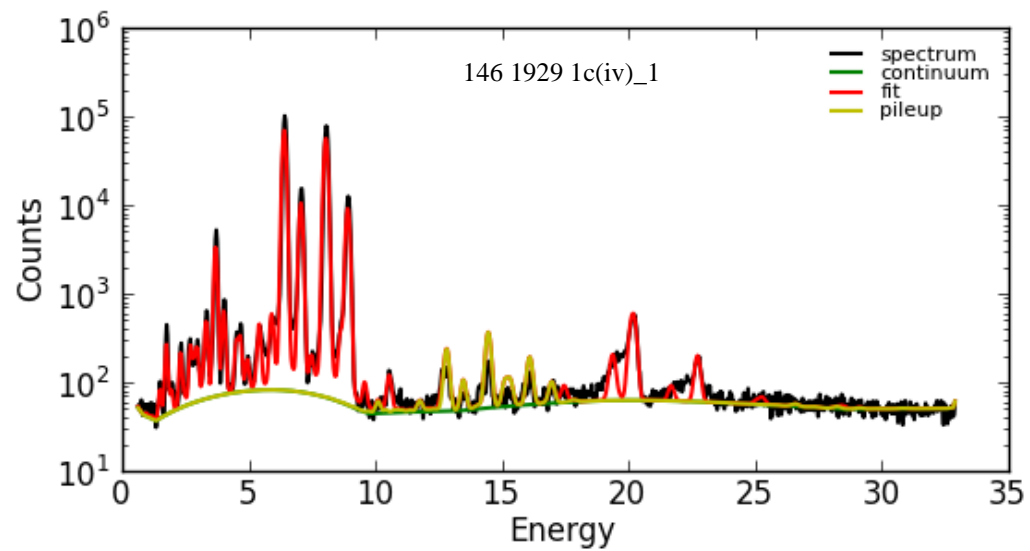
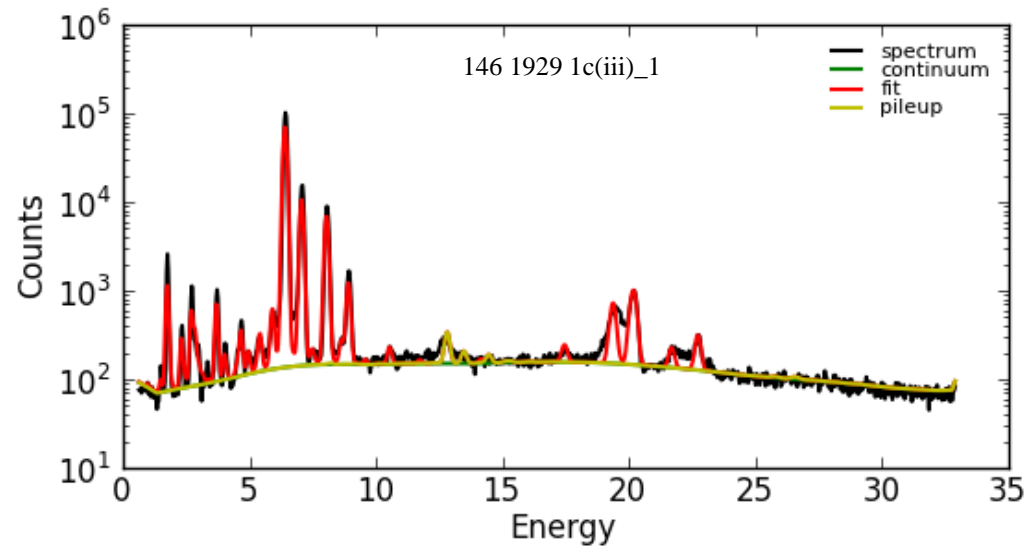
2. 5 Some examples of EDXRF spectrums of analyzed slag samples



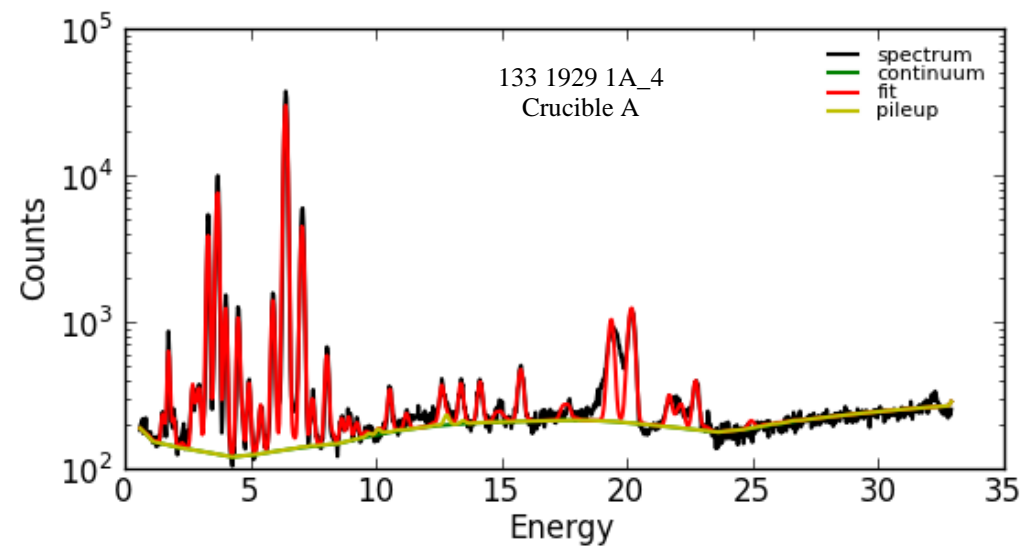
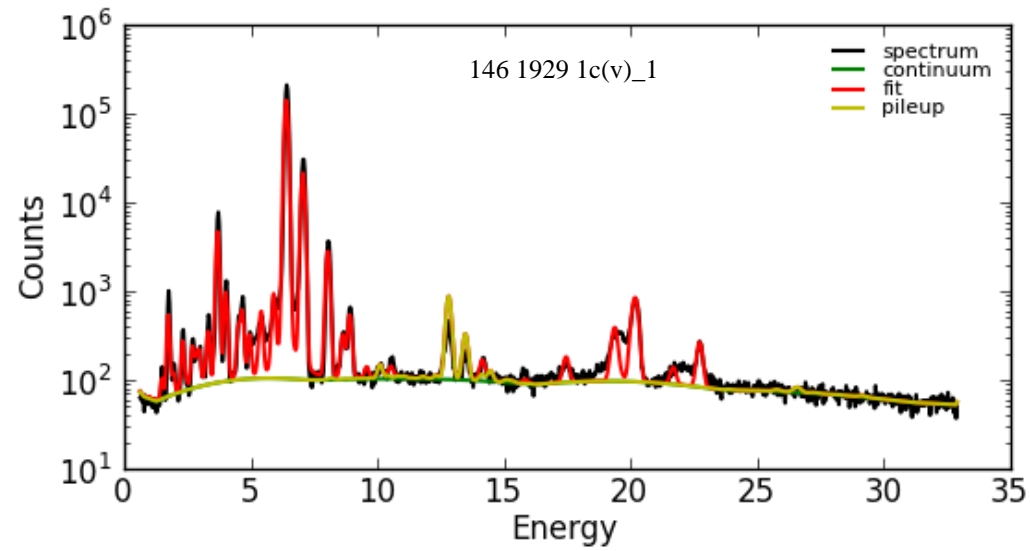
2. 6 Some examples of EDXRF spectrums of analyzed slag samples



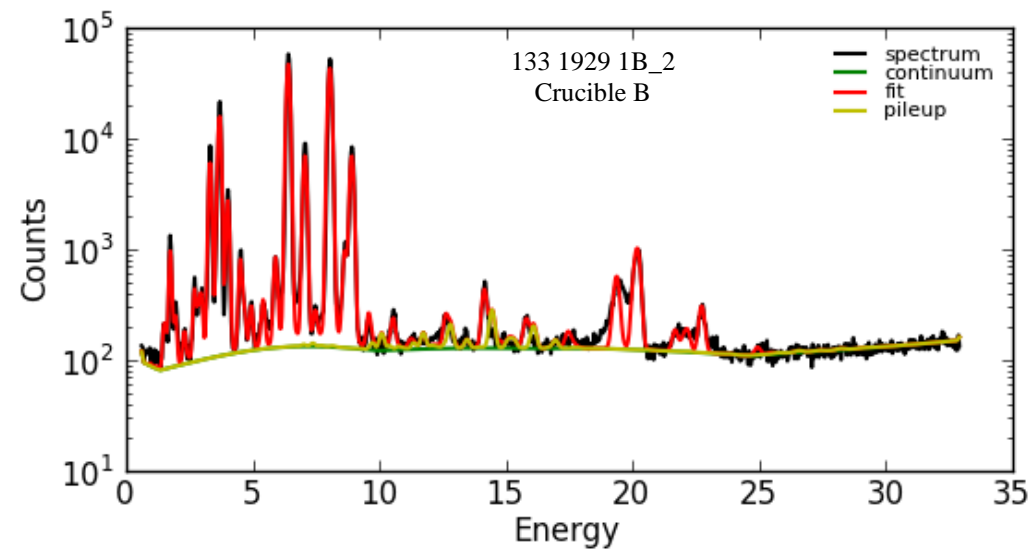
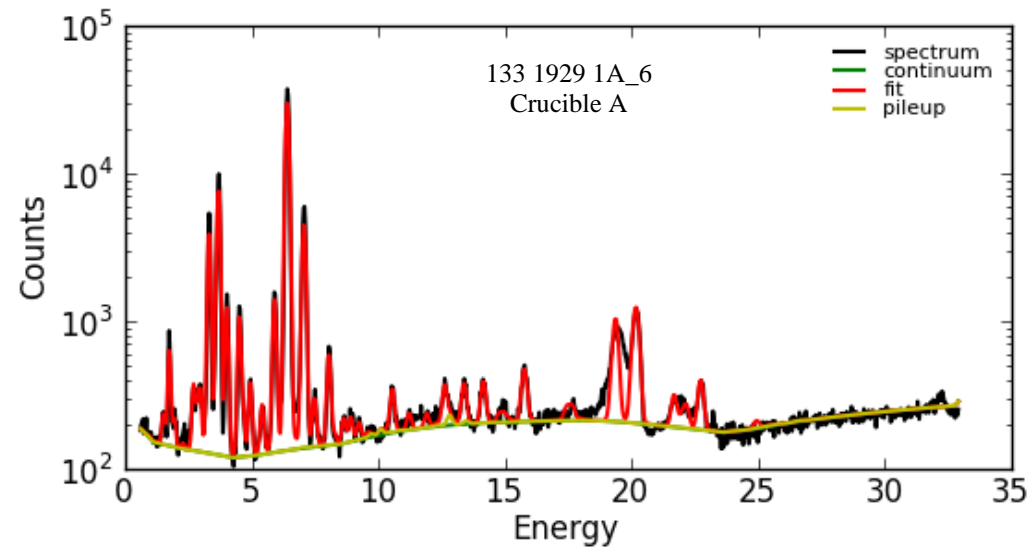
2.7 Some examples of EDXRF spectrums of analyzed slag samples



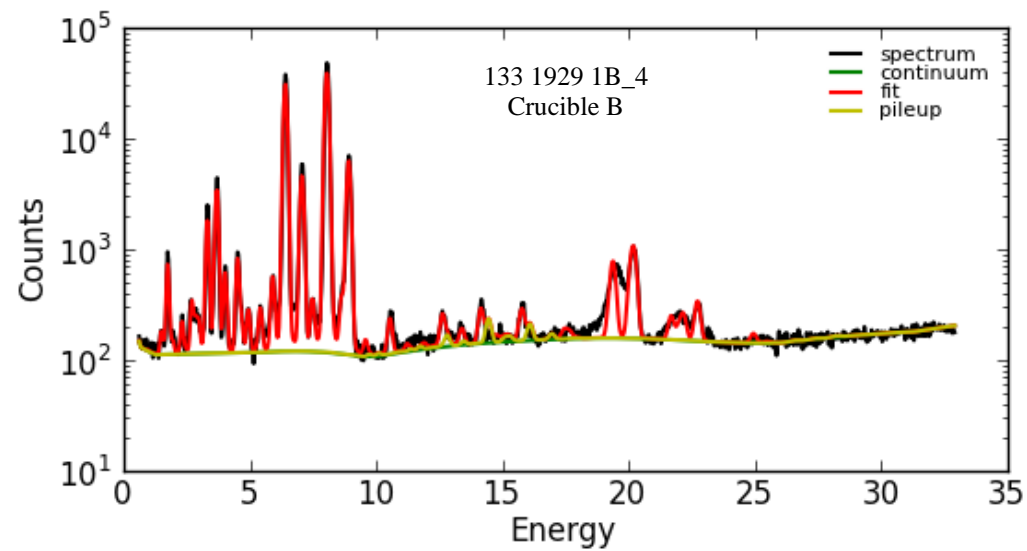
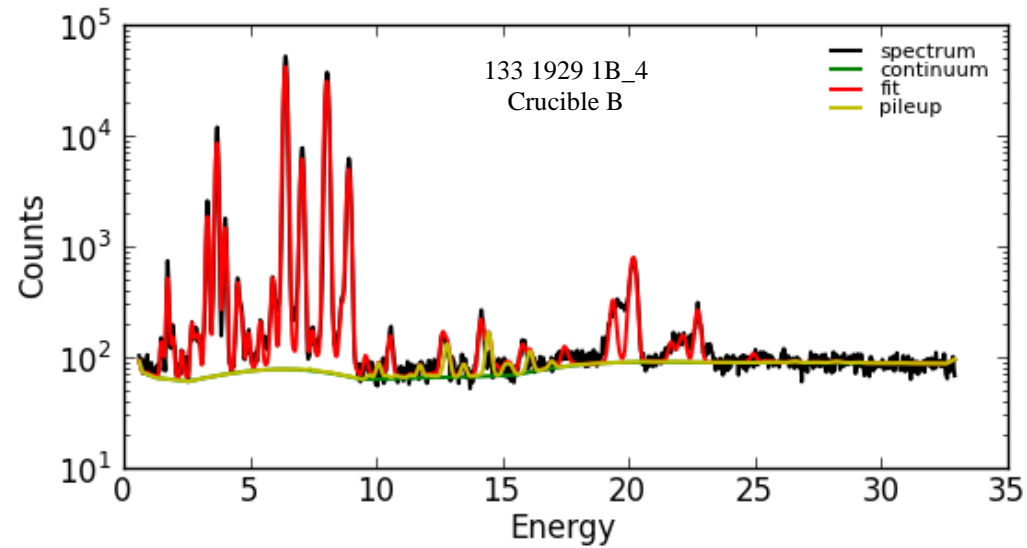
2.8 Some examples of EDXRF spectrums of analyzed slag and crucible samples



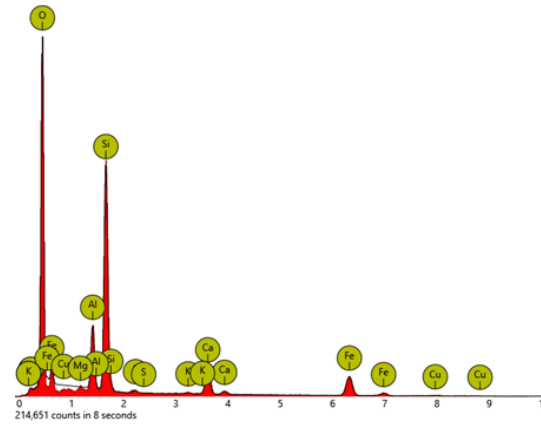
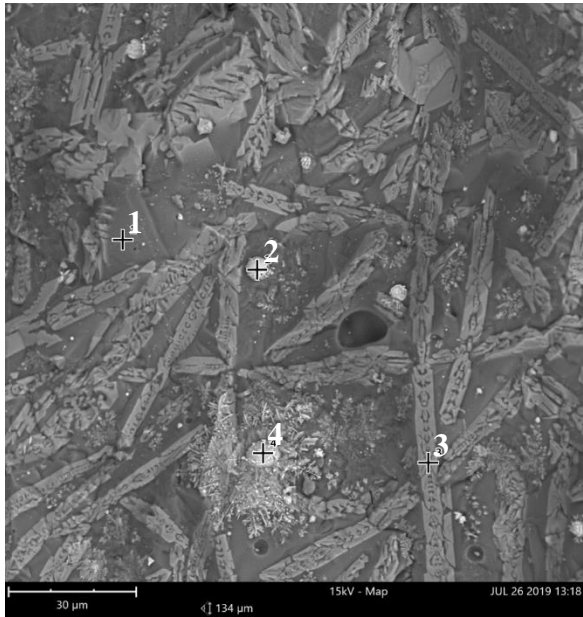
2. 9 Some examples of EDXRF spectrums of analyzed crucible samples



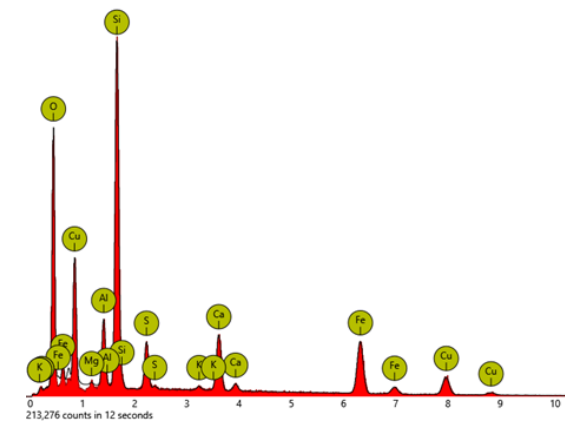
2.10 Some examples of EDXRF spectrums of analyzed crucible samples



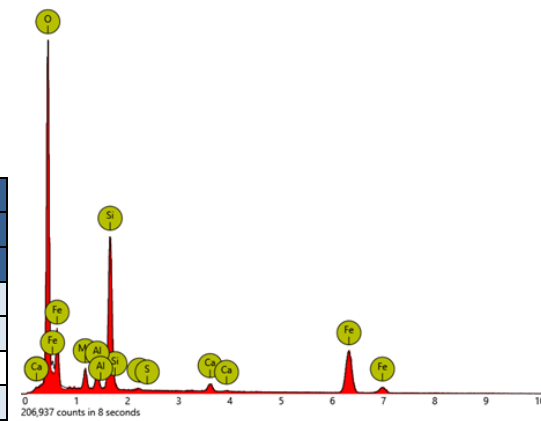
3.1 SEM-EDS backscattered image and spectrums of analyzed spots of sample 133 A929 1(i)



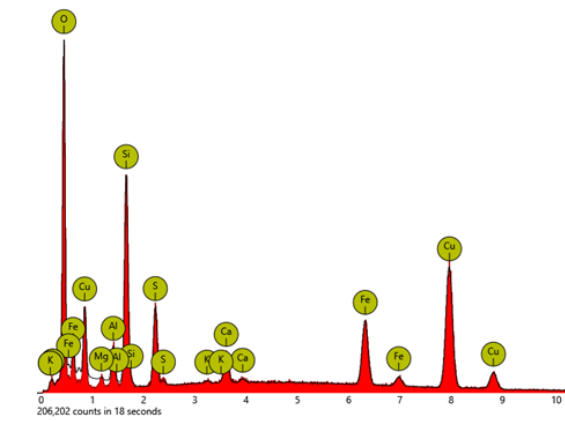
Spot 1



Spot 2



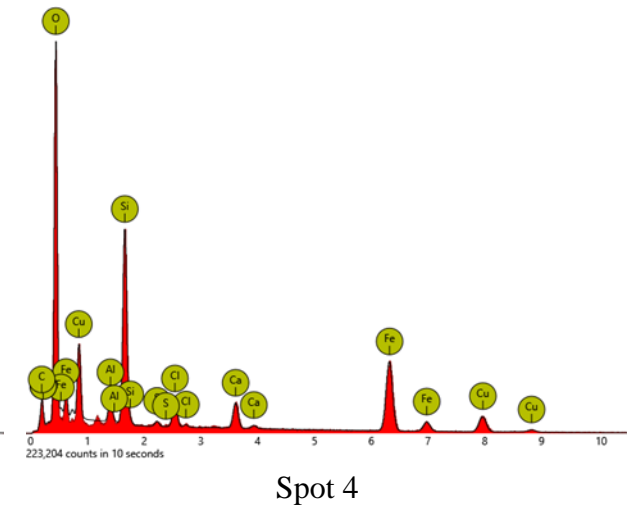
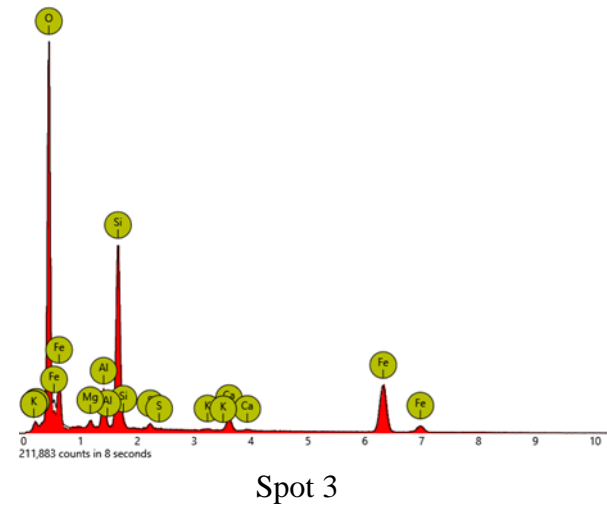
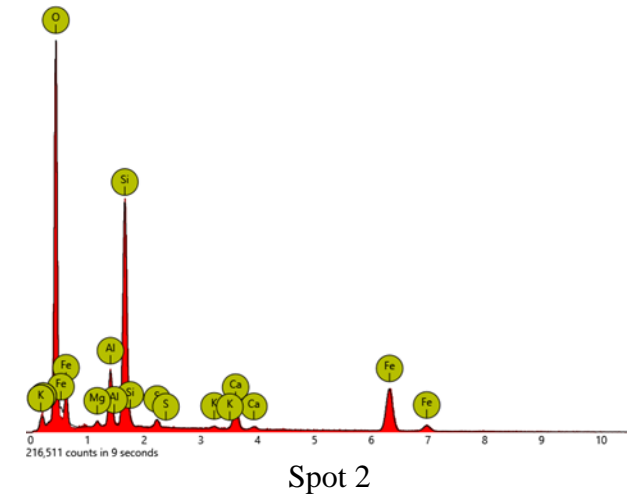
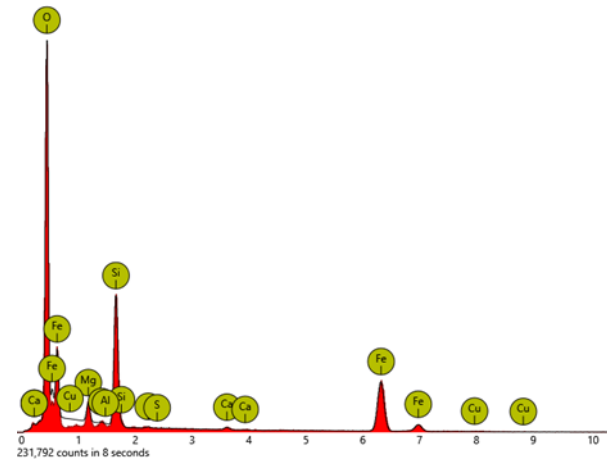
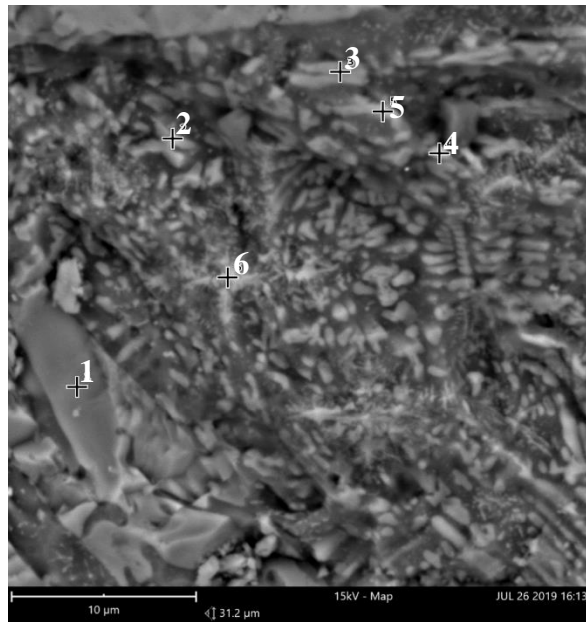
Spot 3



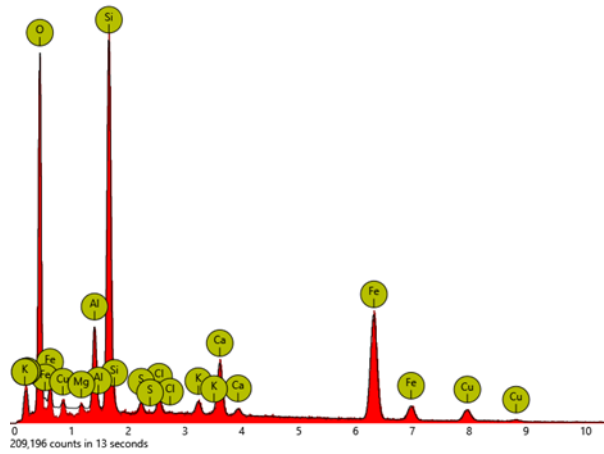
Spot 4

Element	Sample ID			
	133 1(i) Spot 1	133 1(i) Spot 2	133 1(i) Spot 3	133 1(i) Spot 4
O	53.82	27.67	46.45	15.67
Mg	0	0.17	2.51	0.1
AL	6.23	4.38	2.08	1.53
Si	19.9	19.64	15.4	7.5
S	0.34	3.55	0.25	3.13
K	0.19	0.36		0.13
Ca	5.13	6.34	1.56	1.73
Fe	13.54	20.33	31.74	11.45
Cu	0.85	17.54		58.77

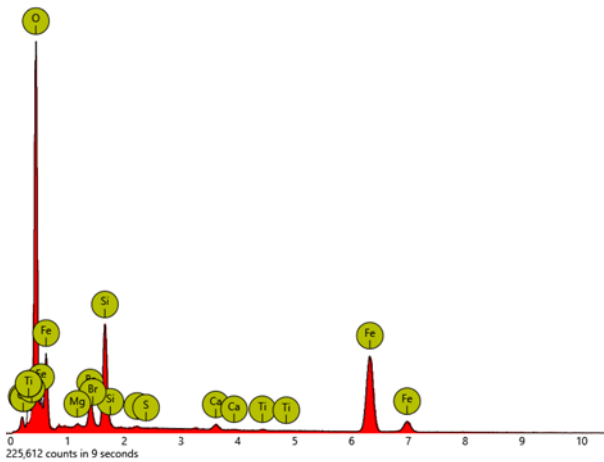
3.2 SEM-EDS backscattered image and spectrums of analyzed spot of sample 133 A929 1(iv)



3.3 SEM-EDS spectrums of analyzed spots of sample 133 A929 1(iv)



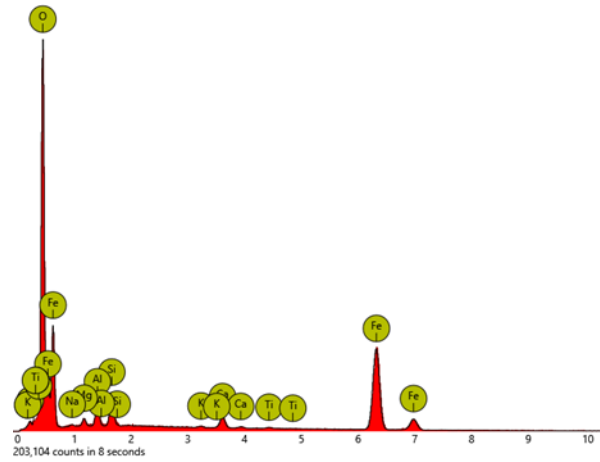
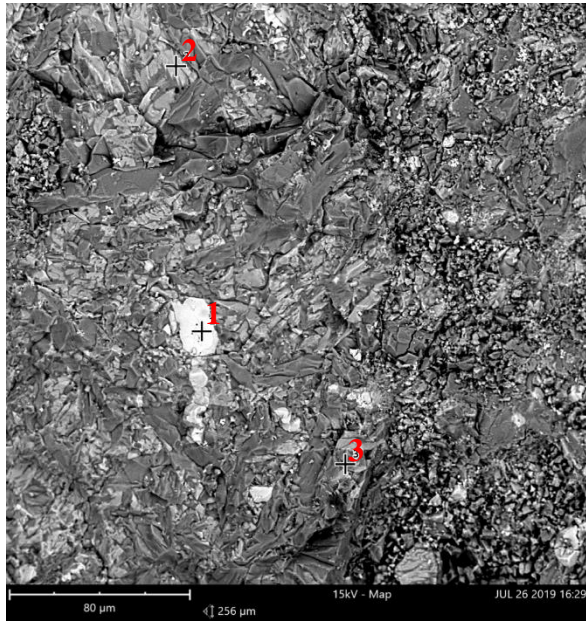
Spot 5



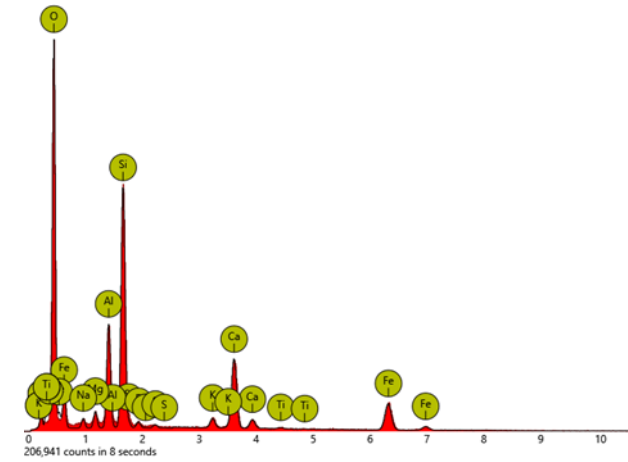
Spot 6

Element	Sample ID					
	133 1(iv)	133 1(iv)	133 1(iv)	133 1(iv)	133 1(iv)	133 1(iv)
	Spot 1	Spot 2	Spot 3	Spot 4	Spot 5	Spot 6
C				7.93		5.17
O	46.14	46.88	46.28	33.8	28.11	39.49
Mg	2.51	0.5	0.77		0.22	0.24
AL	0.15	4.95	3.69	1.89	4.46	
Si	13.12	17.42	15.67	10.45	17.16	7.9
P						
S	0.18	0.87	0.63	0.35	0.72	0.17
Cl				2.08	1.07	
K		0.35	0.24		0.95	
Ca	0.48	3.66	2.23	2.69	4.73	0.7
Ti						0.23
Fe	37.2	25.38	30.49	25.94	33.67	40.72
Cu	0.22			14.87	8.92	
Br						5.38

3.4 SEM-EDS backscattered image and spectrums of analyzed spots of sample 144 A929 1(iii)

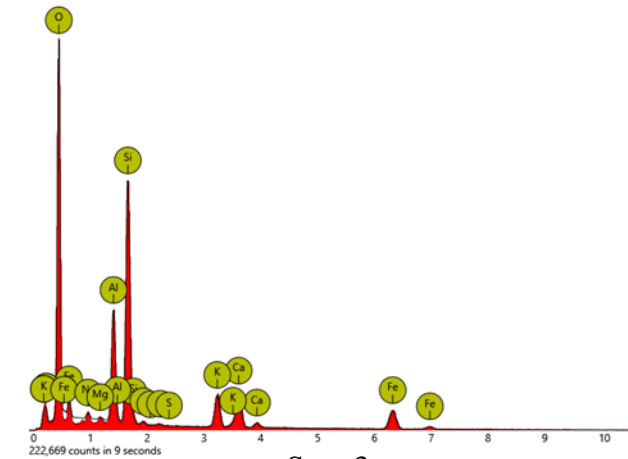


Spot 1



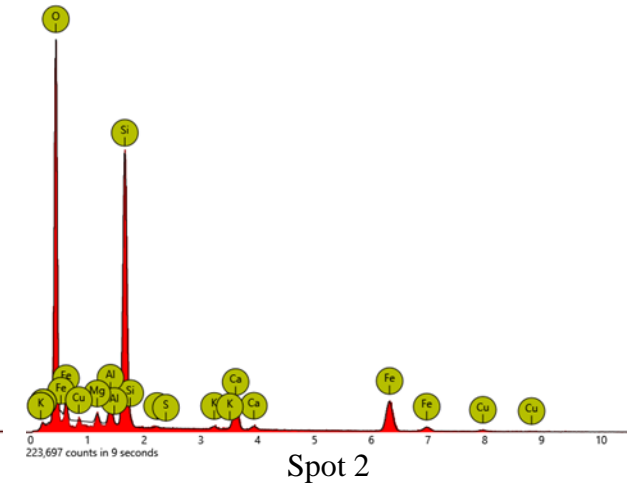
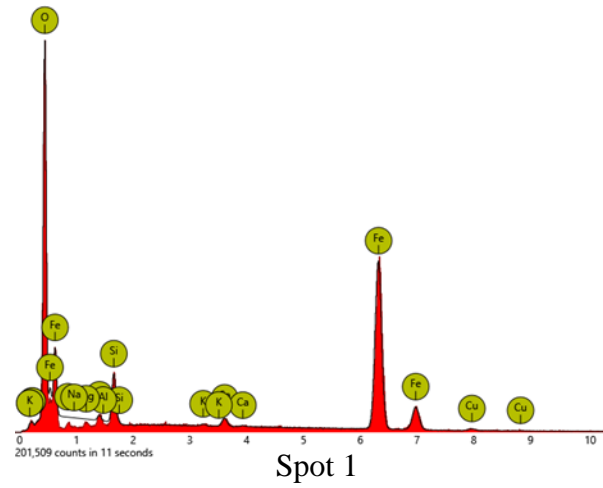
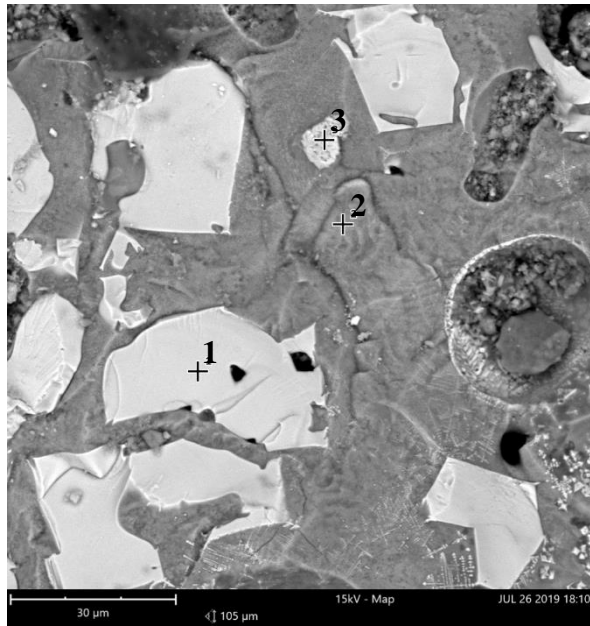
Spot 2

Element	Sample ID		
	144 1a(iii)	144 1a(iii)	144 1a(iii)
	Spot 1	Spot 2	Spot 3
O	39.44	50.09	52.79
Na	0.24	0.9	0.57
Mg	0.98	1.25	0.17
AL	2.75	7.43	8.56
Si	39.44	15.26	16.98
P		0.53	0.26
S		0.31	0.13
K	0.18	1.12	4.24
Ca	1.9	9.68	5.7
Ti	0.21	0.22	
Fe	51.14	13.21	10.6

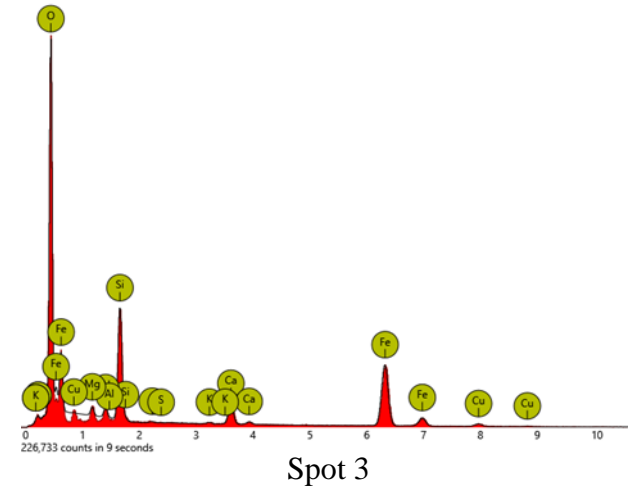


Spot 3

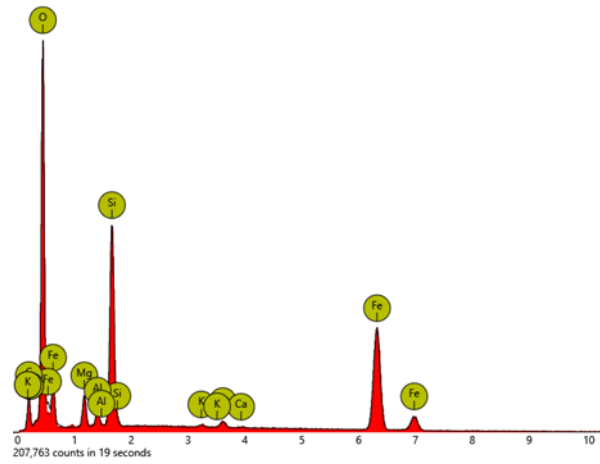
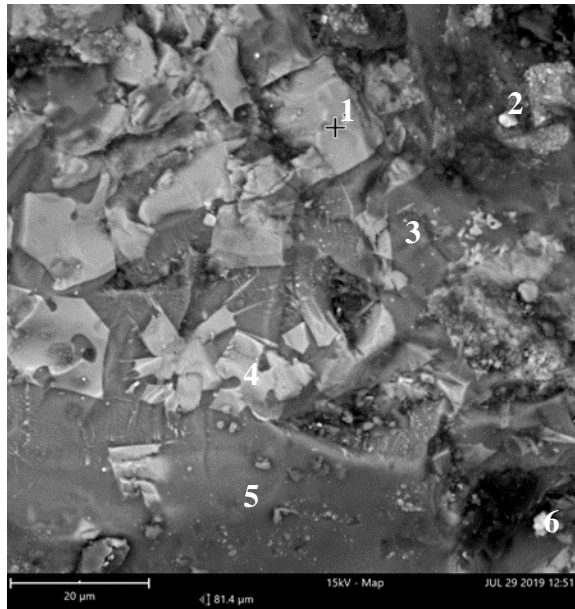
3.5 SEM-EDS backscattered image and spectrums of analyzed spots of sample 144 A929 1(iv)



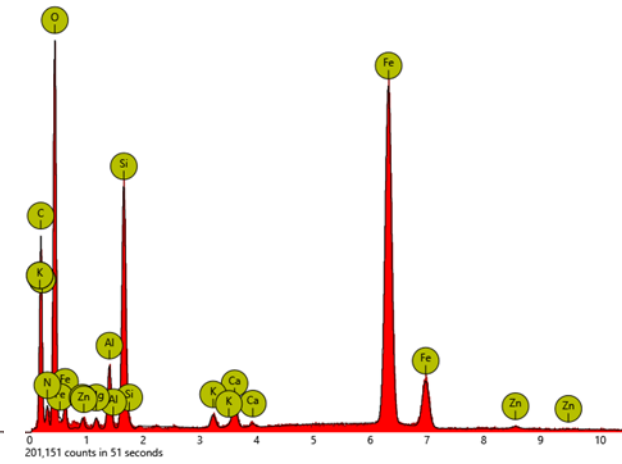
Element	Sample ID		
	144 1a(iv) Spot 1	144 1a(iv) Spot 2	144 1a(iv) Spot 3
	O	25.3	50.35
Mg		0.85	0.99
Al	0.44	2.34	1.01
Si	3.11	20.89	9.69
S		0.18	0.13
K	0.16	0.42	0.21
Ca	0.91	4.72	3.59
Fe	68.25	18.34	37.82
Cu	1.83	1.91	4.01



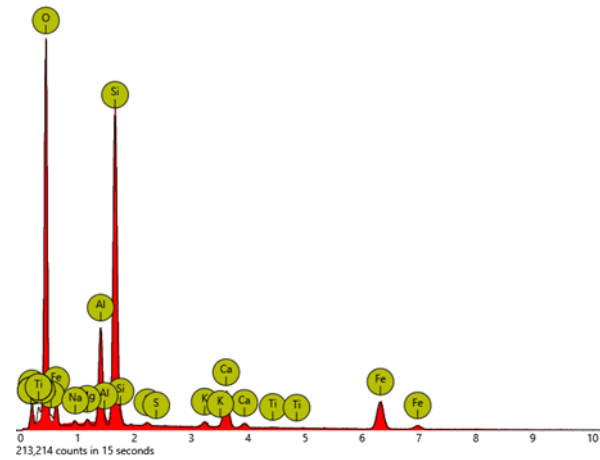
3.6 SEM-EDS backscattered image and spectrums of analyzed spots of sample 146 A929 1(i)



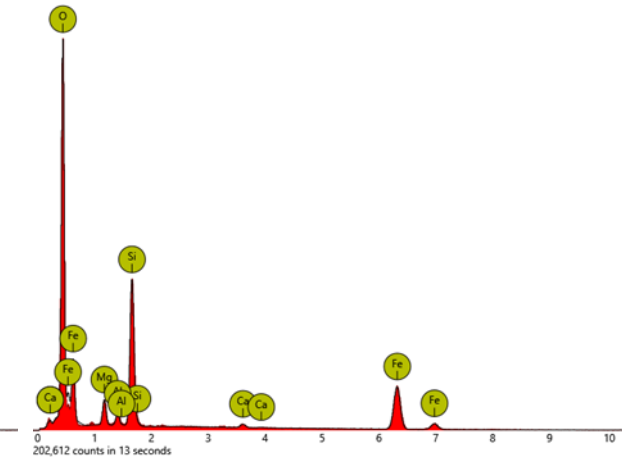
Spot 1



Spot 2

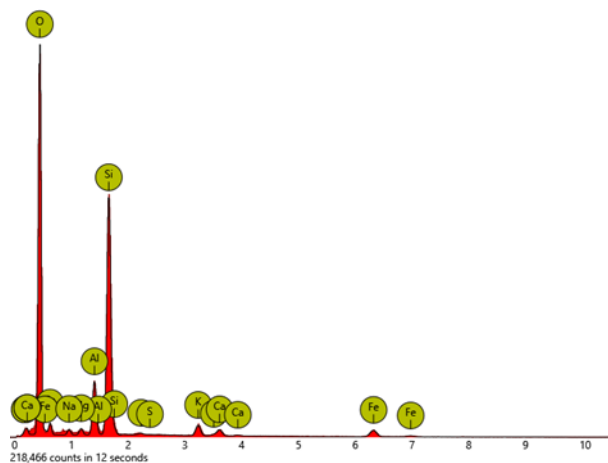


Spot 3

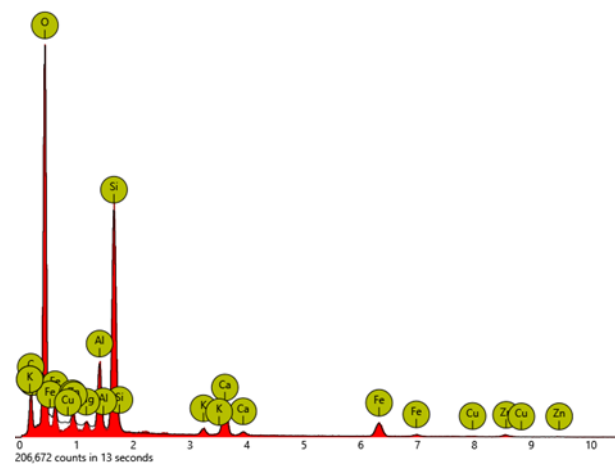


Spot 4

3.7 SEM-EDS spectrums of analyzed spots of sample 146 A929 1(i)



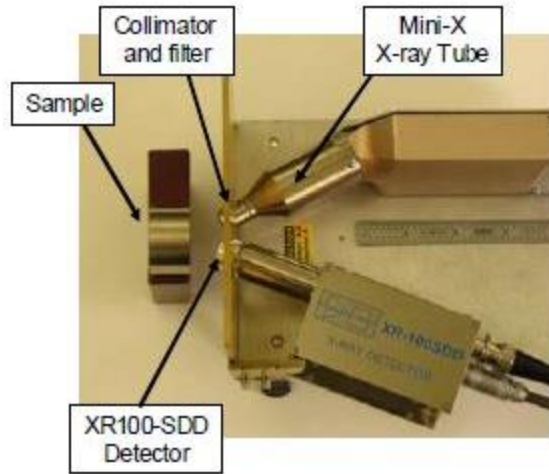
Spot 5



Spot 6

Element	Sample ID					
	146 1c(i)	146 1c(i)	146 1c(i)	146 1c(i)	146 1c(i)	146 1c(i)
	Spot 1	Spot 2	Spot 3	Spot 4	Spot 5	Spot 6
C	9.05	18.07	8.13			13.73
N		2.94				
O	32.78	16.19	47.37	47.79	61.86	52.25
Na			0.41		0.78	
Mg	2.34	0.32	0.45	3.28	0.72	0.27
AL	1.05	1.71	6.48	1.36	5.65	4.68
Si	11.46	5.42	18.38	14.69	22.29	14.08
S			0.26		0.21	
K	0.22	0.48	0.58		1.98	0.76
Ca	0.71	1	4.72	0.71	1.38	4.03
Ti			0.1			
Fe	42.39	52.67	13.11	32.17	5.13	6.95
Cu						0.21
Zn		1.2				3.05

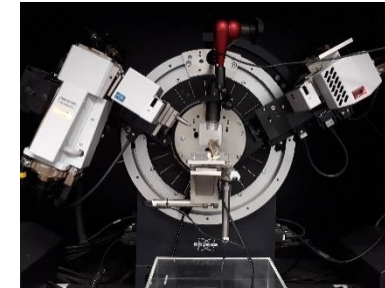
4.1 Images of different analytical instruments and tools used in the present study.



(a) An Amptek Mini-X X-ray fluorescence spectrometer, used for the EDXRF analysis

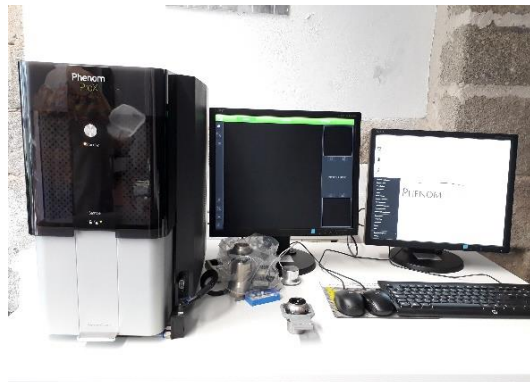


(b) A Brucker D8 Discover Diffractometer used for the powder XRD analysis



(c) A close-up view of Brucker D8 Discover Diffractometer

(d) An agate mortar and pestle, used for preparing the powder samples for the Powder XRD analysis



(e) A Phenom World scanning electron microscope, used for the SEM-EDS analysis



(f) A phenom World scanning electron microscope sample holder



(g) A Leica M205C stereo microscope, used to observe the inclusion in the core of the crucible fragments



(h) An electric saw, used for cutting a small part from the slag samples for the EDXRF analysis